Code Hopping - Direct Sequence Spread Spectrum to Compensate for Intersymbol Interference in an Ultra-Wideband System

by

Sung Han Chung

A thesis submitted to the
Department of Electrical and Computer Engineering
in conformity with the requirements
for the degree of Master of Science (Engineering)

Queen's University
Kingston, Ontario, Canada

August 2004

Your file Votre référence
ISBN: 0-612-99623-9
Our file Notre référence
ISBN: 0-612-99623-9

Abstract

Ultra-Wideband (UWB) has been attracting many researchers for its potential to support a high bit rate in a short range wireless communication system. In order to achieve the high bit rate, a short spreading code is often preferred to a long spreading code in a Direct Sequence Spread Spectrum (DSSS) UWB system. As the symbol period is decreased to support the high bit rate, intersymbol interference (ISI) gets severe in the multipath fading channel. In this thesis, we propose Code Hopping - Direct Sequence Spread Spectrum (CH-DSSS) to compensate for ISI in a UWB system. We also propose a CH pattern search algorithm to find a suboptimal hopping pattern.

To evaluate the performance of the proposed CH-DSSS system, we derive an exact bit error rate (BER) expression in the CH-DSSS system using a Rake receiver for the multipath fading channel. Then, we increase a computational speed by applying the Beaulieu series method (BSM) without sacrificing accuracy. The performance of the CH-DSSS system is evaluated with the Intel channel model that has been adopted by the IEEE 802.15.3a task group. We generate 7000 channels and compute average BER and outage probability.

Computational results show that significant gains are obtained by CH both in the average BER and in the outage probability. Especially, CH with the Gold sequence of length 31 is found to be very good for a non-line of sight (NLOS) channel. Our most important result is for the Gold sequence with 10 Rake fingers at 193.1 Mbps in the NLOS channel, where CH is shown to achieve a 6 dB gain for the outage probability over the system that uses a single optimized sequence all the time.

Acknowledgements

One of the best things that happened to me as an M.Sc. student would be to have Dr. Peter J. McLane as a supervisor. He helped me taste the pleasure of seeking and finding an answer to a problem. I appreciate his kindness and care for his students.

I would like to thank Dr. Iickho Song for his belief in me and support. Without him, I would not be able to start this thesis. I am thankful to his family as well who has been always kind to me and my wife. When I was in difficulty, Dr. Saeed Gazor gave me comfort and courage to keep going on. I appreciate his affection toward students. I also want to thank the Department of Electrical and Computer Engineering and its staff for their excellent work.

I would like to express thanks to friends, Yugang Zhou and Tiago H. Falk. My graduate life would not have been fun without them. I also appreciate Pawel Dmochowski and Kitty K. Y. Wong for their help and friendly mood in the lab.

I would also like to thank the committee members, Dr. Colin MacDougall, Dr. David Thomson, Dr. Saeed Gazor, and Dr. Shahram Yousefi for their helpful advice and comments.

Special thanks should be attributed to Haewon Kim, my wife, since she always has been with me for better or worse. I appreciate her patience, support, and cheer for me.

Finally, I would like to dedicate this thesis to my parents. I am deeply grateful for their love and dedication.

Table of Contents

List of Tables

List of Figures

List of Abbreviations

ADC	Analog Digital Converter
AWGN	Additive White Gaussian Noise
BER	Bit Error Rate
BPSK	Binary Phase Shift Keying
BSM	Beaulieu Series Method
CDM	Code Division Multiplexing
CDMA	Code Division Multiple Access
CH	Code Hopping
CS	Code Selection
CSI	Channel State Information
DSSS	Direct Sequence Spread Spectrum
FCC	Federal Communications Commission
FDM	Frequency Division Multiplexing
GL	Gold-Like
GL(15)	Length 15 Gold-Like Sequence
Gold(31)	Length 31 Gold Sequence
HP	Hopping Pattern
i.i.d.	Independent and identically distributed
ISI	Intersymbol Interference
LOS	Line of Sight
MC	Monte Carlo
Mbps	Mega bit per second
MIMO	Multiple-Input Multiple-Output

M-PAM	M-ary Pulse Amplitude Modulation
MRC	Maximal Ratio Combining
NLOS	None Line of Sight
OFDM	Orthogonal Frequency Division Multiplexing
OOK	On Off Keying
PAM	Pulse Amplitude Modulation
PAN	Personal Area Network
pdf	Probability density function
PPM	Pulse Position Modulation
PRF	Pulse Repetition Frequency
PSD	Power Spectral Density
Q-MC	Quasi-analytic Monte Carlo
RMS	Root Mean Square
S-CDMA	Synchronous Code Division Multiple Access
SI	Self Interference
SISO	Single Input Single Output
SNR	Signal to noise ratio
S-V model	Saleh-Valenzuela model
TDM	Time Division Multiplexing
TH	Time Hopping
UWB	Ultra-Wideband
WGN	White Gaussian Noise
WCDMA	Wideband Code Division Multiple Access
WH	Walsh-Hadamard
WH(16)	Length 16 Walsh-Hadamard Sequence
WH(32)	Length 32 Walsh-Hadamard Sequence

List of Symbols

A	The amplitude of the transmitted signal.
C_m	The coefficient of the Fourier series.
$D(\xi)$	Intersymbol interference term for the Beaulieu series method.
DM_{tot}	Total decision metric for code hopping pattern search.
H_N	$N \times N$ Hadamard matrix.
$\bar{H}_N$	The binary complimentary of the elements in H_N.
K	The number of Rake fingers.
K'	The number of arriving rays in a cluster.
L	The total number of arriving paths.
M	The integer that truncates the infinite summation in the Fourier series for the BSM.
$M(k,\ N_h)$	$k \pmod{N_h}$.
N_c	The processing gain or the length of the spreading sequence.
N_h	The length of a hopping pattern.
$N_{h,\,max}$	The maximum length of a hopping pattern.
$\frac{N_o}{2}$	The spectral density or the variance of white Gaussian noise.
N_{tot}	The total number of spreading sequences.
$P_T(t)$	Rectangular pulse with unit height within $[0, T)$ and zero elsewhere.
$P(\tau)$	The power delay profile
$P_r\{e\}$	Probability of error.
$R_{k,\,m}(\tau)$	Partial cross-correlation function between the spreading sequence for the k-th bit, $a_k(t)$, and the spreading sequence for the m-th bit, $a_m(t)$.

$\hat{R}_{k,\,m}(\tau)$	Partial cross-correlation function between the k-th spreading sequence and the m-th spreading sequence, but all sequences start at $t = 0$.
$R_{n_I}(\tau)$	The autocorrelation function of the imaginary part of white Gaussian noise process.
$R_{n_R}(\tau)$	The autocorrelation function of the real part of white Gaussian noise process.
T	Symbol period.
T_c	Chip period.
T_l	The excess delay of the l-th cluster.
$U_{cn}(\xi)$	The correlated noise term of the Rake combiner output.
U_s	The desired signal term of the Rake combiner output.
$U_{si}(\xi)$	The self interference term of the Rake combiner output.
$U_{isi}(\xi,\ \mathbf{b})$	Intersymbol interference term of the Rake combiner output.
X	Intersymbol interference plus noise term for the Beaulieu series method.
$a_k(t)$	The waveform of the spreading sequence for the k-th bit with code hopping.
$\{a'_0(t), a'_1(t), \cdots a'_{N_h-1}(t)\}$	The set of the hopping sequence selected from the total set of spreading sequences.
$\mathbf{a}' = \{a'_0, a'_1, \cdots a'_{N_h-1}\}$	The hopping pattern of the spreading sequence.
$a^i_{M(k,\,N_h)}$	The i-th chip amplitude for the k-th spreading sequence which is taken from the hopping pattern.
b_k	The k-th data bit.
$b_k(t)$	The waveform of the k-th data bit.
$\hat{b}_k(t)$	The waveform of the k-th detected bit.
$\mathbf{b}$	The vector of the data sequences that contribute to ISI in $U_{isi}(\xi, \mathbf{b})$.
$\mathbf{c}$	All the parameters of channel impulse response or channel state information.
c_l	The complex channel gain of the l-th path.
$c_{k,\,l}$	The channel gain of the k-th multipath component in the l-th cluster.

g_ξ	The coefficient of the desired signal term for bit b_ξ.
g'_ξ	The coefficient of the desired signal term for bit b_ξ with scaling.
$g_{\xi+k}$	The coefficient of the intersymbol interference term in the received signal.
$g'_{\xi+k}$	The coefficient of the intersymbol interference term in the received signal with scaling.
$gcd(\cdot)$	Greatest common devisor.
$h_c(t)$	Discrete time channel impulse response.
m_{li}	The integer part of the distance in units of T between the l-th excess delay and the i-th finger position.
n	Gaussian distributed random variable.
$n(t)$	Complex white Gaussian noise random process.
$n_{_R}(t)$	The real part of complex white Gaussian noise random process.
$n_{_I}(t)$	The imaginary part of complex white Gaussian noise random process.
$p(i)$	The position of the i-th Rake finger.
$p_{k,\,l}$	The real part of the phase in the k-th multipath component in the l-th cluster.
$\Re\{\cdot\}$	Real part.
x_l	The real part of the l-th complex channel gain, c_l.
y_i	The output of the i-th Rake finger.
y_l	The imaginary part of the l-th complex channel gain, c_l.
y_N	The total noise term of the sum of all Rake finger outputs.
y_{N_i}	The noise term of the i-th Rake finger output.
y_{N_R}	The real part of the total noise term.
y_s	The total signal term of the sum of all Rake finger outputs.
y_{s_i}	The signal term of the i-th Rake finger output.
y_{s_R}	The real part of the total received signal term.
y_{tot}	The total Rake finger output of the received signal.
Γ	A cluster decay factor.
Λ	An inter-cluster arrival rate.

Ω_0	The mean power of the first path of the first cluster.
$\prod$	Product operator.
α_l	The magnitude of the complex channel gain of the l-th path.
$\beta_{k,\,l}$	The magnitude of the k-th multipath component in the l-th cluster.
$\delta(\cdot)$	Dirac delta function.
γ	A ray decay factor.
λ	An inter-ray arrival rate.
$\mu_{k,\,l}$	The mean of the k-th multipath component in the l-th cluster.
ω_0	Frequency of the Fourier series.
ϕ_l	The phase of the l-th path.
τ_l	The excess delay of the l-th path.
τ_{li}	The excess delay of the l-th path expressed relative to the i-th finger.
$\tau_{k,l}$	The excess delay of the k-th multipath component in the l-th cluster.
$\tau_{p(i)}$	The excess delay of the i-th Rake finger.
$\tau_{X_{dB}}$	The maximum excess delay (X dB).
σ_τ	The RMS delay spread.
$\tilde{\tau}_{li}$	The fractional part of the distance that constitute τ_{li} relative to m_{li}.
$\bar{\tau}$	The mean excess delay
ξ	Code hopping index.
$*$	Convolution operator.

Chapter 1

Introduction

1.1 Motivation

Recently Ultra-Wideband (UWB) technology has gained much interest for low cost, high rate, short range wireless communication systems. However, UWB raises some challenges. For a high rate system at a transmission rate over 110 Mbps for an indoor wireless channel, there is a relatively longer power delay profile [1] of the channel compared to the symbol period of the UWB system. This fact causes intersymbol interference (ISI). Therefore certain types of ISI mitigation methods may be required for the high rate system. Although an equalizer is a well known scheme to suppress ISI [2], it causes complexity at a receiver. On the other hand, Code Hopping (CH) in Direct Sequence Spread Spectrum (DSSS) can also be used to compensate for ISI maintaining a simple receiver structure compared to that with an equalizer. When CH is used, the impact of ISI terms is due to both the cross-correlation and the auto-correlation functions rather than just due to the latter when a single spreading code system is used. Therefore, for a special case, if multipath components arrive at multiples of the symbol period, CH with orthogonal codes can almost completely remove these ISI terms.

Besides, CH can also reduce performance variability [20]. Although Code Division Multiple Access (CDMA) is a strong and flexible technique for multiple access, if a short code is used, the variability of performance from spreading code to spreading

code is observed [20], [21]. Likewise the performance variability is also expected to be observed in a DSSS UWB system, since the length of spreading sequences tend to be shorter to support a high rate. It is shown in [20] that CH can reduce the performance variability of each user in a short spreading code system.

In addition, CH can also reduce the probability of code collision between uncoordinated systems [26]. Since the short code has a limited number of spreading codes, there is a possibility that the same code is used in a neighboring UWB system. Then, both codes will collide with each other causing severe interference. However if CH is used in a CDMA system, the probability of such a collision will be decreased [26].

Because of the features CH can provide and the characteristics of a high rate UWB system, it is worthwhile to investigate the performance of a CH-DSSS UWB system. Our main application in this thesis is to use CH to compensate for ISI. When CH is not used and the best single DSSS sequence is used, we call this a code selection (CS) system.

1.2 Performance Measure

We employ bit error rate (BER) and outage probability as performance measures. The BER is a well known performance measure and we calculate the average BER over an ensemble of UWB channels. However, when the channel is slowly changing in time, the average BER may be dominated by the worst channel that may only occur rarely. Therefore the average BER may not fully represent the real performance of a system in a slowly fading channel. In such a case, the outage probability often becomes useful as a performance criterion. For each given channel, we obtain the BER and compare it to a threshold. If the BER is higher than the threshold, then we increment an outage count. Then we calculate the percentage of time or channels that is over the threshold to get the outage probability.

1.3 Literature Survey

In the 1960s, Ross [3] studied the transient behavior of antennas with impulse like signals and impulse measurement techniques for the design of wideband radiation elements. Bennett and Ross [4] described the various applications of time domain electromagnetic carrierless baseband pulse technology. After that, the term, Ultra-Wideband, started to appear in the late 1980s with the interest of the U.S. Department of Defense. Most UWB research had been performed under the classification of the U.S. government until 1994. Since then, UWB has been released of restrictions, and much research was carried out on the UWB technology and its application [5].

In the late 1980s, Win and Scholtz [6] described a pulse position modulation based UWB system and a Time Hopping (TH) multiple access scheme. TH-UWB has also been studied in [7] and [8]. Around this time, some companies such as Intel Corp. started to apply DSSS schemes to UWB (DS-UWB). Foerster studied the performance of DS-UWB in the presence of interference [9]. Li and Rusch researched multiuser detection with DS-CDMA UWB in [10]. Ogawa et al. [11] developed signal sources suitable for a DS-UWB system. M-ary UWB using Walsh codes was also proposed in [12].

After the UWB technology was defined by the Federal Communications Commission (FCC), it has experienced major changes in the direction of UWB research and development. For instance, multiband systems became an interesting area of research. Gupta and Tewfik researched the capacity of the UWB with Orthogonal Frequency Division Multiplexing (OFDM) [13]. Gerakoulis and Salmi has researched the OFDM scheme that has the capability of suppressing narrow-band interference [14]. Also, multiuser UWB OFDM with frequency hopping was studied by Saberinia and Tewfik [15]. They also studied UWB-OFDM in a high rate system up to 2 Gbps [16]. Besides, there also has been an approach to generalize single-input single-output (SISO) UWB to multiple-input multiple-output (MIMO) UWB schemes by Weisenhorn and

Hirt [17].

As the demand for a high data rate system is getting stronger, many research groups seem to be interested in short code DSSS CDMA systems. Tang et al. [18] and Parkvall [19] compared long codes and short codes in a DS-CDMA system. Moreover, Parkvall [20] and Honig and Veerakachen [21] reported that if the short code is used, each user with a fixed code can have different performances. Noneaker and Pursley [22] tried to select a single spreading sequence that is robust over a doubly selective fading channel. Instead of finding one good sequence, Parkvall [20] proposed CH to reduce the performance variability by averaging the user performance over spreading sequences. Ünal and Tanik [23] also showed that CH can improve the outage probability in uplink synchronous CDMA systems. They also studied on the capacity improvement by CH in [24]. Orthogonal code hopping multiplexing is considered by Park and Sung [25] to increase the availability of downlink channels. Onizawa and Hasegawa [26] proposed CH to reduce the probability of code collision between uncoordinated neighboring systems. There are other works regarding CH for various purposes including [27] and [28].

Although numerous studies on CH have been reported, to the author's knowledge, there has not been an explicit study on CH to compensate for ISI in a multipath fading channel. Nouguet et al. [29] proposed CH to increase the total symbol period to avoid ISI, but didn't suggest a solution when the excess delay of the channel impulse response is longer than the total symbol period of a system. Tugnait and Ma [30] proposed a blind multiuser detection scheme with CH for a multipath channel, but used an equalizer to suppress the ISI. Moreover, the multipath channel used in the study was simpler (4 paths) than the standard UWB channel model (around 35 significant paths for the non-line of sight channel). Furthermore, most of the work on CH, so far reported, does not consider the design of hopping patterns.

Therefore, this thesis is focused on establishing a good CH pattern search algorithm and on evaluating the performance of CH to compensate for ISI using the UWB

channel model from [42].

1.4 Thesis Contribution

The contributions stated below are relative to assuming perfect channel state information (CSI), timing, and carrier recovery regarding the CH-DSSS system with a Rake receiver. Also, spectral properties of the DSSS UWB system are not considered in this thesis.

1. A CH scheme is proposed to compensate for ISI and is shown to be effective in a DSSS UWB system.

2. An exact error probability analysis is developed for a single user CH-DSSS system with a Rake receiver for a multipath fading channel with ISI, and the Beaulieu series method (BSM) is applied to increase the computation speed for the error probability evaluation without loosing accuracy.

3. A suboptimal CH pattern search algorithm is proposed and it produces hopping patterns with good performance.

4. Relative to not using CH, called code selection (CS), it is found that, for the same performance, the CH scheme requires less number of Rake fingers in the receiver than the CS scheme.

1.5 Thesis Outline

This thesis is composed of 5 chapters. In chapter 1, the introduction and some background is described. Chapter 2 covers the system model and the error probability analysis. Chapter 3 proposes an algorithm to find the suboptimal CS and the suboptimal CH pattern. Chapter 4 gives computational results. Finally, conclusions are made in chapter 5.

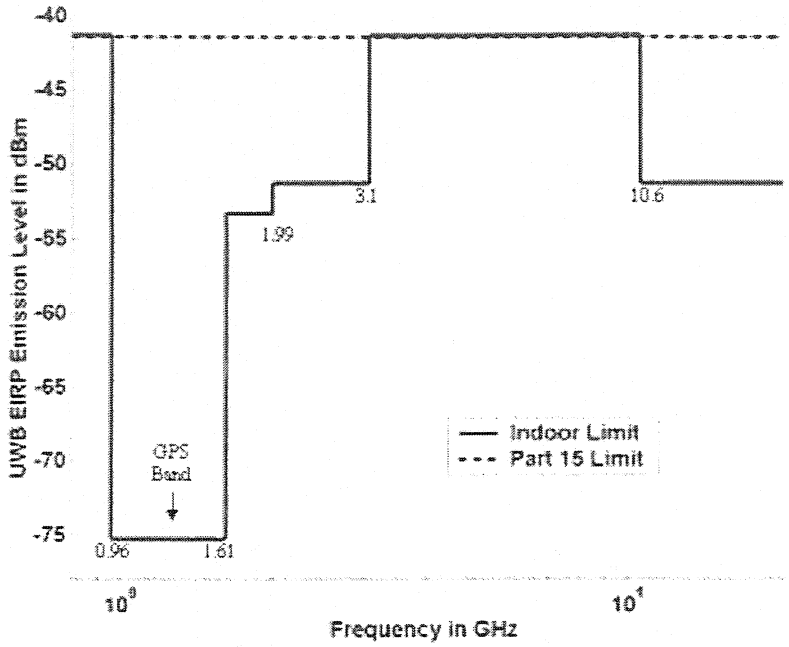

Figure 1.1: Indoor UWB spectral mask by the FCC part 15

1.6 Ultra-Wideband

In this section we briefly describe UWB communication schemes regarding definition, modulation schemes, application, multiple access schemes, and multiband schemes.

1.6.1 Introduction

The FCC has recently defined UWB technology as any wireless transmission method that occupy bandwidth more than 20% of the center frequency or more than 500 MHz of bandwidth [35]. The FCC has assigned the total bandwidth of 7500 MHz for unlicensed use in the 3.1 GHz to 10.6 GHz frequency band. The allocated bandwidth for UWB is the largest ever permitted for the unlicensed use. However, the power spectral density (PSD) measured in 1 MHz is strictly limited in order to avoid the interference with other licensed narrow-band systems. Fig. 1.1 shows the spectral mask set by the FCC [39]. It is also required in [37] that the data rate should be at least 110 Mbps with a 10 m separation between the transmitter and the receiver, and

parameter	requirements
bit rate	110 and 200 Mbps
range	10 and 4 m
power consumption	100 and 250 mW
bit error rate	10^{-5}
colocated piconets	4
co-existence capability	reduced interference to IEEE systems

Table 1.1: Summary of the IEEE 802.15.3a requirements

200 Mbps with a 4 m separation. Since the transmitted power is strictly limited but wide bandwidth is available, UWB is suitable for a short range, high rate system such as a personal area network (PAN). Table 1.1 summarizes other technical requirements given in [38] and [39].

The FCC definition of UWB opened many possibilities for system design. It can be utilized with typical narrow time duration pulse baseband impulse radio [6]. These signals can be Gaussian shaped pulses, their derivatives, and others [31], [32]. Recently, there emerged a use of the technology that employs multiple bands each occupying at least 500 MHz bandwidth. In addition to above two schemes, UWB in a MIMO system and other hybrid schemes are also under study [39].

1.6.2 Application

Since UWB utilizes unlicensed spectrum with wide bandwidth, there is a large number of possible applications, such as positioning, secured transmission, and high rate data communications [33].

First, the very short UWB pulse causes multipath terms to be detected with high resolution [36]. This enables very accurate positioning. A few examples will be in building object tracking, wall penetrating positioning in a hazardous environment, and fine positioning for medical purposes [33]. Besides, geolocation [34] devices are also being developed.

Second, UWB can be used for a high security transmission system. It is the

military which was initially interested in UWB technology due to its potential for security. When operated with low power and short pulses (probably with a hopping scheme), it would be extremely difficult to intercept transmitted signals unless a receiver has the exact timing information.

Lastly, a high data rate indoor communication system has recently become an important area for UWB technology. It can provide a cheap and low power receiver at a high data rate for PAN systems. From an optimistic point of view, it will be able to supplant most present-day indoor wired and wireless communication systems. For example, a DVD player, a TV, a monitor, a computer, and all other peripherals can interconnect via UWB, eliminating most data wires. In this thesis, we consider a high rate (over 110 Mbps), indoor wireless communication system.

1.6.3 Modulation Schemes

In [39], several modulation schemes are mentioned, which have been used for UWB such as on-off keying (OOK), pulse position modulation (PPM), M-ary pulse amplitude modulation (M-PAM), and binary phase-shift keying (BPSK). Fig. 1.2 illustrates various modulation schemes applicable to UWB.

In Fig. 1.2, (a) OOK is based on the natural characteristics of UWB that transmits a pulse "on" for one and "off" for zero. (b) PPM changes the position of a pulse in time with respect to the reference position, so it requires accurate timing devices. (c) PAM changes the amplitude of a pulse. For higher order M-PAM, it may look attractive for a high data rate system, however it is mentioned in [36] that using higher order M-PAM does not necessarily improve the throughput as much as using BPSK (or 2-PAM) with a higher pulse repetition frequency (PRF). This is because M-PAM is generally not a power efficient scheme but a spectrum efficient scheme, while UWB is power constrained technology. Orthogonal modulation schemes are also good candidates because of their power efficient nature. The performance of different modulation schemes in the presence of jamming are compared in [40] and

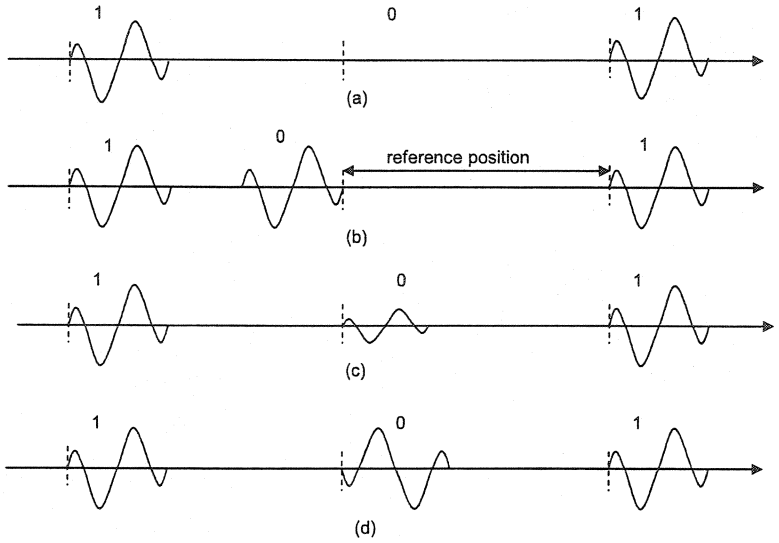

Figure 1.2: Various UWB modulation schemes: (a) OOK, (b) PPM, (c) PAM, (d) BPSK

BPSK (or 2-PAM) is turned out to be one of the good schemes. In this thesis we employ BPSK baseband modulation, in which the information bit is encoded with the polarity of a rectangular pulse.

1.6.4 Multiple Access Schemes

Although multiple access is not considered in this thesis, we briefly mention general multiple access schemes for UWB. In order to make a number of users communicate simultaneously, UWB systems should employ a multiplexing scheme such as time division multiplexing (TDM) or code division multiplexing (CDM).

TDM is readily used in conjunction with TH and PPM [6] - [8] since the nature of the short period signal permits enough room in time to use TDM. While the TH-PPM is well suited for TDM, DSSS based CDM has also been studied [9], [10]. Soon after UWB technology was defined by the FCC [35], another multiple access scheme, frequency division multiplexing (FDM), was added to the list of possible multiple access schemes. Orthogonal Frequency Division Multiplexing (OFDM) has been studied since the definition of UWB by the FCC [13] – [15]. In addition to the

multiple access schemes stated above, some hybrid forms of two or more schemes are also possible [39]. The CH-DSSS scheme needs CDM for multiple access, but we only consider a single user communication system in this thesis.

1.6.5 Singleband and Multiband

One of the major additions in the direction of UWB design could be the multiband scheme. Hence, singleband and multiband will be briefly compared. A singleband scheme is the conventional approach that uses the very short period impulse like signal that occupies the entire permitted bandwidth. This scheme can provide low cost devices especially for the system at a moderate data rate. However for a very high rate system with up to 480 Mbps, it requires a correspondingly high rate, costly, analog to digital converter (ADC) and accurate timing devices [36]. Moreover, if there is the interference of a narrow-band system, we may need an additional device to avoid it.

On the other hand, according to the UWB definition [35], the total bandwidth can be divided into maximum of 15 sub-bands each with 500 MHz bandwidth. This can ease some of the issues that can occur in the singleband scheme. Since the multiband scheme uses a relatively low rate for each subband, the ADC and the timing devices can be less accurate. It decreases the number of resolvable multipath terms causing less ISI, but may also cause deep fading since more multipath terms will be combined within the minimum resolution time. Besides, the multiband scheme can intentionally avoid using a certain band if other narrowband systems use the same band in the proximity of the UWB system. Furthermore, with the use of frequency hopping, the probability of collision with adjacent uncoordinated systems can be reduced [26]. At this point, the multiband scheme seems to be gaining more interest for the above reasons. However there are some drawbacks as well such as the complexity issue that is raised by multi-carrier and frequency hopping schemes.

In this thesis, CH-DSSS in the singleband system is considered, but CH-DSSS can

also be used in the multiband system, since the bandwidth of each subband is still wide enough to incorporate DSSS, OFDM, or coded modulation [36].

1.7 Channel Model

Due to the large bandwidth allocated for UWB, measuring the characteristics of the UWB channel can be a challenging task. It is observed in [1] that in an indoor environment, the excess delay of arriving multipath components can span up to 220 ns. Another interesting feature found in [1] is that the arriving multipath components tend to form clusters in an indoor environment. In this section, we list some of the proposed channel models for UWB and choose one model which will be used for the performance analysis in this thesis.

1.7.1 Various Channel Models

In order to study indoor channel models, it would be desirable to start with [1], which covers a variety of channel measurements in an indoor environment. Although it gives valuable information on the indoor channel, it does not fully cover the characteristics of the UWB channel since the sounding pulse used in the measurement has relatively small bandwidth compared to that of UWB. In 2002, Rusch et al. with Intel Corp. measured a residential indoor channel with the frequency spectrum of 2-8 GHz [43]. It seems this is the best channel measurement for UWB so far reported.

To establish a good channel model, many research groups have proposed various models for the UWB application. In [42] several channel models are compared to the channel measurement from [43] to find the best model. Some of the models compared are the Saleh-Valenzuela(S-V) model [1], the $\Delta - K$ model [44], and the Intel model [42]. It is stated in [36] that the IEEE 802.15.3a channel modelling task group adopted the Intel model [42] for the UWB channel which is based on the S-V model [1] except that the magnitude gain of a multipath ray has the lognormal, rather than the Rayleigh distribution.

1.7.2 Background; Multipath Channel Parameters

Before we further state the characteristics of the Intel channel model, we briefly clarify some of the multipath channel parameters that are used in this model. Multipath channel parameters are well explained in [46].

If we assume the discrete time channel impulse response is time invariant or wide sense stationary, then it can be expressed as

$$h_c(\tau) = \sum_{l=0}^{L-1} c_l \delta(\tau - \tau_l), \tag{1.1}$$

where L is the number of arriving multipaths, and $c_l = \alpha_l e^{j\phi_l}$ is the complex multipath ray gain with positive, real magnitude, α_l, and uniform random phase, ϕ_l, in $[0, 2\pi)$. The excess delay of the l-th path is the relative delay of the l-th arriving path compared to the first arriving path, $\tau_l - \tau_0$. If we ignore propagation delay, we can set $\tau_0 = 0$. Then the excess delay of the l-th path is the same as τ_l.

The power delay profile can be obtained by spatially averaging $|h_c(\tau)|^2$ over a local area and is given by

$$P(\tau) = k|h_c(\tau)|^2, \tag{1.2}$$

where k is an adjustment factor. The mean excess delay is the first moment of the power delay profile and is defined to be

$$\bar{\tau} = \frac{\sum_k \alpha_k^2 \tau_k}{\sum_k \alpha_k^2} \tag{1.3}$$

$$= \frac{\sum_k P(\tau_k)\tau_k}{\sum_k P(\tau_k)}. \tag{1.4}$$

The root mean square (RMS) delay spread is the square root of the second central moment of the power delay profile and is defined to be

$$\sigma_\tau = \sqrt{\bar{\tau^2} - (\bar{\tau})^2}, \tag{1.5}$$

where

$$\bar{\tau^2} = \frac{\sum_k \alpha_k^2 \tau_k^2}{\sum_k \alpha_k^2} \tag{1.6}$$

$$= \frac{\sum_k P(\tau_k)\tau_k^2}{\sum_k P(\tau_k)}. \tag{1.7}$$

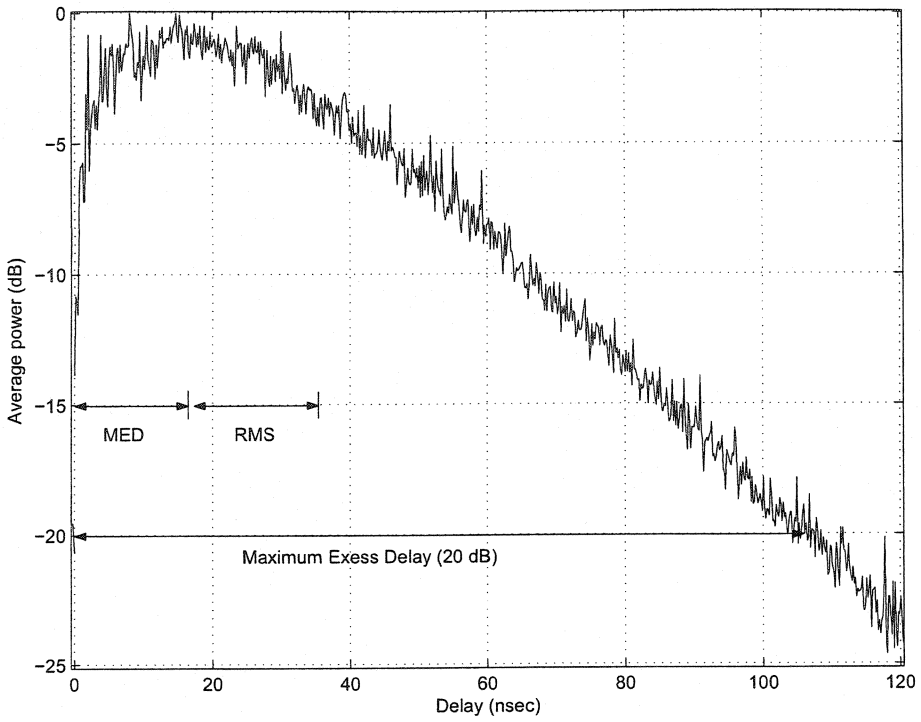

Figure 1.3: The power delay profile of the Non-Line of Sight UWB channel.

The maximum excess delay (X dB) is defined as the excess delay from which the power delay profile starts to fall less than X dB of the strongest path, and can be denoted as

$$\tau_{X_{dB}} - \tau_0.$$

Note that the strongest path does not necessarily arrive at τ_0. Fig. 1.3 shows the example of the power delay profile of the UWB channel obtained from the Intel channel model with the non-line of sight channel parameters in [42].

1.7.3 Intel Channel Model

In this subsection, we describe the Intel channel model in [42]. Intel Corp. proposed a UWB channel model based on the Saleh-Valenzuela (S-V) model [1] except that the lognormal distribution is adopted for the magnitude of arriving multipath rays.

According to the S-V model, the discrete time channel impulse response is given by

$$h(t) = \sum_{l=0}^{L} \sum_{k=0}^{K'} c_{k,\,l}\,\delta(t - T_l - \tau_{k,\,l}), \tag{1.8}$$

where T_l is the excess delay of the l-th cluster, and $\tau_{k,\,l}$ represents the excess delay of the k-th multipath ray relative to the l-th cluster arrival time, T_l. By definition, $\tau_{0,l} = 0$. Also,

$$c_{k,\,l} = p_{k,\,l}\beta_{k,\,l} \tag{1.9}$$

is the channel gain coefficient. $p_{k,\,l} \in \{+1, -1\}$ is the equiprobable random variable that represents the real part of the phase term, which is analogous to $e^{j\phi_{k,\,l}}$ for a complex channel. However, for a BPSK modulation scheme, both models perform the same since only the real part is considered in the demodulation. $\beta_{k,\,l}$ in (1.9) is a lognormally distributed random variable with mean $\mu_{k,\,l}$ and variance σ^2, and is given by

$$\beta_{k,\,l} = 10^{n/20}, \tag{1.10}$$

where n has the normal distribution with mean $\mu_{k,l}$ and variance σ^2, $n \sim N(\mu_{k,\,l}, \sigma^2)$, or equivalently

$$n = 20log_{10}(\beta_{k,\,l}). \tag{1.11}$$

The mean value of n for the k-th ray in the l-th cluster is given by

$$\mu_{k,l} = \frac{10\ln\Omega_0 - 10T_l/\Gamma - 10\tau_{k,\,l}/\gamma}{\ln 10} - \frac{\sigma^2 \ln 10}{20}, \tag{1.12}$$

where Γ and γ are a cluster decay factor and a ray decay factor, respectively. The standard deviation of the lognormal fading term, σ, is empirically found to be 4.8 dB [42]. Moreover, the second moment of $\beta_{k,\,l}$ is given by

$$E[\beta_{k,\,l}^2] = \Omega_0 e^{-T_l/\Gamma} e^{-\tau_{k,\,l}/\gamma}, \tag{1.13}$$

where Ω_0 is the mean power of the first ray of the first cluster. We first set $\Omega_0 = 1$, and generate a channel impulse response. Then the total energy of the channel impulse

response is normalized to one,

$$\sum_{l=0}^{L}\sum_{k=0}^{K}|c_{k,\,l}|^2 = 1. \tag{1.14}$$

Let Λ and λ denote an inter-cluster arrival rate and an inter-ray arrival rate, respectively. Then, the inter-cluster arrival time and the inter-ray arrival time are exponentially distributed and their probability density functions (pdf) can be given as,

$$p(T_l|T_{l-1}) = \Lambda e^{-\Lambda(T_l - T_{(l-1)})}, \qquad l > 0, \Lambda > 0 \tag{1.15}$$

$$p(\tau_{k,\,l}|\tau_{(k-1),\,l}) = \lambda e^{-\lambda(\tau_{k,\,l} - \tau_{(k-1),\,l})}, \qquad k > 0, \lambda > 0, \tag{1.16}$$

respectively. The pdf's in (1.15) and (1.16) are equal to zero for $\Lambda, \lambda \leq 0$.

Even though the delays (inter-arrival time) in (1.15) and (1.16) are continuous random variables, the Intel model [42] quantizes it to the nearest chip period. In our study, the delay is quantized to be a multiple of the chip period in a CH-DSSS system.

1.7.4 Realization of the Intel channel model

Using the Intel channel model described above, we generate three types of UWB channels with different parameters. In the generation of the channels, the minimum resolvable path duration is set to be 167 psec which is the same duration used in the channel measurement in [43]. Fig. 1.4 shows the sample impulse response of the line of sight one (LOS1) channel. Table 1.2 shows the parameters used to generate the UWB channels. It is clearly seen in Fig. 1.4 that the arriving paths are clustered. If we use the length 15 spreading code with chip pulse duration of 167 psec, the symbol period will be 2.505 ns. For a BPSK modulation, the corresponding bit rate will be 399.2 Mbps. Note that the maximum excess delay is much longer than the symbol period, which will cause ISI. Fig. 1.5 shows another type of the line of sight (LOS2) channel with different parameters, and Fig. 1.6 shows the realization of the non-line of sight one (NLOS1) channel with the parameters shown in Table 1.2. These

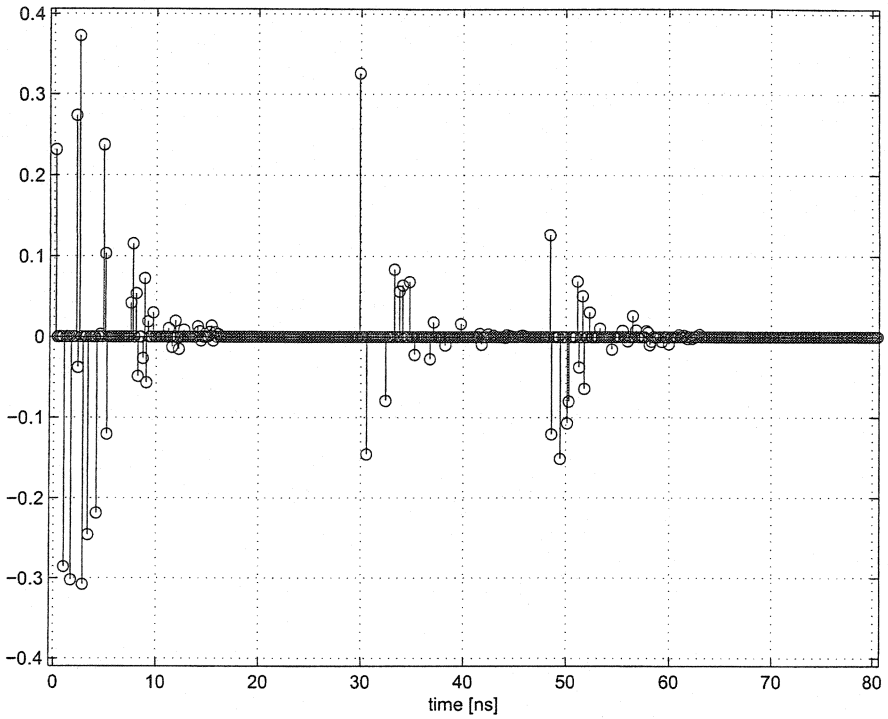

Figure 1.4: The sample realization of the line of sight 1 (LOS1) UWB channel.

parameters are taken from [42]. As expected, the NLOS1 channel in Fig. 1.6 has far more multipath terms than those of the LOS channels in Fig. 1.4 and Fig. 1.5.

channel parameters	**LOS1**	**LOS2**	**NLOS1**
Λ $[1/nsec]$	1/60	1/22	1/11
λ $[1/nsec]$	1/0.5	1/0.94	1/0.35
Γ	16	7.6	16
γ	1.6	0.94	8.5
σ $[dB]$	4.8	4.8	4.8

Table 1.2: UWB channel parameters for LOS1, LOS2, and NLOS1 channels

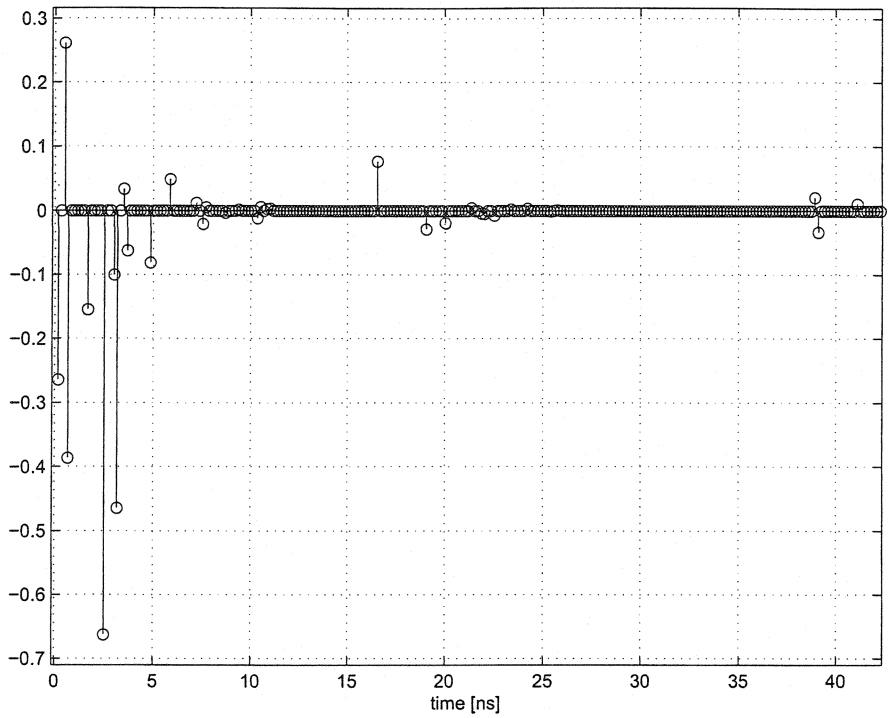

Figure 1.5: The sample realization of the line of sight 2 (LOS2) UWB channel.

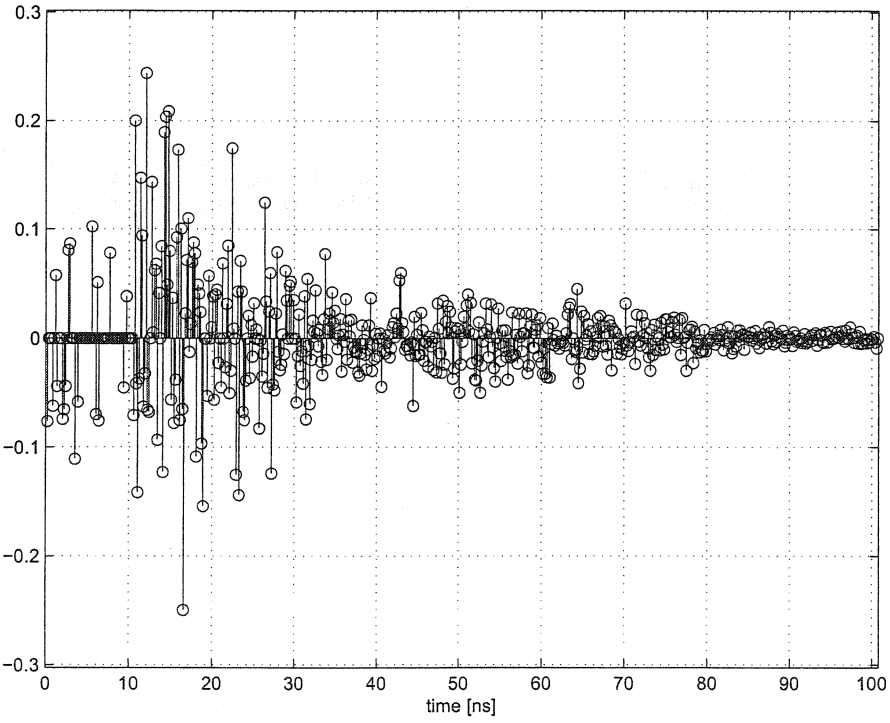

Figure 1.6: The sample realization of the non-line of sight 1 (NLOS1) UWB channel.

1.8 Code Hopping-Direct Sequence Spread Spectrum (CH-DSSS)

1.8.1 Introduction

DSSS systems have been widely studied in recent years due to their features to compensate for jamming, fading, and to prevent eavesdropping. It would be ideal if the spreading sequence had perfect correlation properties in order to minimize the BER of a DSSS system [47]. Many research groups are working to develop the spreading sequence with good correlation properties. However in practice, such an ideal spreading sequence is hard to find.

In a DSSS system, the spreading sequence can be categorized into a long code and a short code. In the long code system, the period of the spreading sequence is generally longer than the symbol period, and the correlation value between users is different from bit to bit [20]. It causes multiple access interference to look random in time, and the average performance of each user becomes similar to each other [20]. In the short code system, on the other hand, the period of the spreading sequence is generally equal to the symbol period. In such a case, the cross-correlation value between users is not changing in time. Therefore, it is possible for some users to have bad performance in a certain environment for a long period of time. This performance variability is reported in [20], [21]. However it is stated in [20] that the short code is preferred for interference suppression and cancellation due to its cyclostationary correlation property that often leads to the low complexity of a system.

In addition to the performance variability between users, similar phenomenon can also occur for a single user system in the channel that causes ISI. It is shown in [22] that there exists a spreading sequence that performs better than the others in a frequency selective fading or a doubly selective fading channel. One of the goals in [22] was to find the robust sequence that performs well in the doubly selective fading channel.

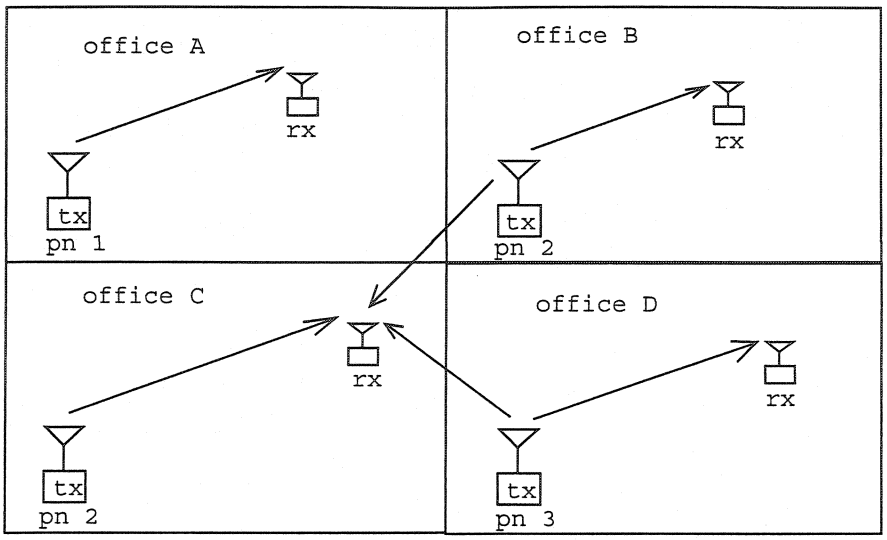

Figure 1.7: Code interference from uncoordinated UWB systems

If a channel is slowly changing in time, the channel parameters can be considered constant for a certain period of time. If a receiver with the assigned code encounters a bad channel, it will experience bad performance until the channel changes. One possible action for the user would be to move out of the bad channel.

Because of the different auto-correlation function of each spreading code, the performance variability can also occur among users with different codes for a multipath fading channel, especially when the maximum excess delay is longer than the symbol period.

CH can be considered as a part of the DSSS scheme in a short code system in which each user changes the spreading sequence in a predetermined way or randomly. Hence, CH makes a short code look like a long code in the sense that the period of the total spreading sequence is longer than the symbol period [30].

1.8.2 Advantages of Code Hopping

There are several advantages that can be obtained by the CH scheme. First, CH can reduce code interference from uncoordinated systems [26], as can also be done by the frequency hopping system with multiband UWB schemes. Since the spreading

sequence is a limited resource, it is possible that a neighboring system may use the same spreading sequence as shown in Fig. 1.7. In this scenario, the receiver in the office C with the spreading sequence 2 (pn 2) gets interfering signals from other offices. The interference from the office D with the spreading sequence 3 (pn 3) may be negligible since each system has different spreading sequences. However, the interference from the office B with spreading sequence 2 (pn 2) could cause a big degradation in performance due to the same spreading sequence in use. Therefore, both users in the office B and the office C will constantly experience severe interference. However, if CH is used in this situation, the probability of using same sequence in the adjacent system will be much reduced [26].

Second, CH can reduce the performance variability of a short code system in a multiuser environment [20]. By sharing the spreading sequences with CH, each user can have average performance [23]. Furthermore, sharing the spreading sequences can also improve outage probability [23] because the correlation property of the spreading sequence is one of the main causes of the uplink interference of a mobile in a cellular Synchronous CDMA (S-CDMA) system. Using CH can improve the performance of the worst case situation by averaging it over the spreading sequences.

Third, if used with an orthogonal code, CH can accommodate more channels than the number of codes available [50]. Many downlink CDMA systems, such as IS-95, CDMA 2000, and WCDMA, adopt the orthogonal code since it can effectively cancel interference [50]. By using orthogonal CH multiplexing in [50], an increase was observed in the number of allocatable downlink channels. Moreover, in the uplink S-CDMA system, the capacity improvement by CH was also observed in [24].

In addition to the advantages of CH described above, it can also be used to compensate for ISI. In a conventional DSSS system, the periodic auto-correlation of the spreading sequence suppresses both self interference (SI) and ISI. Therefore it would be desirable to use the spreading sequence with a good periodic auto-correlation property. There are some spreading sequences with good auto-correlation properties,

such as maximal-length sequences [56], ternary sequences [49], and multi-valued sequences [50]. However the maximal-length sequences and the ternary sequences have a limited number of sequences and the multi-valued sequences induce complexity in implementation.

Furthermore, even an ideal sequence is not good enough to deal with a certain type of ISI. If arriving multipath component has the excess delay at a multiple of symbol period, $\tau = kT$, then there occurs a big ISI term even with the ideal spreading sequence. On the other hand, if CH is used with an orthogonal code, most ISI terms with the excess delay at $\tau = kT$ can be removed. This is due to the fact that the ISI terms occur as both cross-correlation and auto-correlation functions in a CH system, and the cross-correlation values at multiples of the symbol period are all zero. Then the impact of such ISI terms will be nearly removed in a CH system.

1.8.3 Disadvantage of Code Hopping

Although CH can offer several advantages, it also has a drawback. Most asynchronous spreading sequences, such as Gold sequences and maximal-length sequences are designed to have good "periodic" correlation properties [48]. Therefore, these sequences may perform best when the correlation functions of interference terms are periodic. Such a periodic auto-correlation function occurs with a conventional DSSS system with a single code. In the conventional DSSS system, the periodic auto-correlation of the spreading sequence tries to compensate for ISI.

Fig. 1.8 illustrates the brief example of the interference term with a Rake receiver. Assume the transmitted bit b_0 with the spreading sequence a_0 is to be detected and there are two arriving paths with channel gains c_1 and c_2. Then with the DSSS system, the signal term of the received signal to be detected, y_{s_1}, at the first Rake

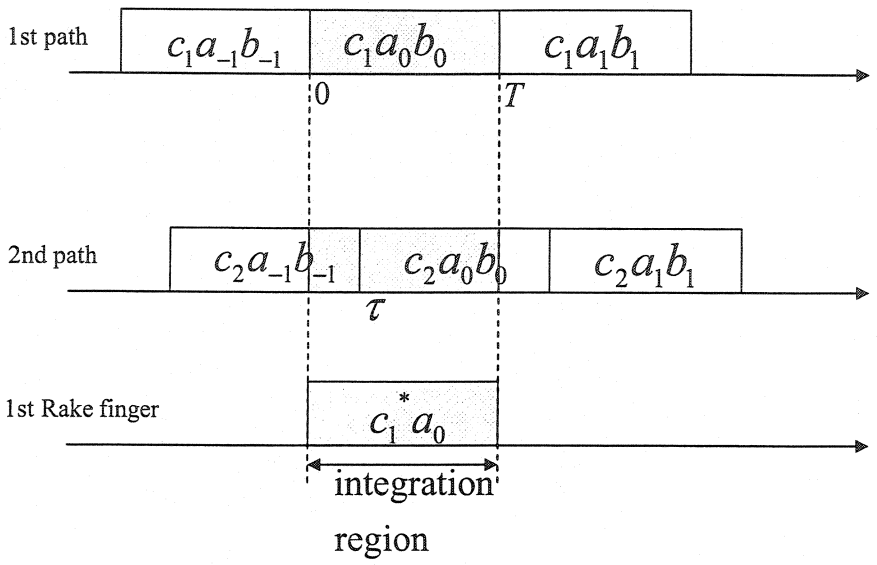

Figure 1.8: Interference terms in the Rake receiver

finger output after correlating c_1^* and a_0 will be given as,

$$\begin{aligned} y_{s_1} &= \{c_1a_0b_0 + c_2(a_{-1}b_{-1} + a_0b_0)\}c_1^*a_0^* \\ &= |c_1|^2b_0 + c_1^*c_2\{R_{-1,\,0}(\tau - T)b_{-1} + R_{0,\,0}(\tau)b_0\} \\ &= |c_1|^2b_0 + c_1^*c_2R_{0,\,0}(\tau)b_0 + c_1^*c_2R_{-1,\,0}(\tau - T)b_{-1}, \end{aligned} \tag{1.17}$$

where $R_{k,\,m}(\cdot)$ is the partial cross-correlation function of the spreading sequence between a_k and a_m. In the last line of (1.17), the first, the second, and the third term represent the desired signal, the SI, and the ISI, respectively. The SI term is the interference coming from the desired bit to be detected, and the ISI term is the interference coming from other bits than the desired bit to be detected. Note that in a conventional DSSS system, the spreading sequence is the same for each bit ($a_{-1} = a_0$). Then the second and the third term in (1.17) can be combined to form a periodic auto-correlation function if $b_{-1} = b_0$, and (1.17) can be given by

$$y_{s_1} = |c_1|^2b_0 + c_1^*c_2(R_{0,\,0}(\tau) + R_{0,\,0}(\tau - T))b_0. \tag{1.18}$$

However, if CH is used, all the interference terms in the DSSS system turn into

partial cross-correlation functions. Therefore, some good properties of the well known spreading sequences can be lost by CH. Thus, in order for CH to effectively suppress ISI, a CH pattern needs to be carefully designed.

1.9 Spreading Sequences

We describe some of the preferred conditions to choose spreading sequences for CH to compensate for ISI and select one class of asynchronous sequences and one class of synchronous sequences for our study.

1.9.1 Preferred Conditions of the Spreading Sequence for Code Hopping

In order to make CH effective, there are some preferences when selecting the class of spreading sequences.

First, the number of available spreading sequences for CH should be large enough to offer diversity in choosing hopping patterns. If the number of spreading sequences is too small, it will be relatively harder to find a good hopping pattern. However as the number of the spreading sequences is increasing for each user, the CH pattern search time may also increase.

Second, as mentioned earlier, among the correlation properties of the spreading sequences, the partial correlation property is more important than the periodic correlation property. Hence, the well known spreading sequences designed for the good periodic correlation property may not necessarily be the best choice for CH.

In addition, when the UWB system is to support a high data rate, the length of the spreading sequence should not be too long.

Considering the conditions mentioned above, we choose Gold-like (GL) and Gold sequences with length 15 and 31, respectively for an asynchronous system, and select Walsh-Hadamard (WH) sequences with length 16 and 32 for a synchronous system.

No.	GL sequence
1	0 1 1 1 1 0 1 0 1 1 0 0 1 0 0
2	0 0 0 0 0 0 0 1 0 0 0 1 0 1 1
3	1 1 0 0 0 1 1 1 0 0 1 0 0 1 1
4	1 0 1 0 0 1 0 0 0 0 1 1 1 1 1
5	1 0 0 1 0 1 0 1 1 0 1 1 0 0 1
6	1 0 0 0 1 1 0 1 0 1 1 1 0 1 0
7	0 0 0 1 1 0 0 1 1 1 0 1 0 0 0
8	0 1 0 0 1 0 1 1 0 1 0 0 0 1 0
9	0 1 1 0 0 0 1 0 0 0 0 0 0 1 1
10	1 1 1 1 0 1 1 0 1 0 1 0 1 0 1
11	1 0 1 1 1 1 1 0 0 1 1 1 1 1 0
12	0 1 0 1 0 0 1 1 1 0 0 0 0 0 1
13	1 1 1 0 1 1 1 0 0 1 1 0 1 1 0
14	0 0 1 1 0 0 0 0 1 0 0 1 1 0 1
15	1 1 0 1 1 1 1 1 1 1 1 1 0 0 0
16	0 0 1 0 1 0 0 0 0 1 0 1 1 1 0

Table 1.3: Gold-like (GL) sequences with length 15

1.9.2 Gold and Gold-like Sequences

The Gold sequence [51], [52] can be generated by sum of the two distinct maximal-length sequences with same period, called the preferred pair. If there is a binary maximal-length sequence, $\mathbf{a}$, with length $N = 2^m - 1$, where m is a positive integer, then the preferred pair, $\mathbf{a}'$, can be generated by sampling every q-th element of $\mathbf{a}$ with cyclic shift, and is denoted as $\mathbf{a}' = \mathbf{a}[q]$. It can be shown that if and only if the greatest common devisor of N and q is 1, $gcd(N, q) = 1$, the sequence $\mathbf{a}'$ is also a maximal-length sequence with period N [53].

However, there is no preferred pair of maximal-length sequences if $m \equiv 0 \ (mod\ 4)$, hence no Gold sequence of length 15. Instead, we can generate the Gold-like (GL) sequence of length 15 which is also well known and has similar properties to the Gold sequence [54] - [57].

The GL and the Gold sequences of length 15 and 31, are listed in Table 1.3 and Table 1.4, respectively, which will be used in Chapter 4.

No.	GL sequence
1	0 1 1 0 1 0 0 1 0 0 0 0 1 0 1 0 1 1 1 0 1 1 0 0 0 1 1 1 1 1 0
2	0 0 1 1 0 1 1 1 0 1 0 1 0 0 0 0 1 0 0 1 0 1 1 0 0 1 1 1 1 1 0
3	0 0 0 0 0 1 1 1 1 0 1 0 1 0 1 1 1 1 0 0 0 0 0 0 1 0 0 0 0 1 0
4	1 0 1 1 0 1 0 0 0 1 0 0 1 0 0 0 1 0 1 1 0 1 0 1 1 0 0 0 1 1 0
5	1 1 0 1 0 0 1 1 1 0 0 0 1 1 1 0 0 1 0 1 1 1 1 1 1 0 0 1 1 1 1
6	0 0 0 1 1 1 0 0 0 0 0 0 0 0 1 1 1 0 0 0 1 0 1 1 1 0 1 1 1 0 1
7	1 0 0 0 0 0 1 1 0 0 0 1 1 0 0 0 0 0 0 1 0 0 0 1 1 1 1 1 1 0 0 0
8	1 0 1 1 1 1 0 1 0 0 1 0 1 1 1 1 0 1 1 1 0 0 1 1 0 1 1 0 0 1 1
9	1 1 0 0 0 0 0 1 0 1 0 0 0 0 0 1 1 1 0 1 0 0 1 0 0 1 0 0 1 0 1
10	0 0 1 1 1 0 0 1 1 0 0 1 1 1 0 0 1 0 0 1 0 0 0 0 0 0 0 1 0 0 1
11	1 1 0 0 1 0 0 0 0 0 1 0 0 1 1 0 0 0 0 1 0 1 0 0 1 0 1 0 0 0 0
12	0 0 1 0 1 0 1 1 0 1 0 1 0 0 1 1 0 0 0 1 1 1 0 1 1 1 0 0 0 1 1
13	1 1 1 0 1 1 0 1 1 0 1 1 1 0 0 1 0 0 0 0 1 1 1 1 0 0 0 0 1 0 0
14	0 1 1 0 0 0 0 0 0 1 1 0 1 1 0 1 0 0 1 0 1 0 1 0 1 0 0 1 0 1 1
15	0 1 1 1 1 0 1 1 1 1 0 0 0 1 0 1 0 1 1 0 0 0 0 1 1 0 1 0 1 0 0
16	0 1 0 0 1 1 0 0 1 0 0 1 0 1 0 1 1 1 1 1 1 0 1 1 1 1 1 0 1 0 1 0
17	0 0 1 0 0 0 1 0 0 0 1 1 0 1 0 0 1 1 0 1 1 0 1 1 0 0 1 0 1 1 0
18	1 1 1 1 1 1 1 1 1 0 1 1 1 0 1 1 0 1 0 0 0 0 0 1 0 1 1 0 1 1 1 0
19	0 1 0 0 0 1 0 1 1 1 1 1 1 0 0 1 0 0 0 1 1 0 0 0 1 0 0 1 1 1 1 1
20	0 0 1 1 0 0 0 0 1 1 1 1 1 0 1 1 0 1 0 1 0 1 1 0 1 1 1 1 1 0 0
21	1 1 0 1 1 0 1 0 1 1 1 0 1 0 0 1 1 0 0 1 1 0 0 1 0 1 1 1 0 1 0
22	0 0 0 0 1 1 1 0 1 1 0 0 1 1 0 0 0 0 0 0 0 1 1 0 0 1 1 0 1 1 1
23	1 0 1 0 0 1 1 0 1 0 0 0 0 1 1 1 0 0 1 1 1 0 0 0 0 1 0 1 1 0 0
24	1 1 1 1 0 1 1 0 0 0 0 1 0 0 0 1 0 1 0 0 0 1 0 0 0 0 1 1 0 1 1
25	0 1 0 1 0 1 1 1 0 0 1 1 1 1 0 1 1 0 1 1 1 1 0 0 1 1 1 0 1 0 1
26	0 0 0 1 0 1 0 1 0 1 1 0 0 1 0 0 0 1 0 0 1 1 0 1 0 1 0 1 0 0 0
27	1 0 0 1 0 0 0 1 1 1 0 1 0 1 1 1 1 0 1 0 1 1 1 0 0 0 1 0 0 1 0
28	1 0 0 1 1 0 0 0 1 0 1 1 0 0 0 0 0 1 1 0 1 0 0 0 1 1 0 0 1 1 1
29	1 0 0 0 1 0 1 0 0 1 1 1 1 1 1 1 1 1 1 1 0 0 1 0 1 0 0 0 1 1 0 1
30	1 0 1 0 1 1 1 1 1 1 1 0 0 0 0 0 1 1 1 1 1 1 1 0 1 0 1 1 0 0 1
31	1 1 1 0 0 1 0 0 1 1 0 1 1 1 1 0 1 1 0 0 1 0 0 1 1 1 1 0 0 0 1
32	0 1 1 1 0 0 1 0 1 0 1 0 0 0 1 0 1 0 1 0 0 1 1 1 0 1 0 0 0 0 1
33	0 1 0 1 1 1 1 0 0 1 0 1 1 0 1 0 0 1 1 1 1 0 1 0 0 0 0 0 0 0 0

Table 1.4: Gold sequences with length 31

1.9.3 Walsh-Hadamard Sequences

The Walsh-Hadamard (WH) sequence is often used to improve the bandwidth efficiency of a DSSS system [56]. One way to generate the WH sequence with block length $N = 2^n$, where n is a positive integer, is to use a Hadamard matrix with recursive procedures [56], which is given by

$$\begin{aligned} H_1 &= [0], \\ H_2 &= \begin{bmatrix} H_1 & H_1 \\ H_1 & \bar{H}_1 \end{bmatrix}, \\ H_{2N} &= \begin{bmatrix} H_N & H_N \\ H_N & \bar{H}_N \end{bmatrix}, \end{aligned}$$

where N is the power of two and $\bar{H}_N$ is the binary complement of the elements in H_N. Since the auto-correlation values of the WH sequences are generally worse than the cross-correlation values, it may not be appropriate to use the WH sequence for the DSSS system for a channel with ISI. However in the CH-DSSS system, since the ISI terms occur as both cross-correlation and auto-correlation functions, CH-DSSS will perform better than DSSS with the WH sequence, as will be shown in the Chapter 4. In addition, we don't lose the orthogonality of the WH sequence by using CH. Table 1.5 and Table 1.6 list the WH sequences with length 16 and 32, respectively, which will be used in Chapter 4.

No.	WH sequence
1	1 1 1 1 1 1 1 1 1 1 1 1 1 1 1 1
2	1 0 1 0 1 0 1 0 1 0 1 0 1 0 1 0
3	1 1 0 0 1 1 0 0 1 1 0 0 1 1 0 0
4	1 0 0 1 1 0 0 1 1 0 0 1 1 0 0 1
5	1 1 1 1 0 0 0 0 1 1 1 1 0 0 0 0
6	1 0 1 0 0 1 0 1 1 0 1 0 0 1 0 1
7	1 1 0 0 0 0 1 1 1 1 0 0 0 0 1 1
8	1 0 0 1 0 1 1 0 1 0 0 1 0 1 1 0
9	1 1 1 1 1 1 1 1 0 0 0 0 0 0 0 0
10	1 0 1 0 1 0 1 0 0 1 0 1 0 1 0 1
11	1 1 0 0 1 1 0 0 0 0 1 1 0 0 1 1
12	1 0 0 1 1 0 0 1 0 1 1 0 0 1 1 0
13	1 1 1 1 0 0 0 0 0 0 0 0 1 1 1 1
14	1 0 1 0 0 1 0 1 0 1 0 1 1 0 1 0
15	1 1 0 0 0 0 1 1 0 0 1 1 1 1 0 0
16	1 0 0 1 0 1 1 0 0 1 1 0 1 0 0 1

Table 1.5: WH sequences with length 16

No.	WH sequence
1	1 1 1 1 1 1 1 1 1 1 1 1 1 1 1 1 1 1 1 1 1 1 1 1 1 1 1 1
2	1 0 1 0 1 0 1 0 1 0 1 0 1 0 1 0 1 0 1 0 1 0 1 0 1 0 1 0
3	1 1 0 0 1 1 0 0 1 1 0 0 1 1 0 0 1 1 0 0 1 1 0 0 1 1 0 0
4	1 0 0 1 1 0 0 1 1 0 0 1 1 0 0 1 1 0 0 1 1 0 0 1 1 0 0 1
5	1 1 1 1 0 0 0 0 1 1 1 1 0 0 0 0 1 1 1 1 0 0 0 0 1 1 1 1 0 0 0 0
6	1 0 1 0 0 1 0 1 1 0 1 0 0 1 0 1 1 0 1 0 0 1 0 1 1 0 1 0 0 1 0 1
7	1 1 0 0 0 0 1 1 1 1 0 0 0 0 1 1 1 1 0 0 0 0 1 1 1 1 0 0 0 0 1 1
8	1 0 0 1 0 1 1 0 1 0 0 1 0 1 1 0 1 0 0 1 0 1 1 0 1 0 0 1 0 1 1 0
9	1 1 1 1 1 1 1 1 0 0 0 0 0 0 0 0 1 1 1 1 1 1 1 1 0 0 0 0 0 0 0 0
10	1 0 1 0 1 0 1 0 0 1 0 1 0 1 0 1 1 0 1 0 1 0 1 0 0 1 0 1 0 1 0 1
11	1 1 0 0 1 1 0 0 0 0 1 1 0 0 1 1 1 1 0 0 1 1 0 0 0 0 1 1 0 0 1 1
12	1 0 0 1 1 0 0 1 0 1 1 0 0 1 1 0 1 0 0 1 1 0 0 1 0 1 1 0 0 1 1 0
13	1 1 1 1 0 0 0 0 0 0 0 0 1 1 1 1 1 1 1 1 0 0 0 0 0 0 0 0 1 1 1 1
14	1 0 1 0 0 1 0 1 0 1 0 1 1 0 1 0 1 0 1 0 0 1 0 1 0 1 0 1 1 0 1 0
15	1 1 0 0 0 0 1 1 0 0 1 1 1 1 0 0 1 1 0 0 0 0 1 1 0 0 1 1 1 1 0 0
16	1 0 0 1 0 1 1 0 0 1 1 0 1 0 0 1 1 0 0 1 0 1 1 0 0 1 1 0 1 0 0 1
17	1 1 1 1 1 1 1 1 1 1 1 1 1 1 1 1 0 0 0 0 0 0 0 0 0 0 0 0 0 0 0 0
18	1 0 1 0 1 0 1 0 1 0 1 0 1 0 0 1 0 1 0 1 0 1 0 1 0 1 0 1 0 1 0 1
19	1 1 0 0 1 1 0 0 1 1 0 0 1 1 0 0 0 0 1 1 0 0 1 1 0 0 1 1 0 0 1 1
20	1 0 0 1 1 0 0 1 1 0 0 1 1 0 0 1 0 1 1 0 0 1 1 0 0 1 1 0 0 1 1 0
21	1 1 1 1 0 0 0 0 1 1 1 1 0 0 0 0 0 0 0 0 1 1 1 1 0 0 0 0 1 1 1 1
22	1 0 1 0 0 1 0 1 1 0 1 0 0 1 0 1 0 1 0 1 1 0 1 0 0 1 0 1 1 0 1 0
23	1 1 0 0 0 0 1 1 1 1 0 0 0 0 1 1 0 0 1 1 1 1 0 0 0 0 1 1 1 1 0 0
24	1 0 0 1 0 1 1 0 1 0 0 1 0 1 1 0 0 1 1 0 1 0 0 1 0 1 1 0 1 0 0 1
25	1 1 1 1 1 1 1 1 0 0 0 0 0 0 0 0 0 0 0 0 0 0 0 0 0 0 0 0 1 1 1 1 1 1 1 1
26	1 0 1 0 1 0 1 0 0 1 0 1 0 1 0 1 0 1 0 1 0 1 1 0 1 0 1 0 1 0
27	1 1 0 0 1 1 0 0 0 0 1 1 0 0 1 1 0 0 1 1 0 0 1 1 1 1 0 0 1 1 0 0
28	1 0 0 1 1 0 0 1 0 1 1 0 0 1 1 0 0 1 1 0 0 1 1 0 1 0 0 1 1 0 0 1
29	1 1 1 1 0 0 0 0 0 0 0 0 1 1 1 1 0 0 0 0 1 1 1 1 1 1 1 1 0 0 0 0
30	1 0 1 0 0 1 0 1 0 1 0 1 1 0 1 0 0 1 0 1 1 0 1 0 1 0 1 0 0 1 0 1
31	1 1 0 0 0 0 1 1 0 0 1 1 1 1 0 0 0 0 1 1 1 1 0 0 1 1 0 0 0 0 1 1
32	1 0 0 1 0 1 1 0 0 1 1 0 1 0 0 1 0 1 1 0 1 0 0 1 1 0 0 1 0 1 1 0

Table 1.6: WH sequences with length 32

Chapter 2

System Model and Error Probability

In this chapter, we describe a CH-DSSS system model and analyze the bit error probability for BPSK modulation. After the exact BER expression of the CH-DSSS system is derived, the Beaulieu Series Method (BSM) is applied to efficiently determine the error probability.

2.1 System Model

We consider a short spreading code, single user CH-DSSS baseband communication system. Fig. 2.1 illustrates the system model. We assume the channel is slowly changing in time, so it is constant at least for a block of data. We also assume the transmitter and the receiver have feedback in the system and CSI is perfectly estimated at the receiver. Then the estimated CSI is sent to the transmitter. At the transmitter, a proper CH pattern is assigned based on the CSI and the correlation functions of the spreading sequences. Then, binary data bits, $b_k \in \{1, -1\}$, are spread by the spreading sequence with CH, $a_k(t)$, and BPSK modulated. Because of CH, each spreading sequence used for each data bit, $a_k(t)$, is generally different from others and follows a pre-determined and periodic hopping pattern. The transmitted signal is fed into a multipath fading channel with the mean excess delay generally longer than a symbol period, and it causes ISI. Then the output of the channel and white

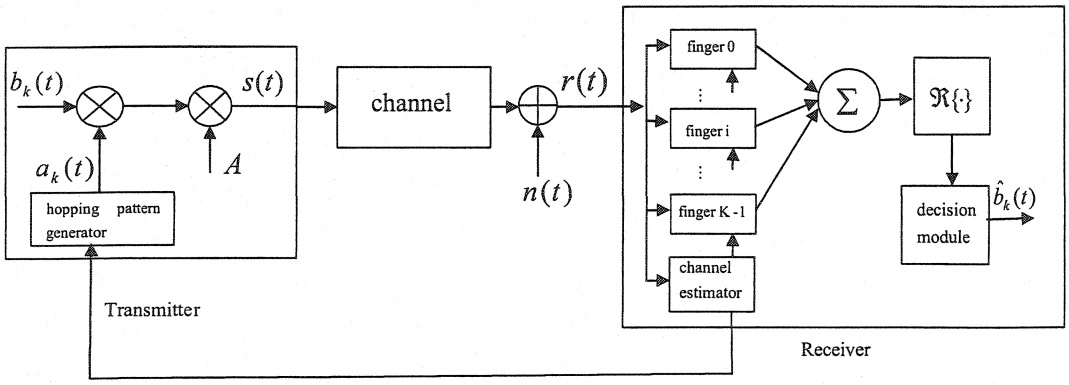

Figure 2.1: The system model of a CH-DSSS system

Gaussian noise (WGN), $n(t)$, are added at the receiver. At the receiver, the scattered received signal energy due to the multipath fading channel is collected with K Rake combiners followed by a hard decision detector.

The main application considered is to apply the CH-DSSS scheme to a UWB channel with ISI. The CH scheme is intended to compensate for ISI and an equalizer is not used in the receiver.

2.2 Main Assumptions

Below are the main assumptions on which the system model and the error probability analysis are based.

1. The channel is slowly changing in time and perfect knowledge of CSI is available for both the transmitter and the receiver. Thus there are no timing errors for chip and bit recovery in the coherent detection procedure used in the receiver.

2. Except for discrete multipath components, the transmitted signal is not distorted during transmission and the carrier is perfectly recovered at the receiver.

3. Data bits, $b_k \in \{1, -1\}$, are independent and identically distributed (i.i.d.) random variables.

4. The additive noise, $n(t)$, is zero mean complex white Gaussian random process.

5. The maximal ratio combining rule is used for the Rake receiver.

6. Each multipath delay and the data symbol period are at multiples of the chip period for the DSSS signal.

2.3 Transmitted Signal

In the system model shown in Fig. 2.1, the symbol period is denoted as T with $T = N_c T_c$, where N_c is the processing gain and T_c is the chip period. We also denote the data waveform as $b_k(t)$, and the CH spreading sequence for the k-th bit is denoted as $a_k(t)$. Moreover, $b_k(t)$ and $a_k(t)$ are assumed to be real. Then, the transmitted signal, $s(t)$, with CH can be represented as

$$s(t) = A \sum_{k=-\infty}^{\infty} b_k(t) a_k(t), \tag{2.1}$$

where A is the amplitude of the transmitted signal, and the data waveform, $b_k(t)$, is given as

$$b_k(t) = b_k P_T(t - kT). \tag{2.2}$$

In (2.2), $b_k \in \{-1, 1\}$ is the k-th information bit, and $P_T(t)$ stands for the rectangular pulse with unit height within [0,T) and zero elsewhere.

To further define the CH spreading sequence for the k-th bit, $a_k(t)$, in (2.1), let N_h denote the length of the hopping pattern. If we define $\{a'_0(t),\ a'_1(t),\ \cdots\ a'_{N_h-1}(t)\}$ as a hopping sequence selected from the total set of the spreading sequences shown in Fig. 2.2, then the CH spreading sequence for the k-th bit, $a_k(t)$, used in (2.1) can be expressed as

$$a_k(t) = a'_{M(k,\ N_h)}(t) = \sum_{i=kN_c}^{(k+1)N_c-1} a^i_{M(k,\ N_h)} P_{T_c}(t - iT_c), \tag{2.3}$$

where

$$M(k,\ N_h) \equiv k \pmod{N_h}. \tag{2.4}$$

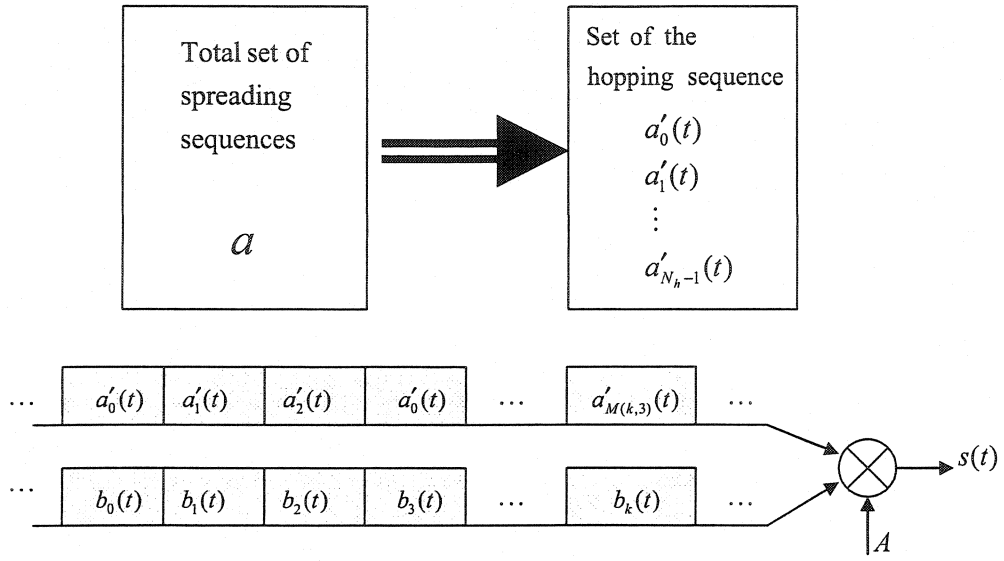

Figure 2.2: The example of the transmitted signal in a CH-DSSS system with $N_h = 3$

In (2.3), $a^i_{M(k,\ N_h)}$ is the i-th chip amplitude for the k-th spreading sequence which is taken from the $M(k,\ N_h)$-th hopping sequence. Fig. 2.2 illustrates the example of the transmitted signal with CH, assuming $N_h = 3$. Since we consider CH, the spreading sequence for the k-th bit is generally different from the spreading sequences for other bits ($a_k(t) \neq a_m(t)$). We will use a periodic hopping pattern with the period of N_h. Therefore the CH spreading sequence used in this system is a short code but acts like a long code in the sense that its period is longer than the symbol period [30].

2.4 Channel Impulse Response

The discrete time channel impulse response with L arriving paths can be modelled as

$$h_c(t) = \sum_{l=0}^{L-1} c_l \cdot \delta(t - \tau_l), \tag{2.5}$$

where $c_l = \alpha_l e^{j\phi_l}$ is the complex channel gain of the l-th arriving path with magnitude α_l and phase ϕ_l, and $\delta(\cdot)$ is the Dirac-delta function. In (2.5), τ_l is the excess delay of the l-th path referenced to τ_0 and it is an integer multiple of T_c. If we ignore propagation delay, we can set $\tau_0 = 0$.

For the error probability analysis later, it is crucial to know the relative delay or the distance between the l-th path and the position of the i-th Rake finger in the receiver, where $(0 \leq i \leq K-1)$. Let τ_{li} denote the excess delay of the l-th path expressed relative to the i-th finger, and $p(i)$ denote the position of the i-th finger, where $(0 \leq p(i) \leq L-1)$. Then we can rewrite τ_{li} with respect to the excess delay of the i-th Rake finger position. Then

$$\tau_l = \tau_{li} = \begin{cases} \tau_{p(i)} - (m_{li}T + \tilde{\tau}_{li}), & \text{if } \tau_l < \tau_{p(i)} \\ \tau_{p(i)} + (m_{li}T + \tilde{\tau}_{li}), & \text{if } \tau_l \geq \tau_{p(i)}, \end{cases} \tag{2.6}$$

where $\tau_{p(i)}$ is the excess delay of the i-th Rake finger position,

$$m_{li} = \lfloor |\tau_l - \tau_{p(i)}|/T \rfloor, \tag{2.7}$$

and

$$\tilde{\tau}_{li} = |\tau_l - \tau_{p(i)}| - m_{li} \cdot T, \tag{2.8}$$

with floor function $\lfloor \cdot \rfloor$. In (2.7), m_{li} is the integer part of the distance in units of T between the l-th excess delay and the i-th finger position, and in (2.8), $\tilde{\tau}_{li}$ is the fractional part of this distance in terms of T_c, the chip period. So, both equations tell us the exact distance of the l-th path, τ_l, from the excess delay of the i-th finger position, $\tau_{p(i)}$. We now explain this notation with an example.

Example 2.1

Let us assume there are three arriving paths (L=3), and we have one Rake finger (K=1). Fig. 2.3 illustrates this example. The symbol period is set to be $T = 15T_c$, where T_c is the chip period. Then, we want to position the 0-th Rake finger $(i = 0)$ to the first arriving path $(p(0) = 1)$. Then, $\tau_{p(0)} = \tau_1$ and each excess delay for the 0-th finger, τ_{l0}, can be expressed as

$$\begin{aligned} \tau_{00} &= \tau_{p(0)} - (m_{00}T + \tilde{\tau}_{00}) = \tau_1 - (0 \cdot T + 7 \cdot T_c) \\ \tau_{10} &= \tau_{p(0)} + (m_{10}T + \tilde{\tau}_{10}) = \tau_1 \\ \tau_{20} &= \tau_{p(0)} + (m_{20}T + \tilde{\tau}_{20}) = \tau_1 + (1 \cdot T + 4 \cdot T_c) \end{aligned}$$

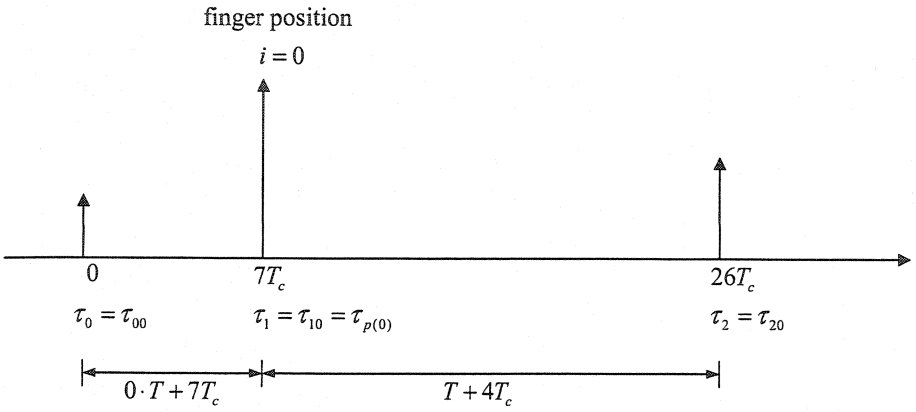

Figure 2.3: The example of the channel model

where τ_{00} represents the excess delay of the 0-th path expressed relative to the 0-th Rake finger, and τ_{10} represents the excess delay of the 1st path expressed relative to the 0-th Rake finger, and so on. Therefore,

$$\begin{aligned} m_{00} &= 0, & \tilde{\tau}_{00} &= 7 \cdot T_c \\ m_{10} &= 0, & \tilde{\tau}_{10} &= 0 \\ m_{20} &= 1, & \tilde{\tau}_{20} &= 4 \cdot T_c. \end{aligned}$$

In this example, the 0-th path ($l = 0$) is less than a symbol period from the 0-th finger position (i=0). The second path ($l = 2$) is greater than a symbol period from the 0-th finger position (i=0).

Similarly, Fig. 2.4 shows the generalized multipath channel model with the notation described in (2.6) - (2.8). With this notation we have written each excess delay of the multipath component, τ_l, in terms of the distance that shows how far it is from the i-th finger position, $\tau_{p(i)}$. The knowledge of this distance between the arriving paths and the i-th finger position helps us understand how the multipath terms interfere in the form of SI or ISI.

2.5 Received Signal

At the receiver K Rake fingers collect the signal energy of multipath terms. They are summed using the Maximal Ratio Combining (MRC) rule assuming perfect CSI. The

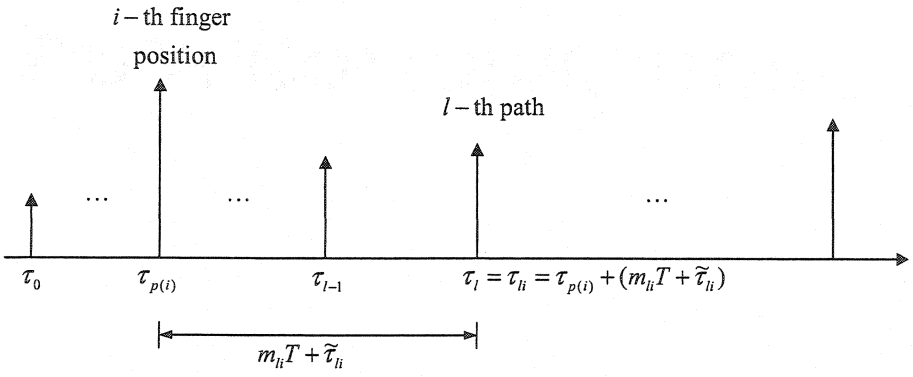

Figure 2.4: A generalized multipath channel model

bit decision is the sign of the MRC combiner output. Fig. 2.5 shows a typical Rake receiver structure. The received signal can simply be expressed as the convolution of $s(t)$ in (2.1) with $h_c(t)$ in (2.5) plus additive white Gaussian noise (AWGN), $n(t)$, given by

$$r(t) = s(t) * h_c(t) + n(t) \tag{2.9}$$

$$= x(t) + n(t), \tag{2.10}$$

where

$$x(t) = \sum_{l=0}^{L-1} c_l \cdot s(t - \tau_l). \tag{2.11}$$

Typically, we have assumed that b_0 is the information to be detected for the error probability analysis when each bit has the same error probability. However, with CH, other bits occur with different performance than b_0. To see this fact, consider the sequence (we set $N_h = 3$)

bit stream	$[\ b_0 \quad b_1 \quad b_2 \quad b_3 \quad b_4 \quad b_5\ ]$
hopping sequence	$[\ a'_0 \quad a'_1 \quad a'_2 \quad a'_0 \quad a'_1 \quad a'_2\ ].$

Note that the performance for b_0 depends on the correlation values $(a'_0,\ a'_1)$, $(a'_0,\ a'_2)$, and $(a'_0,\ a'_0)$. On the other hand, the performance for b_1 depends on the correlation values $(a'_1,\ a'_0)$, $(a'_1,\ a'_2)$, and $(a'_1,\ a'_1)$. These correlation values are different. A similar situation also occurs for bit b_2.

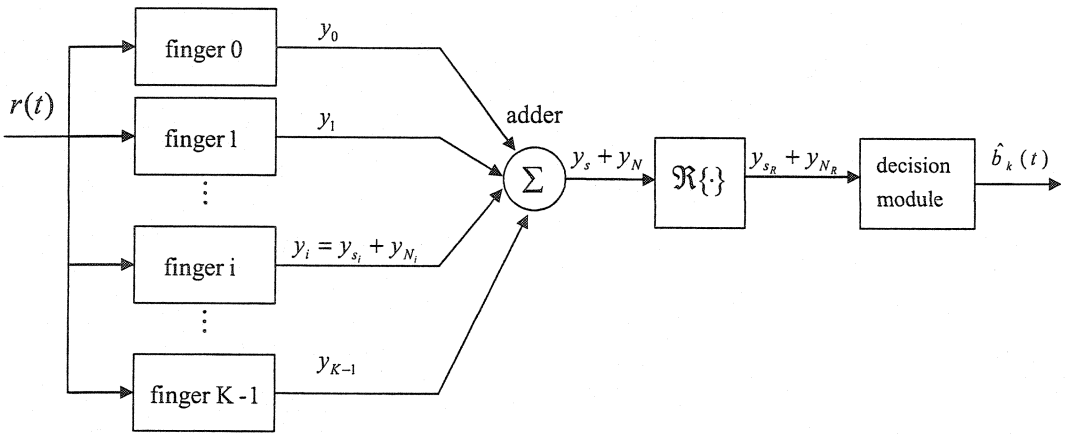

Figure 2.5: The structure of a Rake receiver

We will handle this situation as follows. Let us define a CH index, $\xi = 0,\ 1,\ \cdots N_h - 1$, which indicates the CH sequence in the hopping pattern. Thus, b_0 will be taken to be the bit to be detected when $\xi = 0$. When $\xi = 1$, b_1 will be the bit to be detected, and so on up to $\xi = N_h - 1$. We thus find the error probability for b_ξ as a generic information bit for a given ξ. The error probability thus depends on ξ. Later, we will average the error probability over $\xi = 0,\ 1,\ \cdots N_h - 1$ to get the final average error probability.

If we assume b_ξ is the data bit to be detected, then, using (2.10), the output of the i-th Rake finger shown in Fig. 2.6 is given by

$$\begin{aligned} y_i &= y_i((\xi+1)T + \tau_{p(i)}) && (2.12)\\ &= \int_{\xi T+\tau_{p(i)}}^{(\xi+1)T+\tau_{p(i)}} r(t)\cdot c^*_{p(i)}\cdot a_\xi(t-\tau_{p(i)})dt && (2.13)\\ &= y_{s_i} + y_{N_i}, && (2.14) \end{aligned}$$

where

$$y_{s_i} = \int_{\xi T+\tau_{p(i)}}^{(\xi+1)T+\tau_{p(i)}} x(t)\cdot c^*_{p(i)}\cdot a_\xi(t-\tau_{p(i)})dt \qquad (2.15)$$

is the signal term of the i-th Rake finger output, and $x(t)$ is given in (2.11). Also,

$$y_{N_i} = \int_{\xi T+\tau_{p(i)}}^{(\xi+1)T+\tau_{p(i)}} n(t)\cdot c^*_{p(i)}\cdot a_\xi(t-\tau_{p(i)})dt \qquad (2.16)$$

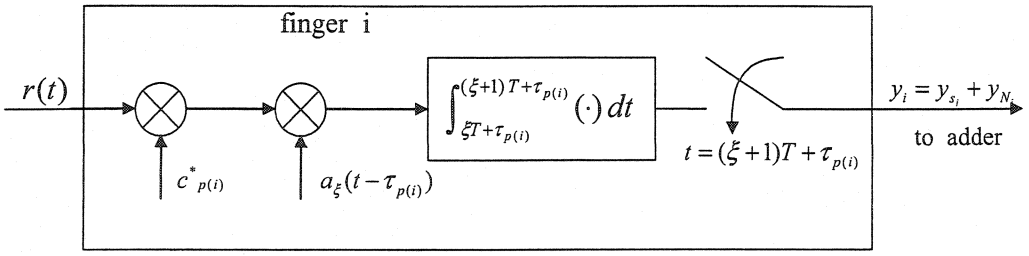

Figure 2.6: The structure of the i-th Rake finger

is denoted as the noise term of the i-th Rake finger output.

2.5.1 Received Signal Term

The signal term, y_{s_i}, in (2.15) is the i-th MRC Rake finger output assuming no noise, $n(t) = 0$. By combining (2.11) with (2.15), y_{s_i} can be expressed as,

$$y_{s_i} = \int_{\xi T+\tau_{p(i)}}^{(\xi+1)T+\tau_{p(i)}} \sum_{l=0}^{L-1} c_l \cdot s(t-\tau_l) \cdot c^*_{p(i)} \cdot a_\xi(t-\tau_{p(i)})dt. \tag{2.17}$$

If we also combine $s(t)$ in (2.1) with (2.17), we have

$$y_{s_i} = \int_{\xi T+\tau_{p(i)}}^{(\xi+1)T+\tau_{p(i)}} \sum_{l=0}^{L-1} c_l A \sum_{k=-\infty}^{\infty} b_k(t-\tau_l)a_k(t-\tau_l) \cdot c^*_{p(i)}a_\xi(t-\tau_{p(i)})dt \tag{2.18}$$

$$= A\sum_{l=0}^{L-1} c_l c^*_{p(i)} \int_{\xi T+\tau_{p(i)}}^{(\xi+1)T+\tau_{p(i)}} \sum_{k=-\infty}^{\infty} b_k(t-\tau_l)a_k(t-\tau_l) \cdot a_\xi(t-\tau_{p(i)})dt. \tag{2.19}$$

Since (2.19) is a sum of L arriving multipath terms, it can be grouped into three cases; the l-th paths that arrive before the i-th Rake finger position ($l < p(i)$), the l-th path that arrives right at the i-th Rake finger position ($l = p(i)$), and the l-th paths that arrive after the i-th Rake finger position ($l > p(i)$). Then we can decompose

(2.19) into three groups as

$$
\begin{aligned}
y_{s_i} = \; & A \sum_{l=0}^{p(i)-1} c_l c_{p(i)}^* \int_{\xi T+\tau_{p(i)}}^{(\xi+1)T+\tau_{p(i)}} \sum_{k=-\infty}^{\infty} b_k(t-\tau_l) a_k(t-\tau_l) a_\xi(t-\tau_{p(i)}) dt \\
& + A c_{p(i)} c_{p(i)}^* \int_{\xi T+\tau_{p(i)}}^{(\xi+1)T+\tau_{p(i)}} \sum_{k=-\infty}^{\infty} b_k(t-\tau_{p(i)}) a_k(t-\tau_{p(i)}) a_\xi(t-\tau_{p(i)}) dt \\
& + A \sum_{l=p(i)+1}^{L-1} c_l c_{p(i)}^* \int_{\xi T+\tau_{p(i)}}^{(\xi+1)T+\tau_{p(i)}} \sum_{k=-\infty}^{\infty} b_k(t-\tau_l) a_k(t-\tau_l) a_\xi(t-\tau_{p(i)}) dt.
\end{aligned}
\tag{2.20}
$$

Then we can combine τ_{li} in (2.6) with (2.20) to get

$$
\begin{aligned}
y_{s_i} = \; & A \sum_{l=0}^{p(i)-1} c_l c_{p(i)}^* \int_{\xi T+\tau_{p(i)}}^{(\xi+1)T+\tau_{p(i)}} \sum_{k=-\infty}^{\infty} b_k(t-\tau_{p(i)}+(m_{li}T+\tilde{\tau}_{li})) \cdot \\
& \qquad a_k(t-\tau_{p(i)}+(m_{li}T+\tilde{\tau}_{li})) \cdot a_\xi(t-\tau_{p(i)}) dt \\
& + A \cdot \alpha_{p(i)}^2 b_0 \int_{\xi T+\tau_{p(i)}}^{(\xi+1)T+\tau_{p(i)}} a_\xi(t-\tau_{p(i)}) \cdot a_\xi(t-\tau_{p(i)}) dt \\
& + A \sum_{l=p(i)+1}^{L-1} c_l c_{p(i)}^* \int_{\xi T+\tau_{p(i)}}^{(\xi+1)T+\tau_{p(i)}} \sum_{k=-\infty}^{\infty} b_k(t-\tau_{p(i)}-(m_{li}T+\tilde{\tau}_{li})) \cdot \\
& \qquad a_k(t-\tau_{p(i)}-(m_{li}T+\tilde{\tau}_{li})) \cdot a_\xi(t-\tau_{p(i)}) dt,
\end{aligned}
\tag{2.21}
$$

where $\alpha_{p(i)}$ is the magnitude of the complex channel gain $c_{p(i)}$. In the first and the third terms in (2.21), the i-th Rake finger position is fixed at $\tau_{p(i)}$ and

$$
\int_{\xi T+\tau_{p(i)}}^{(\xi+1)T+\tau_{p(i)}} \sum_{k=-\infty}^{\infty} b_k(t-\tau_{p(i)} \pm (m_{li}T+\tilde{\tau}_{li})) a_k(t-\tau_{p(i)} \pm (m_{li}T+\tilde{\tau}_{li})) \cdot a_\xi(t-\tau_{p(i)}) dt,
$$

can have at most two non-zero terms since the integration is performed over one symbol period, $[\xi T+\tau_{p(i)},\ (\xi+1)T+\tau_{p(i)})$. The 0-th trace and the 2nd trace in Fig. 2.7 illustrate the remaining two non-zero terms after correlation is done. Note that as at most two terms can contribute to interference at a fixed multipath delay, only at most two symbols give the SI or the ISI in the summation above.

Therefore by considering only the remaining terms after integration, (2.21) can

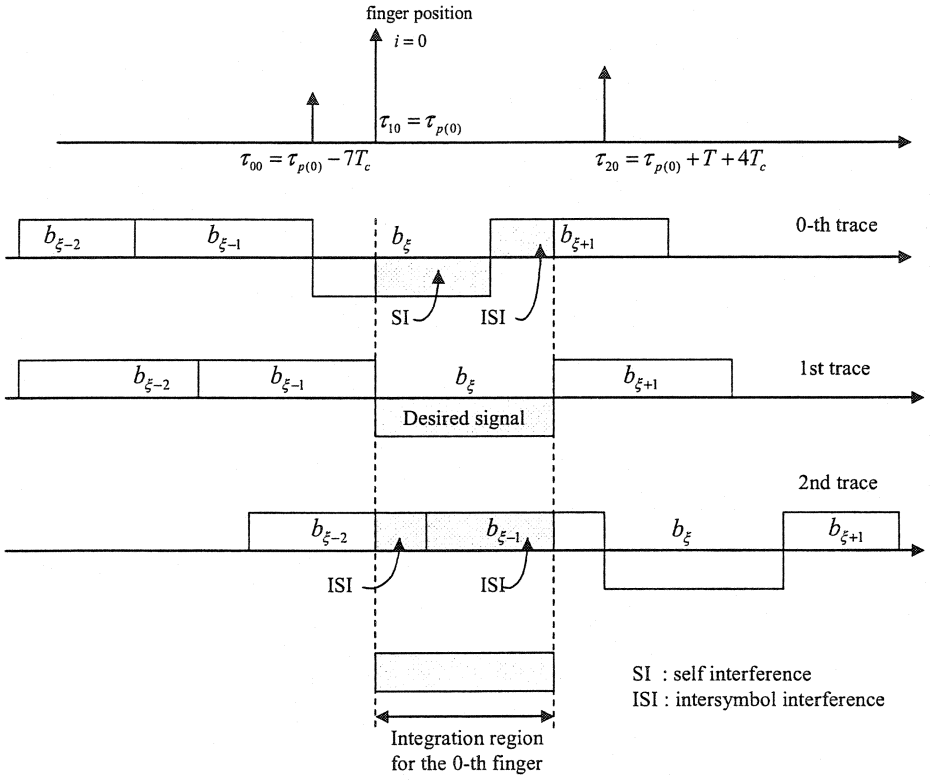

Figure 2.7: The illustration of remaining two terms after the correlation in the i-th Rake finger

be simplified as

$$
\begin{aligned}
y_{s_i} \;=\;& A\sum_{l=0}^{p(i)-1} c_l c^*_{p(i)} \Bigg\{ b_{\xi+m_{li}} \int_{\xi T+\tau_{p(i)}}^{(\xi+1)T+\tau_{p(i)}} a_{\xi+m_{li}}(t-\tau_{p(i)}+(m_{li}T+\tilde{\tau}_{li}))\cdot a_\xi(t-\tau_{p(i)})dt \\
&\qquad + b_{\xi+m_{li}+1} \int_{\xi T+\tau_{p(i)}}^{(\xi+1)T+\tau_{p(i)}} a_{\xi+m_{li}+1}(t-\tau_{p(i)}+(m_{li}T+\tilde{\tau}_{li}))\cdot a_\xi(t-\tau_{p(i)})dt \Bigg\} \\
&+ A\alpha^2_{p(i)} b_\xi T \\
&+ A\sum_{l=p(i)+1}^{L-1} c_l c^*_{p(i)} \cdot \\
&\quad \Bigg\{ b_{\xi-m_{li}-1} \int_{\xi T+\tau_{p(i)}}^{(\xi+1)T+\tau_{p(i)}} a_{\xi-m_{li}-1}(t-\tau_{p(i)}-(m_{li}T+\tilde{\tau}_{li}))\cdot a_\xi(t-\tau_{p(i)})dt \\
&\qquad + b_{\xi-m_{li}} \int_{\xi T+\tau_{p(i)}}^{(\xi+1)T+\tau_{p(i)}} a_{\xi-m_{li}}(t-\tau_{p(i)}-(m_{li}T+\tilde{\tau}_{li}))\cdot a_\xi(t-\tau_{p(i)})dt \Bigg\}. \qquad (2.22)
\end{aligned}
$$

Let the partial cross-correlation function between the k-th sequence and the m-th sequence be defined as

$$R_{k,\,m}(\tau) = \frac{1}{T}\int_{-\infty}^{\infty} a_k(t-\tau)a_m(t)dt.$$

Then, it is possible to express (2.22) in terms of the partial cross-correlation functions given by

$$
\begin{aligned}
y_{s_i} \;=\;& AT\alpha^2_{p(i)} b_\xi \\
&+ AT\sum_{l=0}^{p(i)-1} c_l c^*_{p(i)} \{ b_{\xi+m_{li}} \cdot R_{\xi+m_{li},\xi}(-m_{li}T-\tilde{\tau}_{li}) \\
&\qquad\qquad + b_{\xi+m_{li}+1}\cdot R_{\xi+m_{li}+1,\xi}(-m_{li}T-\tilde{\tau}_{li})\} \\
&+ AT\sum_{l=p(i)+1}^{L-1} c_l c^*_{p(i)} \{ b_{\xi-m_{li}-1}\cdot R_{\xi-m_{li}-1,\xi}(m_{li}T+\tilde{\tau}_{li}) \\
&\qquad\qquad + b_{\xi-m_{li}}\cdot R_{\xi-m_{li},\xi}(m_{li}T+\tilde{\tau}_{li})\}. \qquad (2.23)
\end{aligned}
$$

Let us also define $\hat{R}_{k,m}(\tau)$ as

$$\hat{R}_{k,\,m}(\tau) = \frac{1}{T}\int_{-\infty}^{\infty} \hat{a}_k(t-\tau)\hat{a}_m(t)dt, \qquad (2.24)$$

where $\hat{a}_k(t) = \sum_{i=0}^{N_c-1} a^i_{M(k,\,N_h)} P_{T_c}(t-iT_c)$ is the hopping sequence used for the k-th bit, but all the waveforms of $\hat{a}_k(t)$ start at $t=0$. Then we can further simplify (2.23),

and the signal term of the i-th Rake finger output can be formulated as

$$\begin{aligned} y_{s_i} &= AT\alpha_{p(i)}^2 b_\xi \\ &+ AT \sum_{l=0}^{p(i)-1} c_l c_{p(i)}^* \{ b_{\xi+m_{li}} \cdot \hat{R}_{\xi+m_{li},\xi}(-\tilde{\tau}_{li}) + b_{\xi+m_{li}+1} \cdot \hat{R}_{\xi+m_{li}+1,\xi}(T-\tilde{\tau}_{li}) \} \\ &+ AT \sum_{l=p(i)+1}^{L-1} c_l c_{p(i)}^* \{ b_{\xi-m_{li}-1} \cdot \hat{R}_{\xi-m_{li}-1,\xi}(\tilde{\tau}_{li}-T) \\ &\qquad + b_{\xi-m_{li}} \cdot \hat{R}_{\xi-m_{li},\xi}(\tilde{\tau}_{li}) \}. \end{aligned} \tag{2.25}$$

From (2.25), if the K Rake finger outputs of the received signal are added, we can obtain the total combined signal term as

$$y_s = \sum_{i=0}^{K-1} y_{s_i}, \tag{2.26}$$

or equivalently,

$$\begin{aligned} y_s = \; & ATb_\xi \sum_{i=0}^{K-1} \alpha_{p(i)}^2 \\ & + AT \sum_{i=0}^{K-1} \sum_{l=0}^{p(i)-1} c_l c_{p(i)}^* \{ b_{\xi+m_{li}} \hat{R}_{\xi+m_{li},\,\xi}(-\tilde{\tau}_{li}) + b_{\xi+m_{li}+1} \hat{R}_{\xi+m_{li}+1,\,\xi}(T-\tilde{\tau}_{li}) \} \\ & + AT \sum_{i=0}^{K-1} \sum_{l=p(i)+1}^{L-1} c_l c_{p(i)}^* \{ b_{\xi-m_{li}-1} \hat{R}_{\xi-m_{li}-1,\,\xi}(\tilde{\tau}_{li}-T) + b_{\xi-m_{li}} \hat{R}_{\xi-m_{li},\,\xi}(\tilde{\tau}_{li}) \}, \end{aligned} \tag{2.27}$$

where we define $\sum_{l=0}^{-1}(\cdot) = \sum_{l=L}^{L-1}(\cdot) = 0$. For instance, if $p(i) = 0$, then $\sum_{l=0}^{p(i)-1}(\cdot) = 0$ and if $p(i) = L-1$, then $\sum_{l=p(i)+1}^{L-1}(\cdot) = 0$.

Since we are considering BPSK modulation, detection can be based on the real part of y_s. We denote the complex channel gain as $c_l = x_l + jy_l$, where x_l and y_l are

real values, and if we take the real part of y_s,

$$\begin{aligned}\Re\{y_s\} &= ATb_\xi \sum_{i=0}^{K-1} \alpha_{p(i)}^2 \\ &+ AT \sum_{i=0}^{K-1} \sum_{l=0}^{p(i)-1} (x_l x_{p(i)} + y_l y_{p(i)}) \{ b_{\xi+m_{li}} \hat{R}_{\xi+m_{li},\,\xi}(-\tilde{\tau}_{li}) \\ &\qquad + b_{\xi+m_{li}+1} \hat{R}_{\xi+m_{li}+1,\,\xi}(T-\tilde{\tau}_{li}) \} \\ &+ AT \sum_{i=0}^{K-1} \sum_{l=p(i)+1}^{L-1} (x_l x_{p(i)} + y_l y_{p(i)}) \{ b_{\xi-m_{li}-1} \hat{R}_{\xi-m_{li}-1,\,\xi}(\tilde{\tau}_{li}-T) \\ &\qquad + b_{\xi-m_{li}} \hat{R}_{\xi-m_{li},\,\xi}(\tilde{\tau}_{li}) \}. \end{aligned} \tag{2.28}$$

The total K summed signal term at the output of the adder, y_s, is shown in Fig. 2.5. In (2.28), the first term is the desired signal and the second and the third terms represent the interference including the SI and the ISI. If we recall that the SI term occurs when the distance of the arriving path, τ_l, is less than one symbol period from the i-th finger position, $\tau_{p(i)}$, we can extract the SI term from (2.28), and it can be expressed as

$$b_\xi U_{si}(\xi) = b_\xi \sum_{i=0,\, p(i)\neq l,}^{K-1} \sum_{l=0}^{L-1} (x_{p(i)} x_l + y_{p(i)} y_l) \hat{R}_{\xi,\,\xi}(\tau_l - \tau_{p(i)}), \tag{2.29}$$

where $\hat{R}_{\xi,\,\xi}(\tau_l - \tau_{p(i)}) = 0$, if $|\tau_l - \tau_{p(i)}| \geq T$. Note that $U_{si}(\xi)$ is a function of ξ. Then we can write (2.28) as

$$\Re\{y_s\} = AT \left\{ b_\xi (U_s + U_{si}(\xi)) + U_{isi}(\xi,\, \mathbf{b}) \right\}, \tag{2.30}$$

where

$$U_s = \sum_{i=0}^{K-1} \alpha_{p(i)}^2, \tag{2.31}$$

$$U_{si}(\xi) = \sum_{i=0,\, p(i)\neq l,}^{K-1} \sum_{l=0}^{L-1} (x_{p(i)} x_l + y_{p(i)} y_l) \hat{R}_{\xi,\,\xi}(\tau_l - \tau_{p(i)}), \tag{2.32}$$

and

$$U_{isi}(\xi,\ \mathbf{b}) = \sum_{i=0}^{K-1}\sum_{l=0}^{p(i)-1}(x_l x_{p(i)} + y_l y_{p(i)})\{b_{\xi+m_{li}}\hat{R}_{\xi+m_{li},\,\xi}(-\tilde{\tau}_{li}) + b_{\xi+m_{li}+1}\hat{R}_{\xi+m_{li}+1,\,\xi}(T-\tilde{\tau}_{li})\} + \sum_{i=0}^{K-1}\sum_{l=p(i)+1}^{L-1}(x_l x_{p(i)} + y_l y_{p(i)})\{b_{\xi-m_{li}-1}\hat{R}_{\xi-m_{li}-1,\,\xi}(\tilde{\tau}_{li}-T) + b_{\xi-m_{li}}\hat{R}_{\xi-m_{li},\,\xi}(\tilde{\tau}_{li})\} - b_\xi U_{si}(\xi), \tag{2.33}$$

where we define $\mathbf{b}$ as the vector of the data bit sequence that contributes to the ISI. $U_{isi}(\xi, \mathbf{b})$ in (2.33) is obtained by subtracting (2.29) from the second and the third terms in (2.28). Note that $U_{isi}(\xi,\ \mathbf{b})$ depends on ξ and the data bit sequence, $\mathbf{b}$.

2.5.2 Received Noise Term

As the signal term is expressed in terms of the partial cross-correlation functions, the noise term can also be expressed in a similar way. We start the analysis of the noise term of the i-th Rake finger by rewriting (2.16) as

$$y_{N_i} = \int_{\xi T+\tau_{p(i)}}^{(\xi+1)T+\tau_{p(i)}} c^*_{p(i)} \cdot n(t) \cdot a_\xi(t-\tau_{p(i)})dt. \tag{2.34}$$

In (2.34), $n(t)$ is zero mean complex white Gaussian noise process. Then the total noise term after the adder shown in Fig. 2.5 is the sum of all the noise terms from K Rake finger outputs, and is given by

$$y_N = \sum_{i=0}^{K-1}\int_{\xi T+\tau_{p(i)}}^{(\xi+1)T+\tau_{p(i)}} c^*_{p(i)} \cdot n(t) \cdot a_\xi(t-\tau_{p(i)})dt. \tag{2.35}$$

Since only the real part is considered in the decision module shown in Fig. 2.1, we take the real part of the total noise term, y_N. By denoting $n(t) = n_{_R}(t) + jn_{_I}(t)$, where $n_{_R}(t)$ and $n_{_I}(t)$ are zero mean independent real WGN processes, and the auto-

correlation functions are given by

$$\begin{aligned} R_{n_R}(\tau) &= E[n_R(t+\tau)n_R(t)] \\ &= R_{n_I}(\tau) \\ &= \frac{N_o}{2}\delta(\tau), \end{aligned} \tag{2.36}$$

where N_o is the spectral density or the variance of the WGN noise. Then,

$$\begin{aligned} y_{N_R} &= \Re\{y_N\} \\ &= \Re\left\{\sum_{i=0}^{K-1}\int_{\xi T+\tau_{p(i)}}^{(\xi+1)T+\tau_{p(i)}}(x_{p(i)}-jy_{p(i)})(n_R(t)+jn_I(t))\cdot a_\xi(t-\tau_{p(i)})dt\right\} \\ &= \sum_{i=0}^{K-1}\int_{\xi T+\tau_{p(i)}}^{(\xi+1)T+\tau_{p(i)}}(x_{p(i)}n_R(t)+y_{p(i)}n_I(t))\cdot a_\xi(t-\tau_{p(i)})dt. \end{aligned} \tag{2.37}$$

Let $\mathbf{c}$ be denoted as all the parameters of the channel impulse response in (2.5). If we fix the channel parameters, $\mathbf{c}$, then the real part of the total noise term, y_{N_R}, is a Gaussian distributed random variable, where its mean is

$$\begin{aligned} E[y_{N_R}|\,\mathbf{c}] &= \sum_{i=0}^{K-1}\int_{\xi T+\tau_{p(i)}}^{(\xi+1)T+\tau_{p(i)}} E\left[(x_{p(i)}n_R(t)+y_{p(i)}n_I(t))\right]a_\xi(t-\tau_{p(i)})dt \\ &= 0, \end{aligned} \tag{2.38}$$

and the variance for given $\mathbf{c}$ is

$$\begin{aligned} E[y_{N_R}y_{N_R}|\,\mathbf{c}] &= E\left[\sum_{i=0}^{K-1}\int_{\xi T+\tau_{p(i)}}^{(\xi+1)T+\tau_{p(i)}}(x_{p(i)}n_R(t)+y_{p(i)}n_I(t))\cdot a_\xi(t-\tau_{p(i)})dt\right. \\ &\qquad \left.\times\sum_{j=0}^{K-1}\int_{\xi T+\tau_{p(j)}}^{(\xi+1)T+\tau_{p(j)}}(x_{p(j)}n_R(s)+y_{p(j)}n_I(s))\cdot a_\xi(s-\tau_{p(j)})ds\right] \\ &= \sum_{i=0}^{K-1}\int_{\xi T+\tau_{p(i)}}^{(\xi+1)T+\tau_{p(i)}}\int_{\xi T+\tau_{p(i)}}^{(\xi+1)T+\tau_{p(i)}} E\left[(x_{p(i)}n_R(t)+y_{p(i)}n_I(t))\right. \\ &\qquad \left.\cdot(x_{p(i)}n_R(s)+y_{p(i)}n_I(s))\right]\cdot a_\xi(t-\tau_{p(i)})a_\xi(s-\tau_{p(i)})dt\,ds \\ &\quad + \sum_{i=0,\,i\neq j,}^{K-1}\sum_{j=0}^{K-1}\int_{\xi T+\tau_{p(i)}}^{(\xi+1)T+\tau_{p(i)}}\int_{\xi T+\tau_{p(j)}}^{(\xi+1)T+\tau_{p(j)}} E\left[(x_{p(i)}n_R(t)+y_{p(i)}n_I(t))\right. \\ &\qquad \left.\cdot(x_{p(j)}n_R(s)+y_{p(j)}n_I(s))\right]\cdot a_\xi(t-\tau_{p(i)})a_\xi(s-\tau_{p(j)})dt\,ds \\ &= \qquad (1) \qquad + \qquad (2) \end{aligned} \tag{2.39}$$

In (2.39) the first and the second term indicate the independent noise and the correlated noise, respectively. The first term of (2.39) can be simplified as

$$
\begin{aligned}
(1) = \sum_{i=0}^{K-1} \int_{\xi T+\tau_{p(i)}}^{(\xi+1)T+\tau_{p(i)}} \int_{\xi T+\tau_{p(i)}}^{(\xi+1)T+\tau_{p(i)}} & E\left[x_{p(i)}^2 n_R(t) n_R(s) + y_{p(i)}^2 n_I(t) n_I(s)\right. \\
& \left. + x_{p(i)} y_{p(i)} n_R(t) n_I(s) + x_{p(i)} y_{p(i)} n_R(s) n_I(t)\right] \cdot a_\xi(t-\tau_{p(i)}) a_\xi(s-\tau_{p(i)}) dt\, ds \\
= \sum_{i=0}^{K-1} \frac{N_o}{2}(x_{p(i)}^2 + y_{p(i)}^2) & \int_{\xi T+\tau_{p(i)}}^{(\xi+1)T+\tau_{p(i)}} \int_{\xi T+\tau_{p(i)}}^{(\xi+1)T+\tau_{p(i)}} \delta(t-s) a_\xi(t-\tau_{p(i)}) a_\xi(s-\tau_{p(i)}) dt\, ds \\
= \sum_{i=0}^{K-1} \frac{N_o}{2}(x_{p(i)}^2 + y_{p(i)}^2) & \int_{\xi T+\tau_{p(i)}}^{(\xi+1)T+\tau_{p(i)}} a_\xi(s-\tau_{p(i)}) a_\xi(s-\tau_{p(i)}) ds \\
= \frac{N_o T}{2} & \sum_{i=0}^{K-1} (x_{p(i)}^2 + y_{p(i)}^2),
\end{aligned}
\tag{2.40}
$$

where we used the fact that $E[n_R(t)n_I(s)] = E[n_R(s)n_I(t)] = 0$ since the real part and the imaginary part of the WGN processes are zero mean and independent of each other. Meanwhile, the second term in (2.39) can be simplified as

$$
\begin{aligned}
(2) = \sum_{i=0,\ i\neq j,}^{K-1} \sum_{j=0}^{K-1} \int_{\xi T+\tau_{p(i)}}^{(\xi+1)T+\tau_{p(i)}} & \int_{\xi T+\tau_{p(j)}}^{(\xi+1)T+\tau_{p(j)}} E\left[x_{p(i)} x_{p(j)} n_R(t) n_R(s) + y_{p(i)} y_{p(j)} n_I(t) n_I(s)\right. \\
& \left. + x_{p(i)} y_{p(j)} n_R(t) n_I(s) + x_{p(j)} y_{p(i)} n_R(s) n_I(t)\right] \cdot a_\xi(t-\tau_{p(i)}) a_\xi(s-\tau_{p(j)}) dt\, ds. \\
= \sum_{i=0,\ i\neq j,}^{K-1} \sum_{j=0}^{K-1} \int_{\xi T+\tau_{p(i)}}^{(\xi+1)T+\tau_{p(i)}} & \int_{\xi T+\tau_{p(j)}}^{(\xi+1)T+\tau_{p(j)}} \left\{x_{p(i)} x_{p(j)} \frac{N_o}{2}\delta(t-s) + y_{p(i)} y_{p(j)} \frac{N_o}{2}\delta(t-s)\right\} \\
& \cdot a_\xi(t-\tau_{p(i)}) \cdot a_\xi(s-\tau_{p(j)}) dt \cdot ds \\
= \frac{N_o}{2} \sum_{i=0,\ i\neq j,}^{K-1} \sum_{j=0}^{K-1} & (x_{p(i)} x_{p(j)} + y_{p(i)} y_{p(j)}) \int_{\xi T+\tau_{p(j)}}^{(\xi+1)T+\tau_{p(j)}} a_\xi(s-\tau_{p(i)}) a_\xi(s-\tau_{p(j)}) ds \\
= \frac{N_o T}{2} \sum_{i=0,\ i\neq j,}^{K-1} \sum_{j=0}^{K-1} & (x_{p(i)} x_{p(j)} + y_{p(i)} y_{p(j)}) \hat{R}_{\xi,\,\xi}(\tau_{p(j)} - \tau_{p(i)}).
\end{aligned}
\tag{2.41}
$$

Thus, the second moment of the total noise term given $\mathbf{c}$ is obtained by adding (2.40) and (2.41) to give

$$E[y_{N_R}^2 \mid \mathbf{c}] = \frac{N_o T}{2}\left\{\sum_{i=0}^{K-1}\alpha_{p(i)}^2 + \sum_{i=0,\ i\neq j,}^{K-1}\sum_{j=0}^{K-1}(x_{p(i)}x_{p(j)} + y_{p(i)}y_{p(j)})\hat{R}_{\xi,\,\xi}(\tau_{p(j)} - \tau_{p(i)})\right\}, \tag{2.42}$$

where $\alpha_{p(i)}^2 = x_{p(i)}^2 + y_{p(i)}^2$. Note also that $\hat{R}_{\xi,\,\xi}(\tau_{p(j)} - \tau_{p(i)}) = 0, \quad \text{if } |\tau_{p(j)} - \tau_{p(i)}| \geq T$. Let $N(m, \sigma^2)$ denote the Gaussian distribution with mean, m, and variance, σ^2. Then, for given $\mathbf{c}$, the real part of the total noise term, y_{N_R}, is Gaussian distributed with the statistics given by

$$y_{N_R} \sim N\left(0,\ \frac{N_o T}{2}\left\{\sum_{i=0}^{K-1}\alpha_{p(i)}^2 + \sum_{i=0,\ i\neq j,}^{K-1}\sum_{j=0}^{K-1}(x_{p(i)}x_{p(j)} + y_{p(i)}y_{p(j)})\hat{R}_{\xi,\,\xi}(\tau_{p(j)} - \tau_{p(i)})\right\}\right). \tag{2.43}$$

The second term of the variance in (2.43) is related to the distances between the finger positions that are within the symbol period about each Rake finger. For simplicity, let us denote (2.43) as

$$y_{N_R} \sim N\left(0,\quad \frac{N_o T}{2}\left(U_s + U_{cn}(\xi)\right)\right), \tag{2.44}$$

where

$$U_s = \sum_{i=0}^{K-1}\alpha_{p(i)}^2 \tag{2.45}$$

$$U_{cn}(\xi) = \sum_{i=0,\ i\neq j,}^{K-1}\sum_{j=0}^{K-1}(x_{p(i)}x_{p(j)} + y_{p(i)}y_{p(j)})\hat{R}_{\xi,\,\xi}(\tau_{p(j)} - \tau_{p(i)}). \tag{2.46}$$

$U_{cn}(\xi)$ in (2.46) depends on ξ, and it also implies that the total noise term, y_{N_R}, is correlated between Rake finger outputs.

2.6 Analysis of the Probability of Error

We rewrite (2.30) and (2.44) to derive the probability of error,

$$y_{s_R} = \Re\{y_s\} = AT\{b_\xi(U_s + U_{si}(\xi)) + U_{isi}(\xi,\ \mathbf{b})\} \tag{2.47}$$

$$y_{N_R} = \Re\{y_N\} \sim N\left(0,\ \frac{N_o T}{2}(U_s + U_{cn}(\xi))\right). \tag{2.48}$$

Then the probability of error given $\mathbf{c}$, ξ, $\mathbf{b}$, and $b_\xi = 1$ can be given as

$$\begin{aligned} P_r\{e|\ \mathbf{c}, \xi, \mathbf{b}, b_\xi = 1\} &= P_r\{y_{N_R} < -y_{s_R}\} \\ &= P_r\{y_{N_R} > y_{s_R}\} \\ &= Q\left(\frac{y_{s_R}}{\sigma_{y_{N_R}}}\right) \\ &= Q\left(\sqrt{\frac{A^2T^2}{\frac{N_oT}{2}}} \cdot \frac{U_s + U_{si}(\xi) + U_{isi}(\xi,\ \mathbf{b})}{\sqrt{U_s + U_{cn}(\xi)}}\right) \\ &= Q\left(\sqrt{\frac{2E_b}{N_o}} \cdot \frac{U_s + U_{si}(\xi) + U_{isi}(\xi,\ \mathbf{b})}{\sqrt{U_s + U_{cn}(\xi)}}\right). \end{aligned} \tag{2.49}$$

Similarly, the probability of error given $\mathbf{c}$, ξ, $\mathbf{b}$, and $b_\xi = -1$ can be given as

$$\begin{aligned} P_r\{e|\ \mathbf{c}, \xi, \mathbf{b}, b_\xi = -1\} &= P_r\{y_{N_R} > -y_{s_R}\} \\ &= Q\left(\frac{-y_{s_R}}{\sigma_{y_{N_R}}}\right) \\ &= Q\left(\sqrt{\frac{2E_b}{N_o}} \cdot \frac{U_s + U_{si}(\xi) - U_{isi}(\xi,\ \mathbf{b})}{\sqrt{U_s + U_{cn}(\xi)}}\right). \end{aligned} \tag{2.50}$$

Thus, averaging (2.49) and (2.50) yields

$$\begin{aligned} P_r\{e|\ \mathbf{c}, \xi, \mathbf{b}\} &= \frac{1}{2}\left\{Q\left(\sqrt{\frac{2E_b}{N_o}} \cdot \frac{U_s + U_{si}(\xi) + U_{isi}(\xi,\ \mathbf{b})}{\sqrt{U_s + U_{cn}(\xi)}}\right)\right. \\ &\quad \left. + Q\left(\sqrt{\frac{2E_b}{N_o}} \cdot \frac{U_s + U_{si}(\xi) - U_{isi}(\xi,\ \mathbf{b})}{\sqrt{U_s + U_{cn}(\xi)}}\right)\right\}. \end{aligned} \tag{2.51}$$

We need to average (2.51) over all the data sequences that contribute to the ISI in $U_{isi}(\xi, \mathbf{b})$. Then we can have the probability of bit error given $\mathbf{c}$ and ξ as

$$\begin{aligned} P_r\{e|\ \mathbf{c}, \xi\} &= E_{\mathbf{b}}\left[\frac{1}{2}\left\{Q\left(\sqrt{\frac{2E_b}{N_o}} \cdot \frac{U_s + U_{si}(\xi) + U_{isi}(\xi,\ \mathbf{b})}{\sqrt{U_s + U_{cn}(\xi)}}\right)\right.\right. \\ &\quad \left.\left. + Q\left(\sqrt{\frac{2E_b}{N_o}} \cdot \frac{U_s + U_{si}(\xi) - U_{isi}(\xi,\ \mathbf{b})}{\sqrt{U_s + U_{cn}(\xi)}}\right)\right\}\right] \\ &= \frac{1}{2}E_{\mathbf{b}}\left[Q\left(\sqrt{\frac{2E_b}{N_o}} \cdot \frac{U_s + U_{si}(\xi) + U_{isi}(\xi,\ \mathbf{b})}{\sqrt{U_s + U_{cn}(\xi)}}\right)\right] \\ &\quad + \frac{1}{2}E_{\mathbf{b}}\left[Q\left(\sqrt{\frac{2E_b}{N_o}} \cdot \frac{U_s + U_{si}(\xi) - U_{isi}(\xi,\ \mathbf{b})}{\sqrt{U_s + U_{cn}(\xi)}}\right)\right] \end{aligned} \tag{2.52}$$

The first term and the second term in (2.52) are same after the data bit sequences, $\mathbf{b}$, are averaged. Hence we get

$$P_r\{e|\ \mathbf{c}, \xi\} \ = \ E_{\mathbf{b}}\left[Q\left(\sqrt{\frac{2E_b}{N_o}}\cdot\frac{U_s + U_{si}(\xi) + U_{isi}(\xi,\ \mathbf{b})}{\sqrt{U_s + U_{cn}(\xi)}}\right)\right]. \tag{2.53}$$

Therefore, by averaging (2.53) over the CH index, $\xi = 0,\ 1,\ \cdots\ N_h - 1$, we can finally obtain the probability of bit error given $\mathbf{c}$ as

$$P_r\{e|\ \mathbf{c}\} = \frac{1}{N_h}\sum_{\xi=0}^{N_h-1} E_{\mathbf{b}}\left[Q\left(\sqrt{\frac{2E_b}{N_o}}\cdot\frac{U_s + U_{si}(\xi) + U_{isi}(\xi,\ \mathbf{b})}{\sqrt{U_s + U_{cn}(\xi)}}\right)\right], \tag{2.54}$$

where

$$U_s \ = \ \sum_{i=0}^{K-1}\alpha_{p(i)}^2 \tag{2.55}$$

$$U_{si}(\xi) \ = \ \sum_{i=0,\ p(i)\neq l,}^{K-1}\ \sum_{l=0}^{L-1}(x_{p(i)}x_l + y_{p(i)}y_l)\hat{R}_{\xi,\,\xi}(\tau_l - \tau_{p(i)}) \tag{2.56}$$

$$\begin{aligned} U_{isi}(\xi,\ \mathbf{b}) \ = \ & \sum_{i=0}^{K-1}\sum_{l=0}^{p(i)-1}(x_l x_{p(i)} + y_l y_{p(i)})\{b_{\xi+m_{li}}\hat{R}_{\xi+m_{li},\,\xi}(-\tilde{\tau}_{li}) \\ & \qquad + b_{\xi+m_{li}+1}\hat{R}_{\xi+m_{li}+1,\,\xi}(T - \tilde{\tau}_{li})\} \\ & + \sum_{i=0}^{K-1}\sum_{l=p(i)+1}^{L-1}(x_l x_{p(i)} + y_l y_{p(i)})\{b_{\xi-m_{li}-1}\hat{R}_{\xi-m_{li}-1,\,\xi}(\tilde{\tau}_{li} - T) \\ & \qquad + \ b_{\xi-m_{li}}\hat{R}_{\xi-m_{li},\,\xi}(\tilde{\tau}_{li})\} \\ & - b_\xi U_{si}(\xi) \end{aligned} \tag{2.57}$$

$$U_{cn}(\xi) \ = \ \sum_{i=0,\ i\neq j,}^{K-1}\ \sum_{j=0}^{K-1}(x_{p(i)}x_{p(j)} + y_{p(i)}y_{p(j)})\hat{R}_{\xi,\,\xi}(\tau_{p(j)} - \tau_{p(i)}). \tag{2.58}$$

Note that the result in (2.54) is for the probability of bit error conditioned on $\mathbf{c}$, the channel parameters from the Intel model. This conditioning will be removed to get the final result by averaging over the statistical channel parameters from this model by using the Monte-Carlo simulation method.

2.7 The Beaulieu Series Method

Although (2.54) - (2.58) can provide the exact error probability, the computational burden exponentially grows with the increase of ISI terms, $U_{isi}(\xi, \mathbf{b})$. For exam-

ple, if $U_{isi}(\xi, \mathbf{b})$ consists of 20 data bits, then $Q(\cdot)$ in (2.54) needs to be computed $2^{20} = 1048576$ times to average over all possible data sequences. This number of computations can occur for a NLOS channel in a high rate UWB system, making it impractical to use (2.54). To cope with this concern, one may wish to use Gaussian approximation for the ISI terms. However, it is not clear how many ISI terms are required for the Gaussian approximation to be accurate. Furthermore, for a LOS channel, the number of ISI terms may not be large enough to use the Gaussian approximation. Thus, in order to increase the computational speed without sacrificing any accuracy, the Beaulieu series method (BSM) will be used [58] - [60].

The total signal term at the Rake receiver output in (2.47) and the noise term in (2.48) can be combined to produce the total input signal to the decision module shown in Fig. 2.5, and given by

$$\begin{aligned} y_{tot} &= y_{s_R} + y_{N_R} \\ &= AT\{U_s + U_{si}(\xi)\}b_\xi + AT \cdot U_{isi}(\xi,\ \mathbf{b}) + y_{N_R}. \end{aligned} \tag{2.59}$$

In (2.59), the first term is the desired signal and the second term is the ISI. Note that the SI term, $U_{si}(\xi)$, is also considered as a part of the desired signal because $U_{si}(\xi)$ is deterministic for given $\mathbf{c}$.

In order to use the BSM, we need to obtain the coefficient of the desired signal term and the ISI terms. Let g_ξ be the coefficient of the desired signal term, given by

$$g_\xi = AT\{U_s + U_{si}(\xi)\}. \tag{2.60}$$

Also, let $D(\xi)$ be denoted as the ISI terms in (2.59), and let $g_{\xi+k}$ be denoted as the coefficient of the ISI terms. Then it is possible to numerically obtain $g_{\xi+k}$ from $AT \cdot U_{isi}(\xi,\ \mathbf{b})$ with $U_{isi}(\xi,\ \mathbf{b})$ given in (2.57). The ISI terms will now be given by

$$\begin{aligned} D(\xi) &= AT \cdot U_{isi}(\xi, \mathbf{b}) \\ &= \sum_{\substack{k=-N \\ k \neq 0}}^{N} g_{\xi+k} b_{\xi+k}, \end{aligned} \tag{2.61}$$

where $b_{\xi+k}$ are the data bits that contribute to ISI, and $N = \max(m_{li}) + 1$. Then, we can rewrite (2.59) as

$$y_{tot} = g_\xi b_\xi + D(\xi) + y_{N_R}. \tag{2.62}$$

Example 2.2

To illustrate how to determine $g_{\xi+k}$ in (2.61) we use the parameters in Example 2.1. Recall that the channel parameters are given as

$$\begin{aligned} m_{00} &= 0, \quad \tilde{\tau}_{00} = 7T_c, \\ m_{20} &= 1, \quad \tilde{\tau}_{20} = 4T_c, \\ \tau_{p(0)} &= \tau_1. \end{aligned} \tag{2.63}$$

Let us assume b_0 is the bit to be detected ($\xi = 0$). Then we can substitute the parameters in (2.63) into (2.47) using (2.55), (2.56), and (2.57) to obtain

$$y_{s_R} = AT\{b_0 U_s + b_0 U_{si}(\xi) + U_{isi}(\xi, \mathbf{b})\} \tag{2.64}$$

$$\begin{aligned} &= AT\alpha_1^2 b_0 \\ &\quad + AT(x_0x_1 + y_0y_1)\{b_0 \hat{R}_{0,0}(-7T_c) + b_1 \hat{R}_{1,0}(8T_c)\} \\ &\quad + AT(x_2x_1 + y_2y_1)\{b_{-2}\hat{R}_{-2,0}(-11T_c) + b_{-1}\hat{R}_{-1,0}(4T_c)\} \end{aligned} \tag{2.65}$$

We can rearrange (2.65) with respect to the data bits as

$$\begin{aligned} \Re\{y_s\} = &\quad AT(x_2x_1 + y_2y_1)\hat{R}_{-2,0}(-11T_c)b_{-2} \\ &+ AT(x_2x_1 + y_2y_1)\hat{R}_{-1,0}(4T_c)b_{-1} \\ &+ AT\{\alpha_1^2 + (x_0x_1 + y_0y_1)\hat{R}_{0,0}(-7T_c)\}b_0 \\ &+ AT(x_0x_1 + y_0y_1)\hat{R}_{1,0}(8T_c)b_1. \end{aligned} \tag{2.66}$$

Thus the coefficient of the desired signal term, g_0, and the coefficients of the ISI

term, g_k can be given as

$$\begin{aligned} g_0 &= AT\{\alpha_1^2 + (x_0x_1 + y_0y_1)R_{0,\,0}(-7T_c)\} \\ g_{-2} &= AT(x_2x_1 + y_2y_1)R_{-2,\,0}(-11T_c) \\ g_{-1} &= AT(x_2x_1 + y_2y_1)R_{-1,\,0}(4T_c) \\ g_1 &= AT(x_0x_1 + y_0y_1)R_{1,\,0}(8T_c). \end{aligned}$$

Therefore, if the channel impulse response is given, g_ξ and $g_{\xi+k}$ can be numerically obtained from $AT \cdot U_{isi}(\xi,\ \mathbf{b})$.

Continuing from (2.62), we can derive the probability of error given $\mathbf{c}$, ξ, and $b_\xi = 1$, as

$$\begin{aligned} Pr\{e|\ \mathbf{c}, \xi, b_\xi = 1\} &= Pr\{D(\xi) + y_{N_R} < -g_\xi\} \qquad (2.67) \\ &= Pr\{D(\xi) + y_{N_R} > g_\xi\}. \qquad (2.68) \end{aligned}$$

Moreover, the probability of error given $\mathbf{c}$, ξ, and $b_\xi = -1$ is obtained as

$$Pr\{e|\ \mathbf{c}, \xi, b_\xi = -1\} = Pr\{D(\xi) + y_{N_R} > g_\xi\}. \qquad (2.69)$$

Hence, averaging (2.68) and (2.69) yields

$$\begin{aligned} Pr\{e|\ \mathbf{c}, \xi\} &= Pr\{D(\xi) + y_{N_R} > g_\xi\} \\ &= Pr\left\{\frac{D(\xi)}{\sigma_{y_{N_R}}(\xi)} + y'_{N_R} > \frac{g_\xi}{\sigma_{y_{N_R}}(\xi)}\right\} \\ &= Pr\left\{X - \frac{g_\xi}{\sigma_{y_{N_R}}(\xi)} > 0\right\} \\ &= \sum_{m=-\infty}^{\infty} C_m \cdot e^{-jm\omega_0/\sigma_{y_{N_R}}(\xi)} \cdot E_X\left[e^{jm\omega_0 X}\right], \qquad (2.70) \end{aligned}$$

where

$$\begin{aligned} y'_{N_R} &\sim N(0,\ 1), \qquad (2.71) \\ X &= \frac{D(\xi)}{\sigma_{y_{N_R}}(\xi)} + y'_{N_R}, \qquad (2.72) \\ C_m &= \begin{cases} \frac{1}{j\pi m}, & m = \text{odd} \\ 0, & m = \text{even}, \end{cases} \qquad (2.73) \end{aligned}$$

and

$$E_X\left[e^{jm\omega_0 X}\right] = e^{-m^2\omega_0^2/2} \cdot \prod_{\substack{k=-N \\ k\neq 0}}^{N} \cos\left(\frac{g_{\xi+k}}{\sigma_{y_{N_R}}(\xi)} m\omega_0\right). \tag{2.74}$$

It is shown in [59] that combining (2.73) and (2.74) into (2.70), and simplifying yields

$$Pr\{e|\ \mathbf{c}, \xi\} = \frac{1}{2} - \frac{2}{\pi} \sum_{\substack{m=1 \\ m=odd}}^{\infty} \frac{1}{m} e^{-m^2\omega_0^2/2} \cdot \sin\left(\frac{m\omega_0 g_\xi}{\sigma_{y_{N_R}}(\xi)}\right) \cdot \prod_{\substack{k=-N \\ k\neq 0}}^{N} \cos\left(\frac{m\omega_0 g_{\xi+k}}{\sigma_{y_{N_R}}(\xi)}\right). \tag{2.75}$$

Therefore if we average (2.75) over the CH index, ξ, then the probability of bit error can be formulated as

$$Pr\{e|\ \mathbf{c}\} = \frac{1}{2} - \frac{2}{N_h\pi} \sum_{\xi=0}^{N_h-1} \sum_{\substack{m=1 \\ m=odd}}^{M} \frac{1}{m} e^{-m^2\omega_0^2/2} \cdot \sin\left(\frac{m\omega_0 g_\xi}{\sigma_{y_{N_R}}(\xi)}\right) \cdot \prod_{\substack{k=-N \\ k\neq 0}}^{N} \cos\left(\frac{m\omega_0 g_{\xi+k}}{\sigma_{y_{N_R}}(\xi)}\right), \tag{2.76}$$

where we truncated the infinite summation of m to M. The accuracy of the BSM is verified in [59] that it is almost the same as the exact error probability in the practical region of BER values, while the computational speed is significantly increased. The BER of the BSM will be compared to the other methods in Chapter 4.

Chapter 3

Hopping Pattern Design

Based on the error probability analysis in Chapter 2, we establish a criterion to search for a good CH pattern given CSI and the correlation functions of spreading sequences.

3.1 Code Selection Criterion

In the error probability analysis from (2.54) to (2.58) on page 48, the key factor that governs the BER is the argument inside the $Q(\cdot)$ function in (2.54) excluding the E_b/N_o term, given by

$$\frac{U_s + U_{si}(\xi) + U_{isi}(\xi,\ \mathbf{b})}{\sqrt{U_s + U_{cn}(\xi)}} \quad = \quad \frac{g'_\xi + U_{isi}(\xi,\ \mathbf{b})}{\sqrt{U_s + U_{cn}(\xi)}}, \tag{3.1}$$

where

$$g'_\xi \quad = \quad U_s + U_{si}(\xi). \tag{3.2}$$

From (2.61) on page 49, $U_{isi}(\xi, \mathbf{b})$ can be expressed as

$$\begin{aligned} U_{isi}(\xi, \mathbf{b}) \quad &= \quad \frac{1}{AT} \sum_{\substack{k=-N \\ k \neq 0}}^{N} g_{\xi+k} b_{\xi+k} \\ &= \quad \sum_{\substack{k=-N \\ k \neq 0}}^{N} g'_{\xi+k} b_{\xi+k}, \end{aligned} \tag{3.3}$$

where

$$g'_{\xi+k} \quad = \quad g_{\xi+k}/AT. \tag{3.4}$$

As stated in Section 2.7, $g'_{\xi+k}$ can be numerically obtained from (2.57) on page 48. If we assume each data bit, $b_{\xi+k} \in \{1, -1\}$, is an i.i.d. random variable, we can obtain the mean and variance of $U_{isi}(\xi, \mathbf{b})$. Since $b_{\xi+k}$ has zero mean, $U_{isi}(\xi, \mathbf{b})$ also has zero mean, and the variance is given by,

$$\begin{aligned}
\sigma^2_{U_{isi}(\xi)} &= E\left[U_{isi}(\xi, \mathbf{b}) \cdot U_{isi}(\xi, \mathbf{b})\right] \\
&= E\left[\sum_{\substack{k=-N \\ k\neq 0}}^{N} g'_{\xi+k} b_{\xi+k} \sum_{\substack{m=-N \\ m\neq 0}}^{N} g'_{\xi+m} b_{\xi+m}\right] \qquad (3.5) \\
&= \sum_{\substack{k=-N \\ k\neq 0}}^{N} g'^{\,2}_{\xi+k} E\left[b^2_{\xi+k}\right] + \sum_{\substack{k=-N \\ k\neq 0,\ k\neq m,}}^{N} \sum_{\substack{m=-N \\ m\neq 0}}^{N} g'_{\xi+k} g'_{\xi+m} E\left[b_{\xi+k}\, b_{\xi+m}\right] \qquad (3.6) \\
&= \sum_{\substack{k=-N \\ k\neq 0}}^{N} g'^{\,2}_{\xi+k}. \qquad (3.7)
\end{aligned}$$

Let $\mathbf{a}' = [a'_0\ a'_1\ \cdots\ a'_{N_h}]$ denote a CH pattern to be evaluated. In order to approximately minimize the probability of error, we wish to find the CH pattern, $\mathbf{a}'$, that maximizes (3.1) over the CH index, ξ, and the data bit sequence, $\mathbf{b}$. Because $U_{isi}(\xi,\ \mathbf{b})$ is a random variable, the minimum standard deviation is preferred to approximately minimize the probability of error. Moreover, the error probability will often be dominated by the worst sequence in the CH pattern, $\mathbf{a}'$, which has the smallest value of (3.1). Thus, we choose the minimum value of (3.1) over ξ, or equivalently by taking the negative of the g'_ξ, we can find the maximum value of a decision metric given by

$$DM_{(1)}(\mathbf{a}') = \max_{\text{all } \xi} \left\{ \frac{-g'_\xi + \sigma_{U_{isi}(\xi)}}{\sqrt{U_s + U_{cn}(\xi)}} \right\}. \qquad (3.8)$$

Equation (3.8) represents the worst sequence among the CH pattern, $\mathbf{a}'$.

In addition to (3.8), we include one more component of a decision metric. Since the probability of error will also be dominated by the peak value of the ISI term, $\max\{U_{isi}(\xi, \mathbf{b})\}$, implying the worst ISI case, we also want to find the CH pattern

that has the minimum value of $\max\{U_{isi}(\xi, \mathbf{b})\}$. Therefore we can have the second decision metric given by

$$\begin{aligned} DM_{(2)}(\mathbf{a}') &= \max_{\text{all } \xi} \left\{ \frac{-g'_\xi + \max\{U_{isi}(\xi, \mathbf{b})\}}{\sqrt{U_s + U_{cn}(\xi)}} \right\} \\ &= \max_{\text{all } \xi} \left\{ \frac{-g'_\xi + \sum_{k=-N,\, k\neq 0}^{N} |g'_{\xi+k}|}{\sqrt{U_s + U_{cn}(\xi)}} \right\}. \end{aligned} \tag{3.9}$$

Hence, by averaging the arguments of $\max\{\cdot\}$ in (3.8) and (3.9), we can have the total decision metric as

$$DM_{tot}(\mathbf{a}') = \max_{\text{all } \xi} \left\{ \frac{-g'_\xi + \frac{1}{2}\{\sigma_{U_{isi}(\xi)} + \sum_{k=-N,\, k\neq 0}^{N} |g'_{\xi+k}|\}}{\sqrt{U_s + U_{cn}(\xi)}} \right\}. \tag{3.10}$$

Using (3.10) which represents the worst case in the CH pattern $\mathbf{a}'$, we want to find a CH pattern, $\tilde{\mathbf{a}}'$, that minimizes this decision metric for given CSI, and this operation can be expressed as

$$\arg \left\{ \min_{\text{all } \mathbf{a}'} \{DM_{tot}(\mathbf{a}')\} \right\} = \tilde{\mathbf{a}}'. \tag{3.11}$$

Then we choose $\tilde{\mathbf{a}}'$, as the best CH pattern for given CSI.

3.2 Stage-wise Code Hopping Pattern Search

We use (3.10) to determine the goodness of a CH pattern for given CSI and the set of spreading sequences. The optimal CH pattern may be found by calculating (3.11) for all possible combinations of CH patterns. However this exhaustive search is not attractive from a practical point of view due to computational complexity. Instead, we propose a stage-wise method to find the suboptimal CH pattern.

3.2.1 Stage 1: Code Selection Search

Let N_{tot} denote the total number of spreading sequences available at the receiver. At the stage 1, we use (3.11) over all N_{tot} spreading sequences and find the best code. We denote the best code found as the best code selection (CS), and naturally the

length of the CH pattern is 1 ($N_h = 1$), which implies no CH. If CS is to be used in a system, we can stop at the stage 1. If CH is possible, we proceed to the stage 2 to find a CH pattern.

3.2.2 Stage 2: Code Hopping Pattern Search

At the stage 2, we increment the length of the CH pattern ($N_h = N_h + 1$), by concatenating N_{tot} spreading sequences to the CS sequence found at the stage 1. Hence, a new set of the N_{tot} number of CH patterns with length $N_h = 2$ is generated. Then using (3.11) we find the best CH pattern from the N_{tot} candidates of the CH patterns, and save the corresponding value of $DM_{tot}(\mathbf{a}')$. If the $DM_{tot}(\mathbf{a}')$ value of the previous stage is smaller than that of the present stage, we choose the CH pattern of the previous stage and stop. However, if the $DM_{tot}(\mathbf{a}')$ value of the present stage is smaller than that of the previous stage, we then repeat the stage 2 until the $DM_{tot}(\mathbf{a}')$ value of the present stage is no longer smaller than that of the previous stage. This implies no more gain is obtained by increasing the length of the CH pattern, N_h. Therefore the length of the CH pattern is variable but it can also be fixed arbitrarily. In addition, if it reaches the maximum length, $N_{h,max}$, preset by the system, then we also stop the search. The flowchart of the stage-wise method is shown in Fig 3.1.

3.3 Complexity and Performance

The stage-wise CH pattern search algorithm may not be optimal in searching for the best CH pattern but it does reduce computational complexity over the exhaustive search. For the example of a length N_h CH pattern with the set of N_{tot} spreading sequences, the number of $DM_{tot}(\mathbf{a}')$ computations required by the exhaustive search method is given by

$$(N_{tot})^{N_h},$$

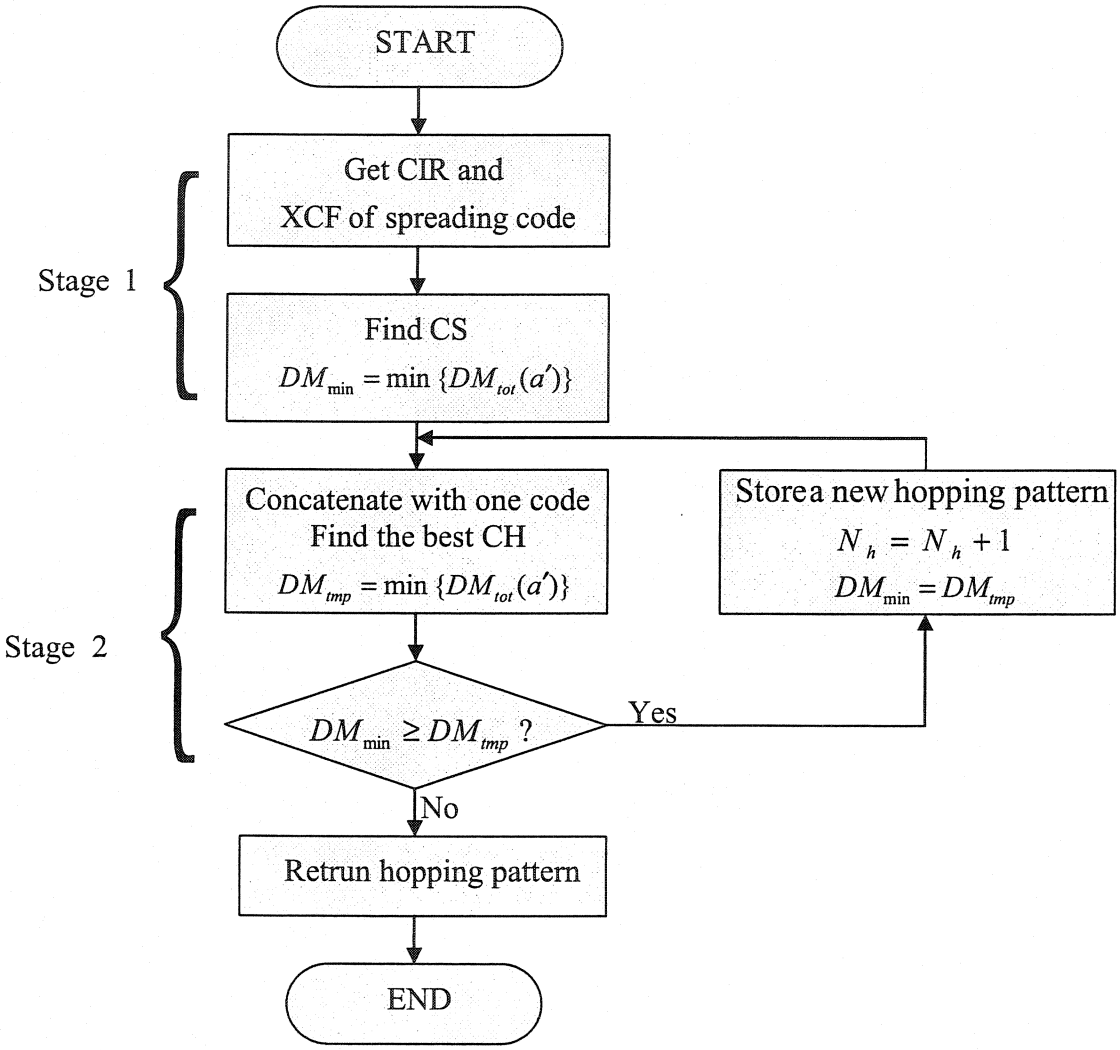

Figure 3.1: Flowchart of the stage-wise CH pattern search method

where we allowed the same sequence to be used in a different location. On the other hand, the stage-wise method only requires

$$N_h \cdot N_{tot}$$

computations.

Since we empirically found that a good CH pattern almost always contains the CS found at the stage 1, it seems reasonable to start with the stage 1 for the CH pattern search. Furthermore, this method proceeds to the next stage only when a certain gain is achieved by increasing the length of the CH pattern. Therefore, CH with the stage-wise search method always performs better than or equal to CS.

Note that the CH pattern search time gets longer if the number of multipath terms increases. Although the stage-wise method significantly reduces the computational complexity over the exhaustive search, it still takes some time to calculate the variance of the ISI term, $\sigma^2_{U_{isi}(\xi)}$, in (3.7) for the NLOS channel. In such a case, we can only consider multipath terms whose strengths are above a certain level. For example, we can ignore multipath terms whose arriving energy is less than -23dB of the strongest path in searching for the CH pattern. Then we can further reduce the computational burden without much sacrificing the efficiency of the CH pattern search. However all the multipath terms are considered in the computation of the error probability.

Chapter 4

Computational Results

We consider a multipath fading channel with AWGN for the performance evaluation of the CS and the CH system. In the multipath fading channel, we assume the channel is constant during the computation of BER. The system model used in this chapter is described in Fig. 2.1 on page 30 and is representative of a baseband UWB system.

The CS system uses the selection of the best code for a given channel, while the CH system chooses a CH pattern found by the algorithm described in Chapter 3. Then we compare the performance of CS with that of CH. Note that we do not evaluate the performance of a conventional DSSS system with a single fixed sequence, since it is obvious that the performance of CS will be always better than or equal to that of the conventional DSSS system. In fact, it is more appropriate to compare the CH system with the CS system than with the conventional DSSS system because CS and CH induce relatively similar complexity. For both CS and CH, CSI is required at the transmitter to assign good spreading sequences. Moreover, the receiver needs to store all the spreading sequences for despreading the received signal. However, for the CH system, the CH pattern search, and the changing tap values in the Rake receiver for the CH pattern will cause slightly higher complexity relative to the CS system.

Our goal is to design a CH system that outperforms a CS system relative to certain performance criteria. First, we clarify the parameters used for the computation of BER, and then analyze the performance for the multipath fading channel generated by the Intel model [42].

4.1 Simulation Parameters

4.1.1 Parameters for the Transmitter

We employ the baseband rectangular pulse for the CH-DSSS system with the chip period $T_c = 0.167\ ns$, and the symbol period is given as

$$T = \begin{cases} 2.505\ ns\ (399.2\ Mbps), & \text{for the GL sequence with length 15} \\ 2.672\ ns\ (374.2\ Mbps), & \text{for the WH sequence with length 16.} \\ 5.177\ ns\ (193.1\ Mbps), & \text{for the Gold sequence with length 31} \\ 5.344\ ns\ (187.1\ Mbps), & \text{for the WH sequence with length 32.} \end{cases}$$

In order to speed up the CH pattern search, we set a threshold in the channel impulse response. If the energy of the channel impulse response is 23 dB less than the energy of the strongest path, we ignore such multipath terms with low energy. However all of the multipath terms in the CSI are considered in the error probability analysis.

The algorithm described in Chapter 3 is used to design the CH pattern. Moreover, the length of the CH pattern is variable, and we set the maximum length to be 5, $N_{h,\,max} = 5$. The loss caused by setting $N_{h,\,max} = 5$ will not be noticeable since the average length of the CH pattern is not very long, and it will be covered later in Section 4.4.1.

4.1.2 Parameters for the Channel Model

In generating the statistical channel, the resolution of the minimum resolvable path is set to be 0.167 ns which approximately produces a 6 GHz bandwidth. This follows from the Intel model (see Section 1.7.3). For the simulation of average BER and outage probability, 7000 statistical channels are generated using the Intel model, and the characteristics of the generated channels are compared with those in Intel model [42]. The reason why 7000 channels were used will be given later in Section 4.3. We compare the mean excess delay ($\bar{\tau}$), the RMS delay spread (τ_{rms}), and the number of significant paths greater than -10 dB energy of the strongest path (NP_{10dB}) in Table 4.1. The characteristics of both the Intel model in [42] and the generated channels

Intel model	LOS1	LOS2	NLOS1
mean excess delay $\bar{\tau}$ $[ns]$	4	3	17
RMS delay spread τ_{rms} $[ns]$	9	5	15
average NP_{10dB}	7	4	35

generated channel	LOS1	LOS2	NLOS1
mean excess delay $\bar{\tau}$ $[ns]$	4.72	2.65	17.94
RMS delay spread τ_{rms} $[ns]$	8.93	4.85	17.08
average NP_{10dB}	6.89	3.96	34.19

Table 4.1: Characteristics of generated LOS1, LOS2, and NLOS1 channels averaged over 7000 channels

to be used are listed in Table 4.1. Also, the channel parameters to generate these channels are described in Table 1.2 on page 16.

The maximum deviation of the generated channels from the Intel model is about 2 ns for the RMS delay spread of the NLOS1 channel. If we recall that the maximum excess delay of the NLOS1 channel can span up to 100 ns as seen in Fig. 1.6 on page 17, it seems the 2 ns difference of the RMS delay spread is tolerable.

According to the channel measurement in [43] and the Intel channel model in [42], it appears the LOS1 channel may occur for a 4 m separation between the transmitter and the receiver, the LOS2 channel may occur for less than a 4 m separation, and the NLOS1 channel may occur with a 10 m separation.

4.1.3 Parameters for BER and Outage Probability Analysis

In order to analyze BER, we need to simulate over AWGN and ISI. Here, we have 3 types of the BER analysis method; the Monte Carlo method (MC), the Quasi-analytic Monte Carlo method (Q-MC), and the BSM.

The MC method simulates over both the AWGN and the ISI, and the simulation stops when 200 errors are counted for each E_b/N_o. Hence for the target BER $= 10^{-4}$, this provides 95% confidence within 20% tolerance (see Appendix A).

The Q-MC method employs the $Q(\cdot)$ function to analytically calculate the BER

conditioned on the ISI as in equation (2.54) - (2.58) on page 48. Then it exhaustively averages the BER over the ISI terms. As stated earlier, if there are 20 data bits contributing to ISI for a NLOS channel, then the $Q(\cdot)$ function needs to be averaged over $2^{20} = 1048576$ possible ISI data sequences. Thus, in order to reduce the simulation time for the NLOS1 channel, we randomly generate the data sequence with length 10^5 and average the $Q(\cdot)$ function over the generated data sequence.

The BSM uses Fourier series to represent the probability of error, and then calculates the expected value of the ISI terms. We set $\omega_0 = 2\pi/600$, and $M = 1600$, which are the parameters for the Fourier series in the BSM as in equation (2.76) on page 52.

In the literature [36], [39], and [41], the uncoded target BER is set to be 10^{-3}, and with possible error-correction coding, the total target BER should be less than 10^{-5}. Therefore, for the outage probability calculation without coding, we set the outage threshold to be 10^{-4} and 10^{-5} for the LOS channel. For the NLOS channel, the outage threshold of 10^{-4} and 10^{-3} are used. Note that for the outage threshold 10^{-4} and 10^{-3}, error-correction coding is needed for acceptable performance.

4.2 The Simulation of a Single Multipath Fading Channel

To verify the three BER analysis methods and to understand the characteristics of CS and CH, we first consider a single multipath fading channel. This is for tutorial value only. Later, we evaluate the average BER and the outage probability for an ensemble of channels from the Intel model [42], which is felt to be of practical value.

4.2.1 Comparison of Performance Analysis Methods

The MC method, the Q-MC method, and the BSM are compared in this section. In the simulation, we use the MC method to confirm the validity of the Q-MC method. Then, we verify the accuracy of the BSM using the Q-MC method.

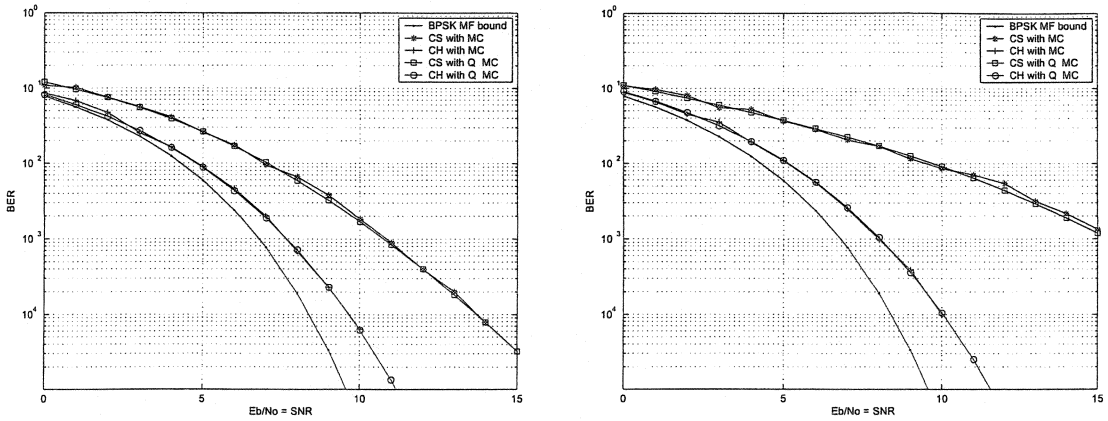

(a) WH(16) sequence at 374.2 Mbps, HP = (4 9 10 8)

(b) GL(15) sequence at 399.2 Mbps, HP = (12 7 15 5)

Figure 4.1: The comparison of the MC and the Q-MC with 10 fingers for a single LOS1 channel (Channel Number = 3588)

First, we compare the MC method with the Q-MC method. We generate a single LOS1 channel, and then compare the BER of the MC with the Q-MC method. Fig. 4.1 shows the BER of the WH(16) sequence and of the GL(15) sequence with a single LOS1 channel. In the figure, HP denotes the hopping pattern. As can be seen in Fig. 4.1, the MC and the Q-MC methods agree well each other. Due to the simulation time, the MC and the Q-MC methods are compared in the limited BER region down to 10^{-4}. Therefore it is verified that the Q-MC method is correct for the BER above 10^{-4}, and we assume this method is also valid for the BER below 10^{-4}.

Next, we compare the Q-MC method with the BSM. The BER of the Q-MC and the BSM are compared in Fig. 4.2. As is seen in the figure, the BSM gives identical performance to that of the Q-MC method. However, for the BER below 10^{-15}, or E_b/N_o over 35 dB, the BER of the BSM may start to oscillate and fail due to the numerical instability. However, the BSM with the parameters given in Section 4.1.3 is safe to use in the region of our interest, such as BER down to $10^{-6} \sim 10^{-7}$.

Since we have compared and verified the three BER analysis methods, we will mainly use the BSM in finding the average BER, and the outage probability. We do

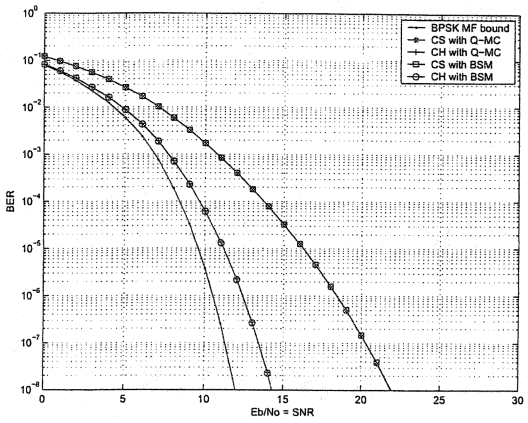

(a) WH(16) sequence at 374.2 Mbps, HP = (4 9 10 8)

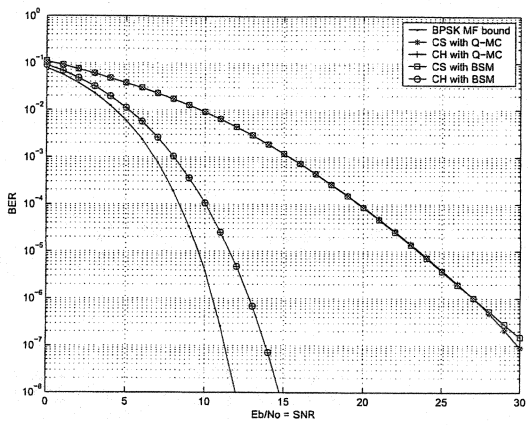

(b) GL(15) sequence at 399.2 Mbps, HP = (12 7 15 5)

Figure 4.2: The comparison of the Q-MC and the BSM with 10 fingers for a single LOS1 channel

such as the BSM is more computationally efficient than the other two methods.

4.2.2 A single LOS1 Multipath Fading Channel

We evaluate the performance of CH for a single LOS1 multipath fading channel. The single LOS1 channel used is shown in Fig. 1.4 on page 16.

The BER of all the WH(16) and the GL(15) sequences with 5 Rake fingers for the single LOS1 channel is shown in Fig. 4.3. Due to the different auto-correlation functions of all the sequences, the performance of each sequence varies in the multipath fading channel. Therefore, the proper assignment of the sequence or CS can significantly improve BER when the channel is slowly changing in time. If the channel is changing quickly or averaged over time or space, all of the sequences will produce similar performance. Note that in Fig. 4.3, the GL(15) sequence generally performs better than the WH(16) sequence because the auto-correlation function of the GL(15) sequence is more controlled than that of the WH(16) sequence. However such a disadvantage of the WH(16) sequence can be improved by CH because it turns the impact of the ISI terms into both cross-correlation and auto-correlation functions.

Fig. 4.4 shows the BER of the same LOS1 channel with CH. In Fig. 4.4(a) the

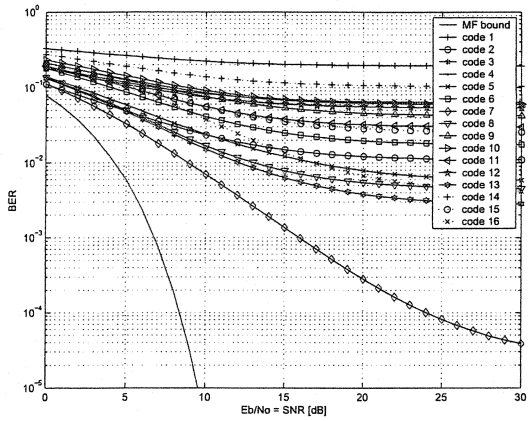

(a) WH(16) all sequences at 374.2 Mbps

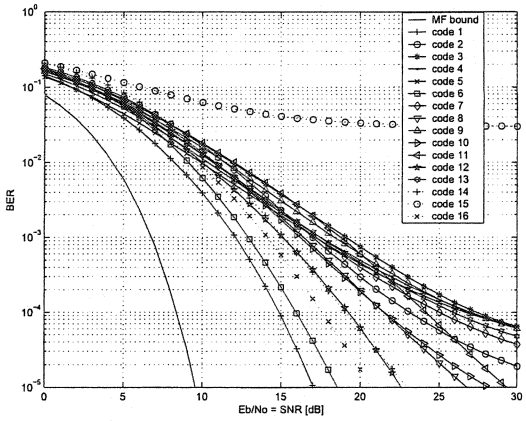

(b) GL(15) all sequences at 399.2 Mbps

Figure 4.3: The BER of all sequences with 5 fingers for a single LOS1 channel

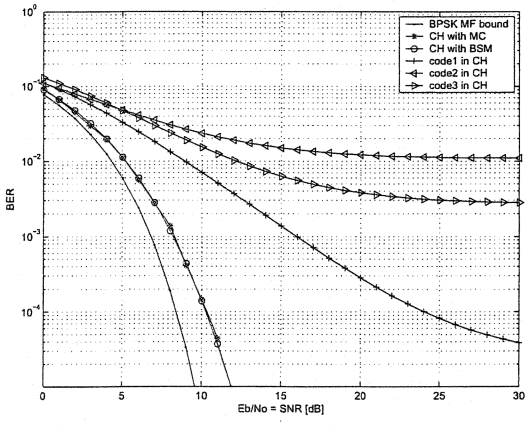

(a) WH(16) CH at 374.2 Mbps, HP = (7, 2, 3)

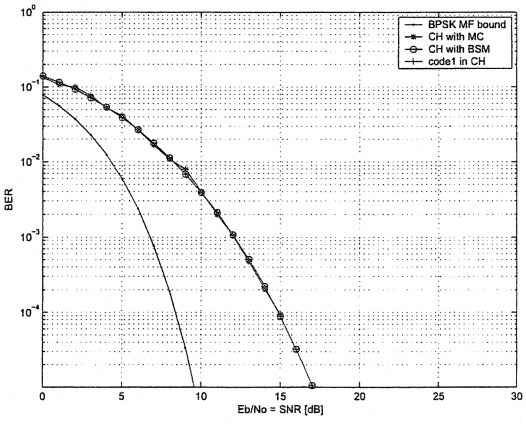

(b) GL(15) CH at 399.2 Mbps, HP = (1)

Figure 4.4: The BER of CH with 5 fingers for a single LOS1 channel

length 3 CH pattern was found with the WH(16) sequence. Note that the BER of the individual sequence used in CH is also shown in the figure, and each of them with the WH(16) sequence has poor BER. However, when they are combined for CH, it shows significant improvement by effectively compensating for ISI. On the other hand, for the GL(15) sequence shown in Fig. 4.4(b) the CH pattern search algorithm could not find the CH pattern that performs better than the best CS shown in Fig. 4.3(b). Thus it simply selected CS even for the CH case. This can often happen with the GL(15) sequence because it has relatively well controlled cross-correlation and auto-correlation functions. However, as the number of ISI terms gets larger such as for the NLOS1 channel, it has higher probability to find a good CH pattern. Moreover, more reliable performance measures will be discussed in the next section; average BER and outage probability. There, CH will be beneficial for both the WH(16) and the GL(15) sequences.

Fig. 4.5 illustrates the number of Rake fingers versus the BER of the WH(16) sequence. It is observed that CH can reduce the number of fingers required to achieve a certain BER. For example, if the BER of 10^{-4} is required for 12 dB, CS needs at least 9 fingers to achieve it, while CH needs only 5 fingers. Therefore for the same E_b/N_o, CH will be able to reduce the number of Rake fingers required at the receiver causing less complexity. In other words, if the same number of Rake fingers are used, then CH can reduce the transmitted power required at the receiver to get a certain BER. For example, if the number of fingers is fixed to 9, the CS method with WH(16) sequence needs about 12 dB to get the BER of 10^{-4}, while the CH method needs about 8.5 dB. Therefore with a given complexity of the receiver, the CH can provide a more power efficient method with a slight increase in complexity. Note that the CH pattern in Fig. 4.5 may be different for each number of fingers since the CH pattern search algorithm also depends on the number of Rake fingers as well as the CSI and the spreading sequence.

Similarly, Fig. 4.6 shows the number of fingers versus the BER of the GL(15)

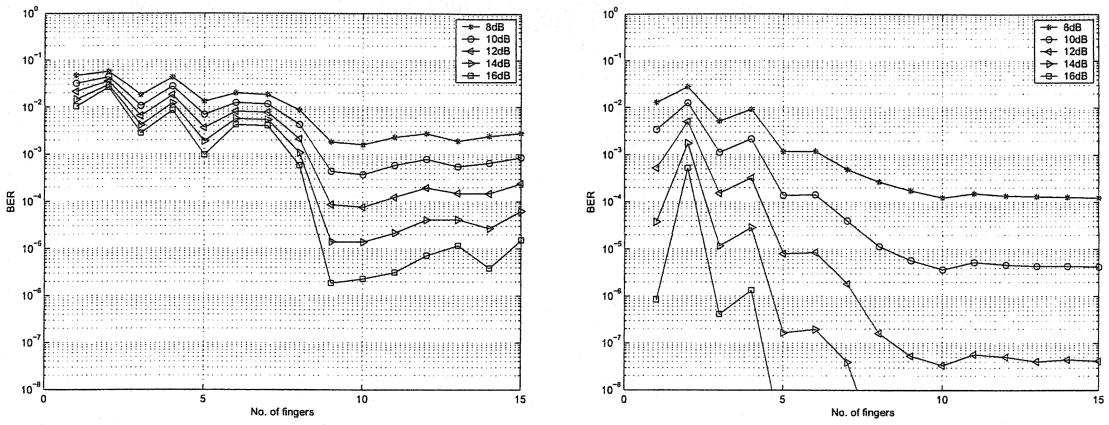

(a) WH(16) with CS at 374.2 Mbps

(b) WH(16) with CH at 374.2 Mbps

Figure 4.5: The number of fingers vs. the BER of the WH(16) sequence for a single LOS1 channel

sequence. Since the CH pattern search algorithm could not find better CH patterns for most of the fingers with the GL(15) sequence, the BER curves with CH are similar to those with CS. However CH shows a lower BER with 4 fingers with which a better CH pattern was found. Therefore CH is always better than or equivalent to CS, but CH with the GL(15) sequence is not beneficial for this single channel.

4.2.3 A Single LOS2 Multipath Fading Channel

We investigate another single LOS channel (LOS2) of which the channel parameters are given in Table 4.1. The LOS2 channel has the shorter mean excess delay and the less number of significant paths compared to those of the LOS1 channel. Fig. 1.5 on page 17 shows the single LOS2 channel used in the simulation.

Fig. 4.7 shows the BER of all sequences for the LOS2 channel. In the figure, the error floor is not observed because there are not many ISI terms. It is observed that wider performance variability occurs with the WH(16) sequence than with the GL(15) sequence. This is due to the poor auto-correlation function of the WH(16) sequence, which causes the SI and the ISI terms to influence the BER. Since the SI term in (2.56) on page 48 is deterministic for the given CSI and the spreading sequence, it can be helpful by properly selecting the sequence. In fact the low BER curves in Fig.

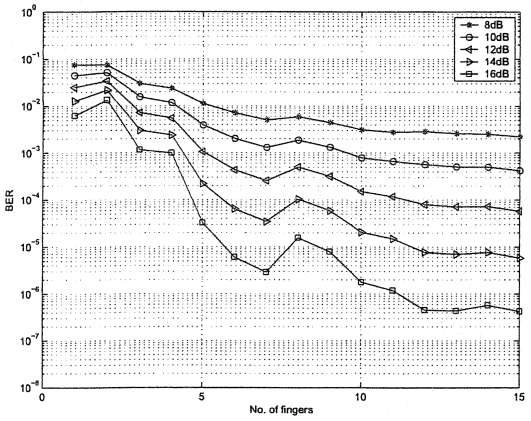

(a) GL(15) with CS at 399.2 Mbps

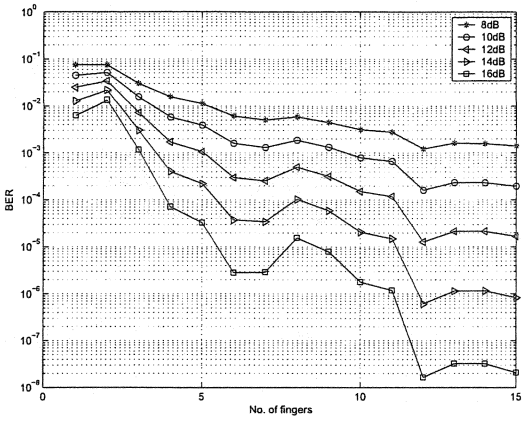

(b) GL(15) with CH at 399.2 Mbps

Figure 4.6: The number of fingers vs. the BER of GL(15) sequence for a single LOS1 channel

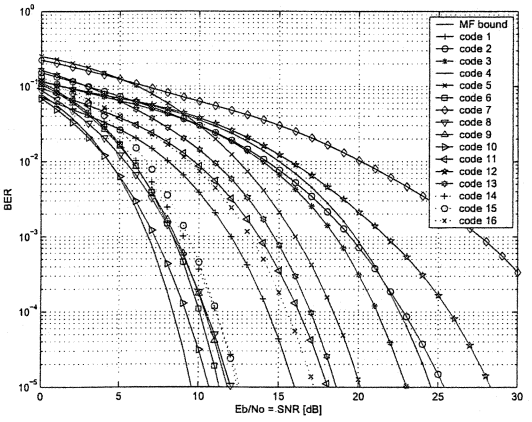

(a) WH(16) all sequences at 374.2 Mbps

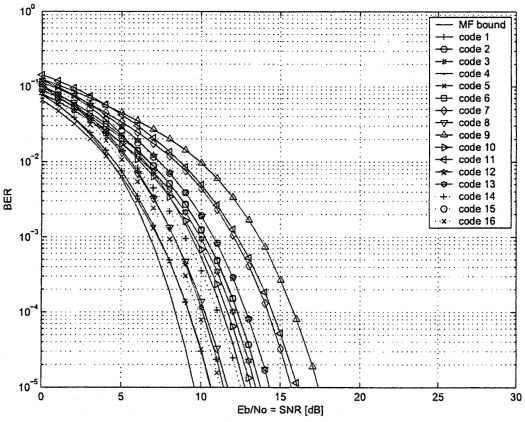

(b) GL(15) all sequences at 399.2 Mbps

Figure 4.7: The BER of all sequences with 5 fingers for a single LOS2 channel

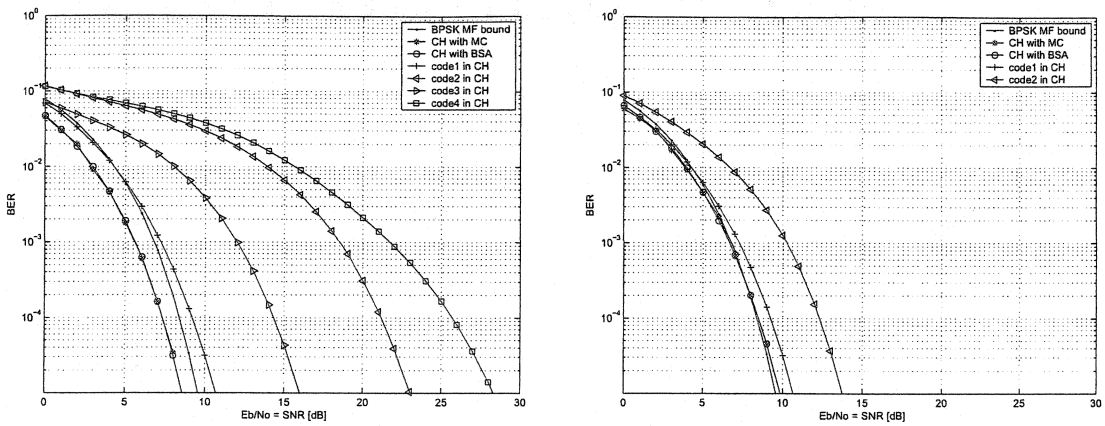

(a) WH(16) CH at 374.2 Mbps, HP = (10, 3, 1, 12)

(b) GL(15) CH at 399.2 Mbps, HP = (5, 2)

Figure 4.8: The BER of CH with 5 fingers for a single LOS2 channel

4.7 are achieved by the SI terms that is aiding the desired signal term.

Fig. 4.8 shows the BER of CH for the same LOS2 channel. It is notable that the WH(16) sequence with CH has lower BERs than the matched filter bound in this figure. This can be explained in several ways.

First, from (2.59) on page 49, the matched filter output of the received signal can be expressed as

$$y_{tot} = AT\{U_s + U_{si}(\xi)\}b_\xi + AT \cdot U_{isi}(\xi,\ \mathbf{b}) + y_{N_R}. \tag{4.1}$$

In a long code DSSS system, since the spreading sequence and its auto-correlation function is virtually random, both the SI term, $U_{si}(\xi)$, and the ISI term, $U_{isi}(\xi,\ \mathbf{b})$, are considered random, so both of them are desired to be suppressed as much as possible. Therefore, in (4.1), only $AT \cdot U_s b_\xi$ is considered as a signal term although more energy than just $AT \cdot U_s b_\xi$ is received. If we assume the spreading sequence has ideal auto-correlation function, $U_{si}(\mathbf{a})$ and $U_{isi}(\xi,\ \mathbf{b})$ will become zero, and then (4.1) will be given by

$$y_{tot} = AT \cdot U_s b_\xi + y_{N_R}. \tag{4.2}$$

In such an ideal case, the BER of CH will become the same as that of the matched filter bound. In this situation, we have forced other received signal terms, $AT \cdot U_{si}(\xi)b_\xi$ and

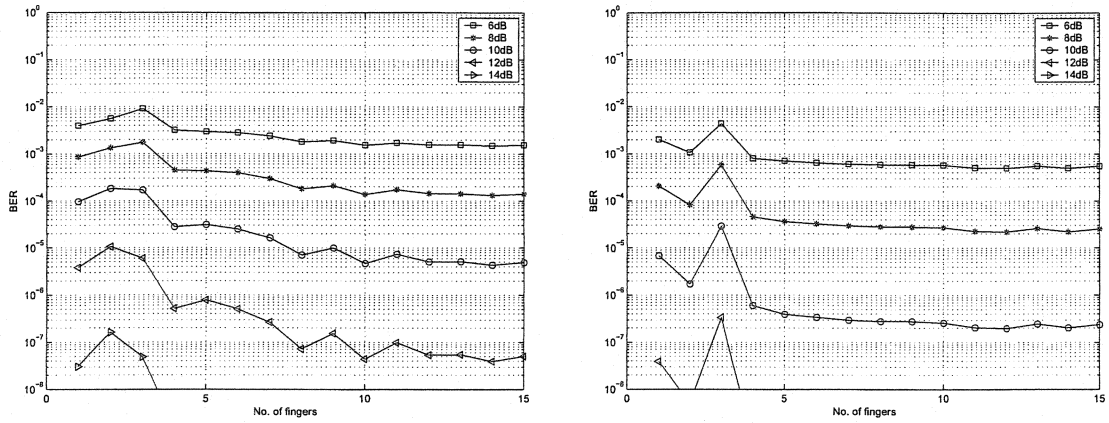

(a) WH(16) with CS at 374.2 Mbps

(b) WH(16) with CH at 374.2 Mbps

Figure 4.9: The number of fingers vs. the BER of the WH(16) sequence for a single LOS2 channel

$AT \cdot U_{isi}(\xi,\ \mathbf{b})$ to zero. However with a short code DSSS system, since the spreading sequence does not change in time, $U_{si}(\xi)$ is not random anymore. Therefore $AT \cdot U_{si}(\xi)$ can also be considered as a signal term. Furthermore, by properly selecting the spreading sequence, this term can positively add to the desired signal term, $AT \cdot U_s b_\xi$. Then, for a certain multipath fading channel, it is possible to achieve lower BER than the matched filter bound.

Second, the matched filter bound is the BER for the AWGN channel with a single arriving path, while the BER of CH is for a multipath fading channel plus AWGN. If we use the CH method for the AWGN channel, the BER of CH becomes the same as that of the matched filter bound because there will be no SI nor ISI term in the AWGN channel. Hence, in fact, it is not appropriate to compare the matched filter bound with CH for a multipath fading channel. However the matched filter bound can still give us a useful reference to see how good the CH method is. Therefore the matched filter bound will be used as the reference throughout this chapter.

Fig. 4.9 and Fig. 4.10 show the number of fingers versus the BER of the WH(16) sequence and of the GL(15) sequence, respectively. Note that in Fig. 4.9(b), when the number of fingers were increased from 2 to 3, the BER actually increased. Then

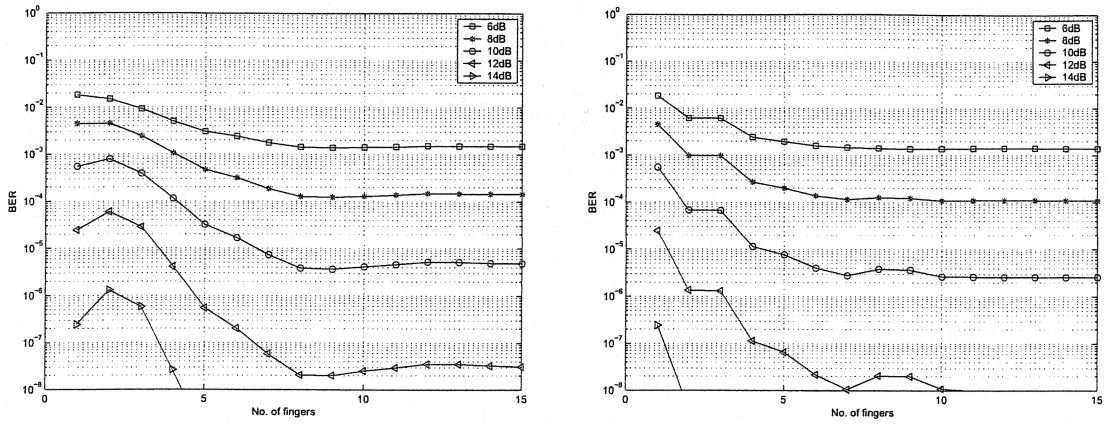

(a) GL(15) with CS at 399.2 Mbps

(b) GL(15) with CH at 399.2 Mbps

Figure 4.10: Number of fingers vs. BER of the GL(15) sequence for a single LOS2 channel

the BER starts to saturate as the number of fingers increases. Similar results are observed with the GL(15) sequence in Fig. 4.10

4.2.4 A Single NLOS1 Multipath Fading Channel

The single NLOS1 channel to be evaluated is shown in Fig. 1.6 on page 17. Due to the large number of multipath terms, the system is anticipated to suffer severe ISI. For the single NLOS1 channel, we consider two different bit rates. First, we evaluate the performance of the WH(16) and the GL(15) sequences at a high rate ($\approx$ 400 Mbps). Next, we lower the bit rate by increasing the processing gain and evaluate the performance. Besides, we also consider the WH sequence with length 32, WH(32), and the Gold sequence with length 31, Gold(31), for the same NLOS1 channel.

The Single NLOS1 Multipath Fading Channel at a High Rate

Fig. 4.11 shows the BER of all sequences with 20 fingers for a single NLOS1 channel. It is seen that both the WH(16) and the GL(15) sequences have the poor BER due to the ISI. Note that as the number of ISI terms gets larger, the individual GL(15) sequence starts to outperform the WH(16) sequence.

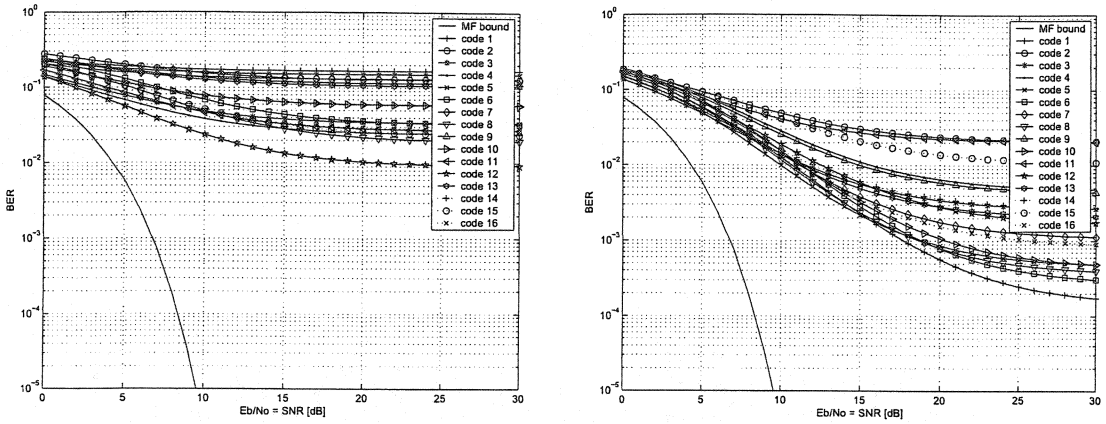

(a) WH(16) all sequences at 374.2 Mbps (b) GL(15) all sequences at 399.2 Mbps

Figure 4.11: The BER of all sequences with 20 fingers for a single NLOS1 channel

Fig. 4.12 shows the BER of CH and of each sequence used in CH with 20 fingers. When CH is used for the same NLOS1 channel, the significant improvement is achieved with the WH(16) sequence as well as with the GL(15) sequence.

Fig. 4.13 and Fig. 4.14 show the number of fingers versus the BER of the WH(16) sequence and the GL(15) sequence, respectively. It is notable that increasing the number of fingers does not linearly improve the BER, implying that simply choosing the strongest arriving paths for Rake fingers may not be the optimum combining method. However, we use this combining method throughout the simulation.

As will be shown later, for the performance of average BER and outage probability, the WH(16) and the GL(15) sequences are not good enough for the NLOS1 channel. However, this was not observed for the single NLOS1 channel. Thus, we need to consider the BER at a lower bit rate by increasing the processing gain.

There are a few ways to increase the processing gain or the length of the spreading sequence. It is possible to double the processing gain by extending the GL(15) and the WH(16) sequences. For example, if the original spreading sequence is [1101], then we can double the processing gain by repeating the each chip of the spreading sequence to yield a new sequence, [11110011]. If this method is used, it may be simpler to design a variable rate system depending on the condition of the channel. However

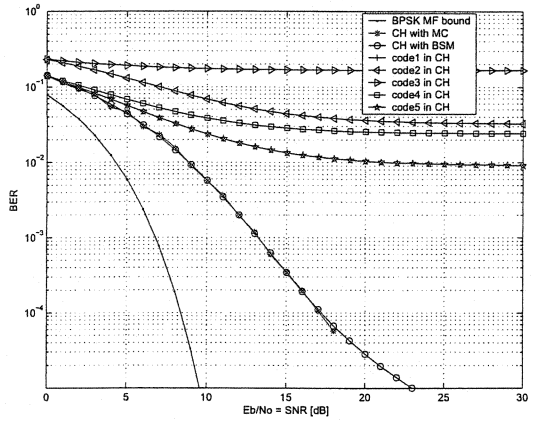

(a) WH(16) CH at 374.2 Mbps, HP=(12 6 14 12)

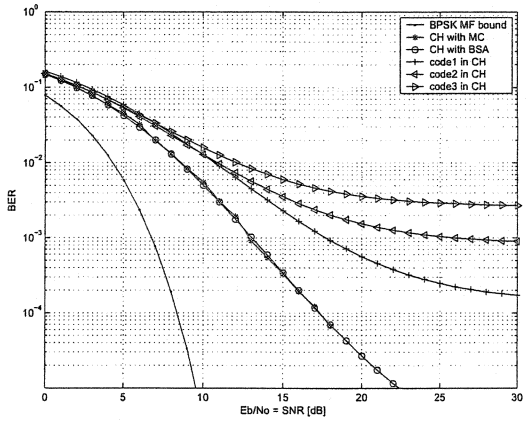

(b) GL(15) CH at 399.2 Mbps, HP=(1 16 4)

Figure 4.12: The BER of CH with the WH(16) and the GL(15) sequences with 20 fingers for a single NLOS1 channel

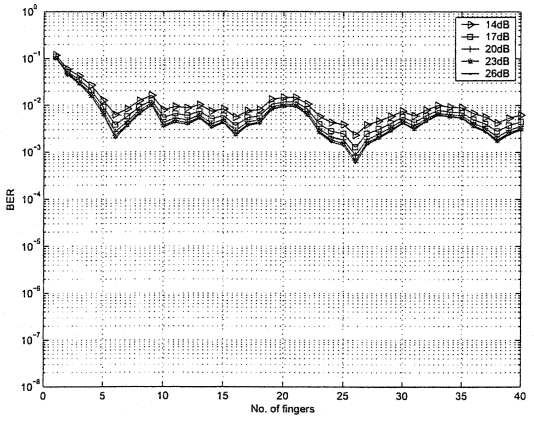

(a) WH(16) with CS at 374.2 Mbps

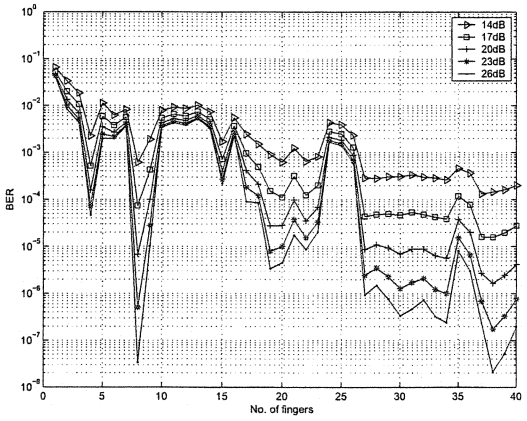

(b) WH(16) with CH at 374.2 Mbps

Figure 4.13: The number of fingers vs. the BER of the WH(16) sequence for a single NLOS1 channel

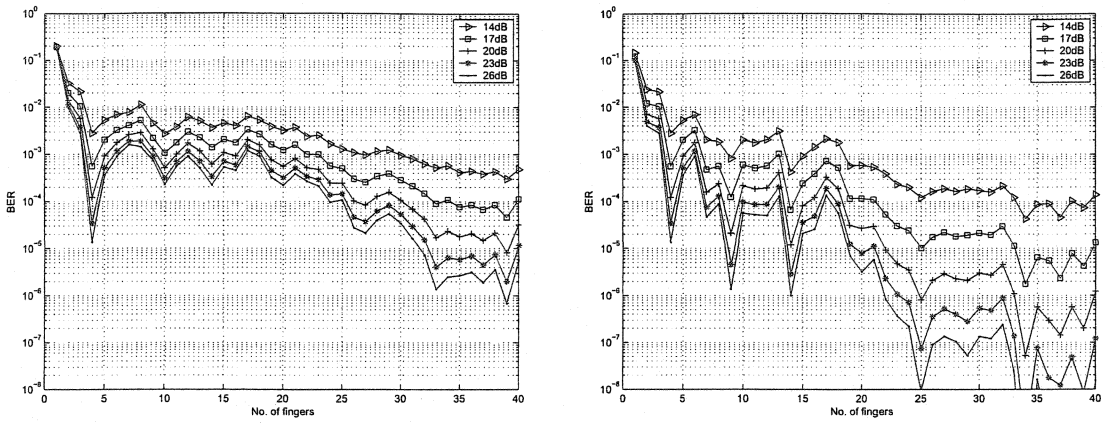

(a) GL(15) with CS at 399.2 Mbps

(b) GL(15) with CH at 399.2 Mbps

Figure 4.14: The number of fingers vs. the BER of the GL(15) sequence for a single NLOS1 channel

the extended sequences may have inferior correlation properties to other sequences with the same length. A more typical method to double the processing gain would be to use the WH(32) sequence and the Gold(31) sequence. We will first consider the performance of extended WH(32) and the extended GL(30) sequences, and then investigate the WH(32) and the Gold(31) sequences later.

The Single NLOS1 Multipath Fading Channel at a Lower Rate Using the Extended WH(32) and the Extended GL(30) Sequences

Fig. 4.15 shows the BER of all extended sequences with 20 fingers. If we compare this figure with the high rate one shown in Fig. 4.11, a significant gain is observed by lowering the bit rate. Fig. 4.16 shows the BER of CH with the extended sequences. Note that in Fig. 4.16(a), the stage-wise CH pattern search algorithm did not find the best CS but found the second best CS in the hopping pattern. Since the criterion developed in chapter 3 does not compute the actual BER but approximately evaluates the performance of sequences, the CS found by the stage-wise search method is not always the best in BER. However such an occurrence is rare. Fig. 4.17 and Fig. 4.18 shows the number of fingers versus the BER of CH with the extended WH(32) sequence and with the extended GL(30) sequence, respectively.

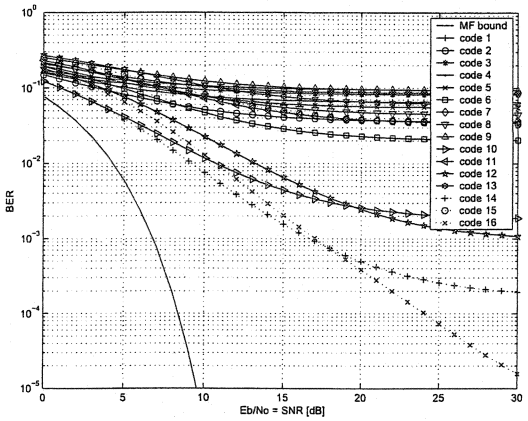

(a) Extended WH(32) all sequences at 187.1 Mbps

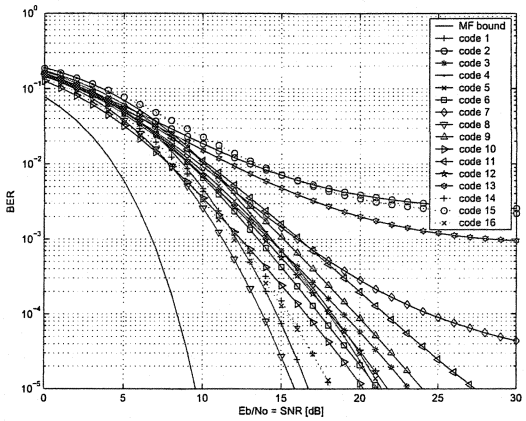

(b) Extended GL(30) all sequences at 199.6 Mbps

Figure 4.15: The BER of all extended sequences with 20 fingers for a single NLOS1 channel

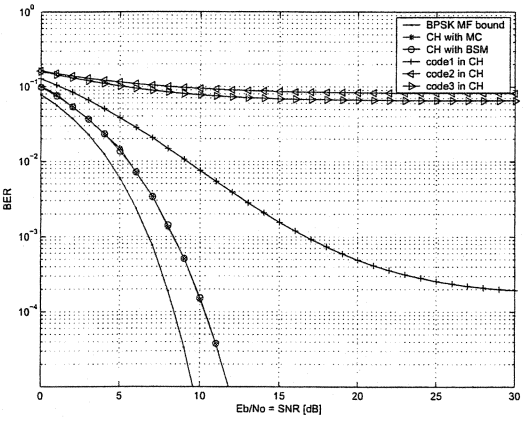

(a) Extended WH(32) CH at 187.1 Mbps, HP=(14 3 1)

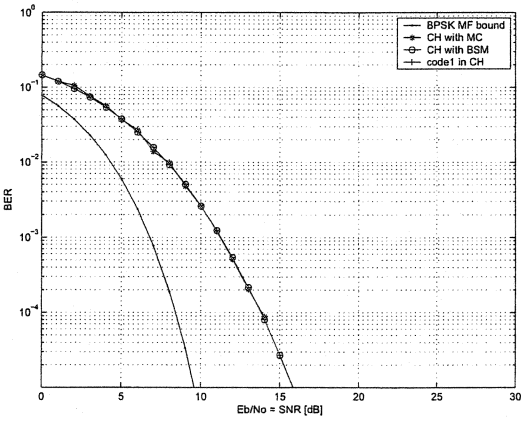

(b) Extended GL(15) CH at 199.6 Mbps, HP=(8)

Figure 4.16: The BER of CH with the extended WH(32) and the extended GL(15) sequences with 20 fingers for a single NLOS1 channel

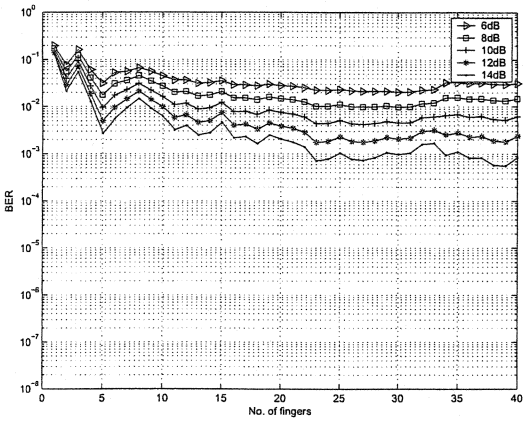

(a) Extended WH(32) with CS at 187.1 Mbps

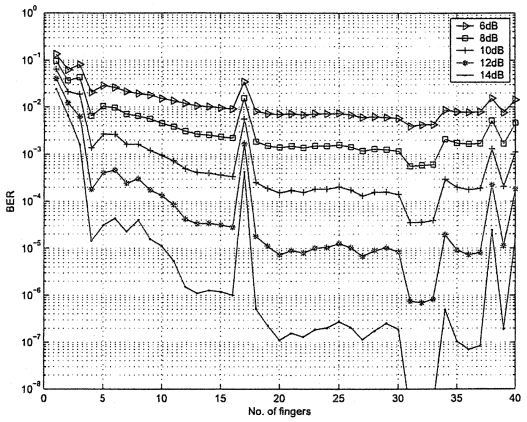

(b) Extended WH(32) with CH at 187.1 Mbps

Figure 4.17: The number of fingers vs. the BER of the extended WH(16) sequence for a single NLOS1 channel

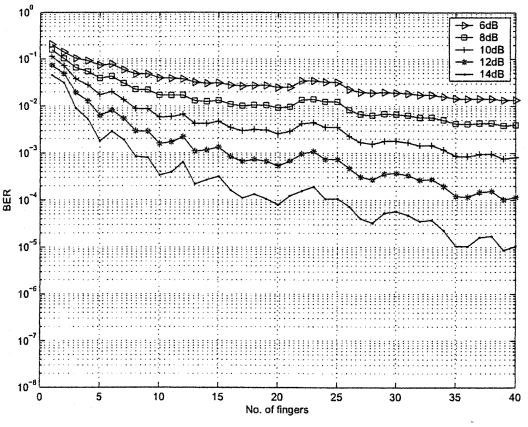

(a) Extended GL(30) with CS at 199.6 Mbps

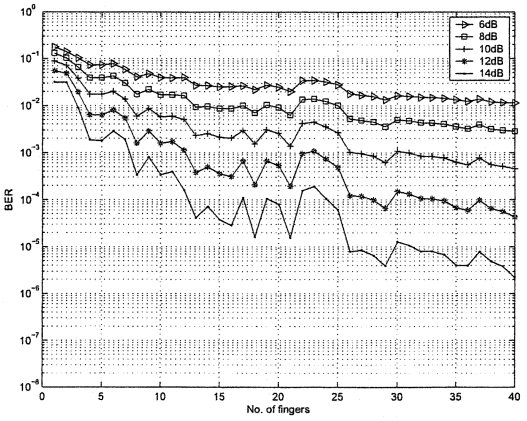

(b) Extended GL(30) with CH at 199.6 Mbps

Figure 4.18: The number of fingers vs. the BER of the extended GL(15) sequence for a single NLOS1 channel

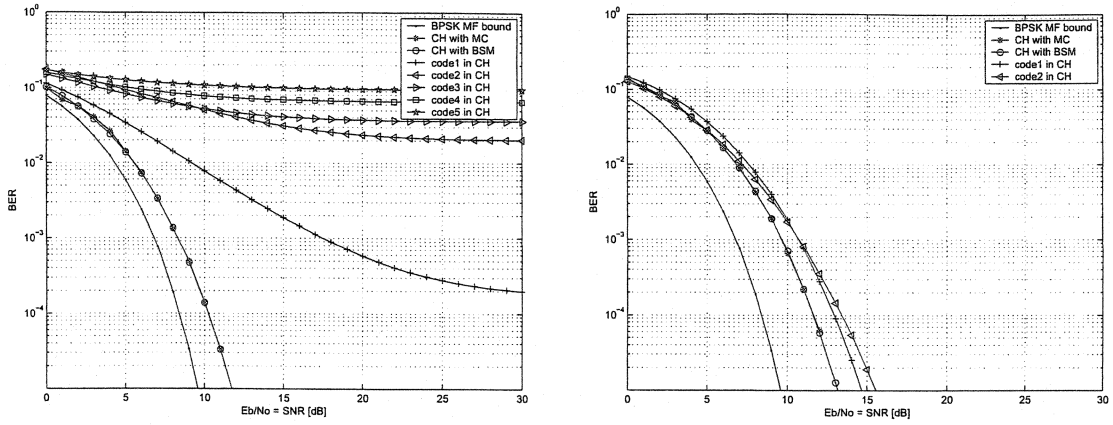

(a) WH(32) CH at 187.1 Mbps, HP=(28 30 3 1 7)

(b) Gold(31) CH at 193.1 Mbps, HP=(8 31)

Figure 4.19: The BER of CH with the WH(32) and the Gold(31) sequences with 20 fingers for a single NLOS1 channel

The Single NLOS1 Multipath Fading Channel at a Lower Rate Using the WH(32) and the Gold(31) Sequences

We now evaluate the performance of CH with the WH(32) sequence and the Gold(31) sequence. We do not show the BER curves of all sequences using the WH(32) and the Gold(31) sequences, but the BER curves are similar to those of the extended sequences.

Fig. 4.19 shows the BER of CH with the WH(32) and the Gold(31) sequences with 20 fingers for a single NLOS1 channel. Also, Fig. 4.20 and Fig. 4.21 shows the number of fingers versus BER of CH with the WH(32) sequence and with the Gold(31) sequence, respectively.

By comparing Fig. 4.12 with Fig. 4.16 and Fig. 4.19, we can see that increasing the processing gain significantly decreases the BER at the cost of the lower bit rate. Moreover, the WH(32) and the Gold(31) sequences perform slightly better than the extended WH(32) and the extended GL(30) sequences. However, if the above sequences are used for a single multipath channel, all of the sequences will show the identical performance.

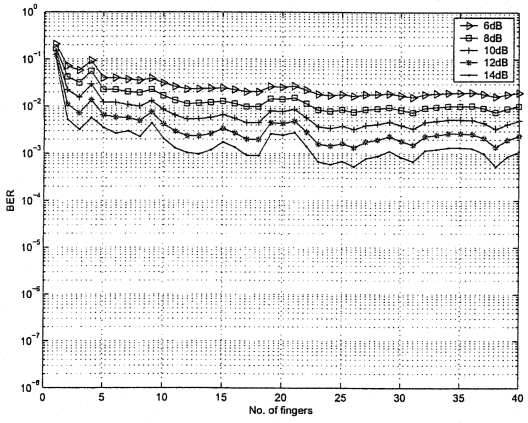

(a) WH(32) with CS at 187.1 Mbps

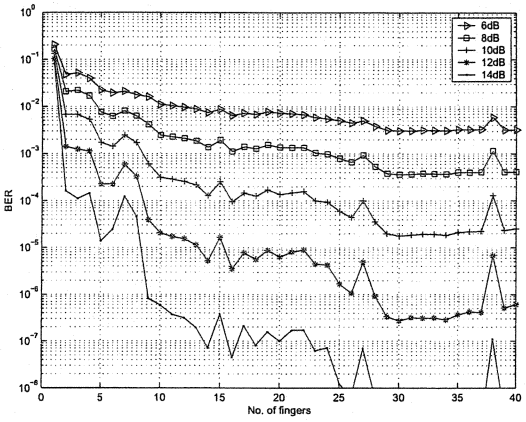

(b) WH(32) with CH at 187.1 Mbps

Figure 4.20: The number of fingers vs. the BER of the WH(32) sequence for a single NLOS1 channel

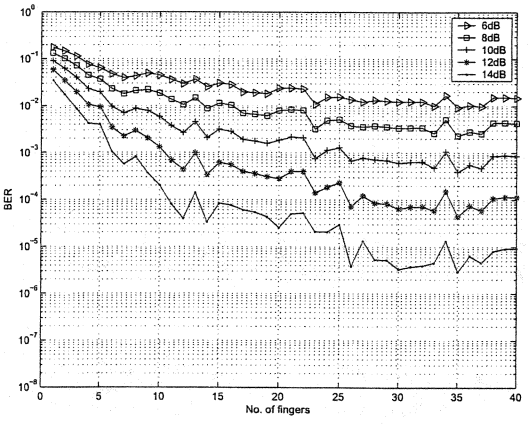

(a) Gold(31) with CS at 193.1 Mbps

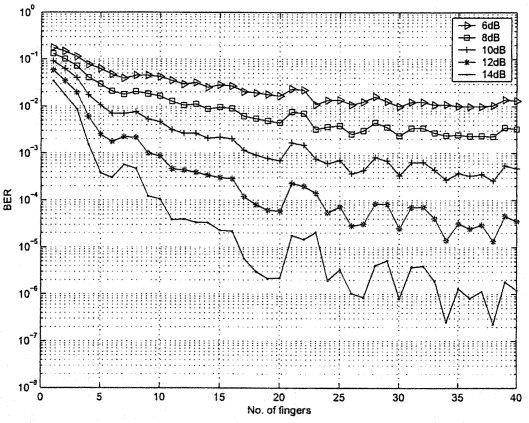

(b) Gold(31) with CH at 193.1 Mbps

Figure 4.21: The number of fingers vs. the BER of the Gold(31) sequence for a single NLOS1 channel

4.3 The Average BER and the Outage Probability of the Multipath Fading Channel

In this section, we evaluate the performance of CS and CH for the average BER and the outage probability. They are the most important performance criteria in this thesis. We first generate 7000 channels from the Intel model [42] using the parameters shown in Table 1.2 on page 16. If the target outage probability is 2 %, 7000 channels can provide 95 % confidence with 30 % tolerance (see Appendix A). We also empirically found that, 7000 and 5000 channels are good enough for the average BER and the outage probability to maintain the computational results within the confidence interval, respectively. To verify the confidence interval shown in Appendix A, we have generated two sets of 7000 channels with different set of random variables and computed the average BER and the outage probability. Then we checked that the results of two different set of 7000 channels were almost identical and met the confidence interval.

For each channel, using the CH pattern search algorithm described in Chapter 3, we find the suboptimal CH pattern and compute the BER using the BSM. The average BER is obtained by averaging each BER over 7000 channels. Then we also calculate the outage probability over the same 7000 channels. To calculate the outage probability, we obtain the probability that the BER of the NLOS1 channel is higher than a threshold for each E_b/N_o. Since the channel is assumed to be slowly changing in time, we put more emphasis on the outage probability than the average BER. If many bit errors occur in a certain bad channel, it significantly degrades the average BER. Then, we need to average over a large number of channels to average out that effect. However for the outage probability, many bit errors in a bad channel means one outage. In other words, the bad channel does not dominate the performance of the outage probability. Therefore for the slowly fading channel, the outage probability requires less number of channels to produce a reliable results than that for the average BER. For instance, as stated above, we have found that 5000 channels are sufficient for

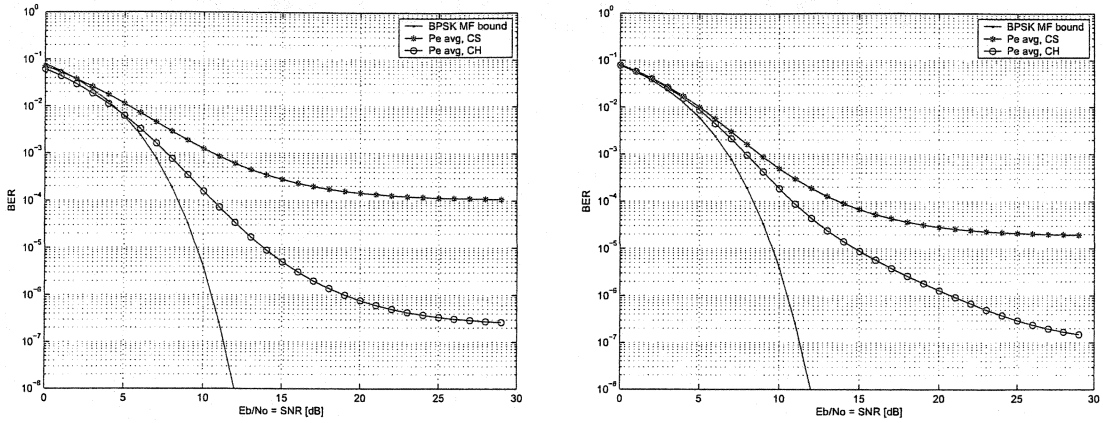

(a) WH(16) CH at 374.2 Mbps (b) GL(15) CH at 399.2 Mbps

Figure 4.22: Average BER with 10 fingers over 7000 LOS1 channels

the outage probability while 7000 channels are needed for the average BER. Moreover, the outage probability in this thesis can mean a spatial outage as well as a time outage.

4.3.1 The average BER and the Outage Probability for the LOS1 Channel

Performance with 10 Rake fingers

Fig. 4.22 shows the average BER with 10 fingers over 7000 LOS1 channels, and the characteristics of the LOS1 channel is shown in Table 4.1. For CS, the GL(15) sequence exhibits lower error floor than that of the WH(16) sequence. However, when CH is used, both sequences show similar performance. Fig. 4.22 also shows that for the BER of 10^{-4}, CH can achieve more than a 10 dB gain with the WH(16) sequence, while about a 2.5 dB gain is achieved with the GL(15) sequence. The gain by CH gets bigger as the target BER goes lower such as 10^{-5}.

Recall that the CH pattern can be sometimes identical to CS as the CH patterns of length 1 could be chosen. The frequency of this event is discussed later in Section 4.4.1. We found that CH contained the CH patterns of at least length two a significant number of times.

The outage probability of the LOS1 channel is shown in Fig. 4.23 with the 10^{-4}

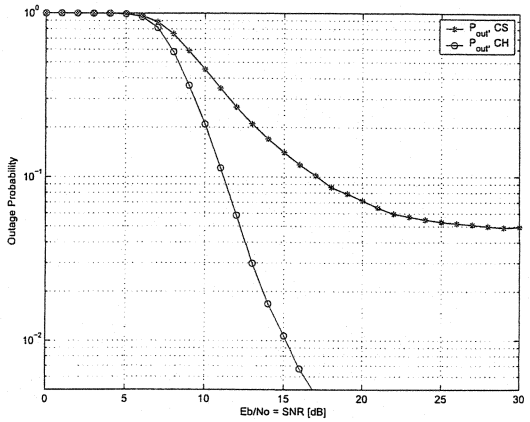

(a) WH(16) CH at 374.2 Mbps

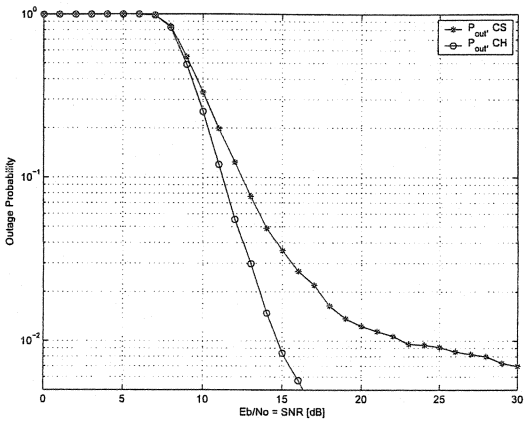

(b) GL(15) CH at 399.2 Mbps

Figure 4.23: Outage probability with 10 fingers over 7000 LOS1 channels, Th = 10^{-4}

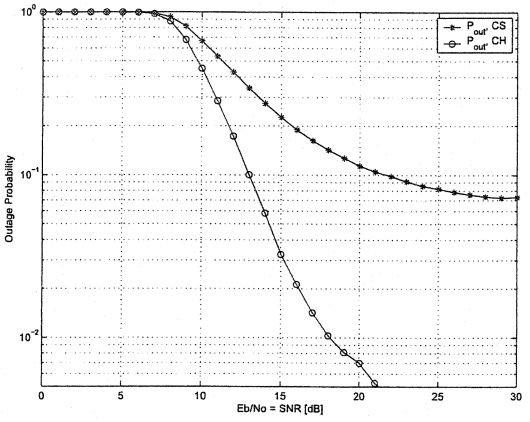

(a) WH(16) CH at 374.2 Mbps

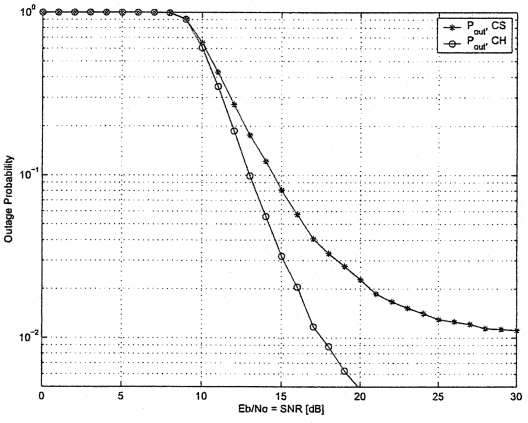

(b) GL(15) CH at 399.2 Mbps

Figure 4.24: Outage probability with 10 fingers over 7000 LOS1 channels, Th = 10^{-5}

threshold. If the 2% outage is tolerable in a system, CH with both the WH(16) sequence and the GL(15) sequence requires around 13.7 dB to meet the target outage. On the other hand, CS with the WH(16) sequence cannot meet the target outage due to the high error floor, and CS with the GL(15) sequence requires around 17.5 dB for the target outage. Therefore, the significant improvement of CH is observed with the WH(16) sequence, while the gain of CH with the GL(15) sequence is about 3.8 dB.

Fig. 4.24 shows another outage probability with the different threshold (Th=10^{-5}). It is seen that CH needs extra 2.5 dB to lower the outage threshold from 10^{-4} to 10^{-5},

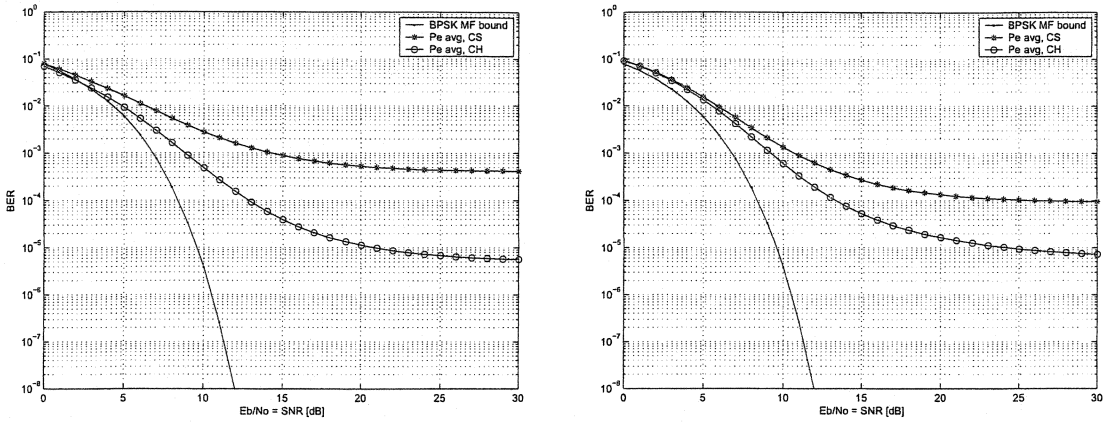

(a) WH(16) CH at 374.2 Mbps (b) GL(15) CH at 399.2 Mbps

Figure 4.25: Average BER with 5 fingers over 7000 LOS1 channels

while CS needs extra 4.5 dB with the GL(15) sequence.

Therefore, for the LOS1 channel, CH is better than CS with both the WH(16) and the GL(15) sequences for the average BER and for the outage probability.

Performance with 5 Rake fingers

We decrease the number of Rake fingers to 5 and simulate over the same LOS1 channels. Fig. 4.25 shows the average BER of the WH(16) and the GL(15) sequences with 5 fingers over 7000 LOS1 channels. Fig. 4.26 and Fig. 4.27 show the outage probability with 5 fingers over 7000 LOS1 channels using the 10^{-4} and the 10^{-5} threshold, respectively.

The performance with 5 fingers are similar to the previous results with 10 fingers, but it requires approximately 3 - 4 dB higher E_b/N_o to achieve the same performance. Moreover, the gain of CH with 5 fingers over CS is even bigger (over 9 dB).

4.3.2 The average BER and the Outage Probability for the LOS2 Channel

Performance with 10 Rake fingers

The average BER of CH over 7000 LOS2 channels are shown in Fig. 4.28. The characteristics of the LOS2 channel are described in Table 4.1. Since the LOS2

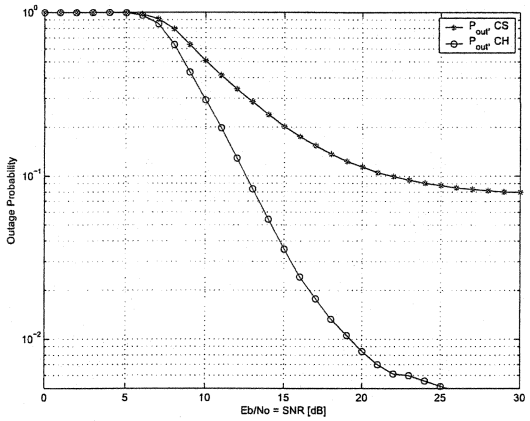

(a) WH(16) CH at 374.2 Mbps

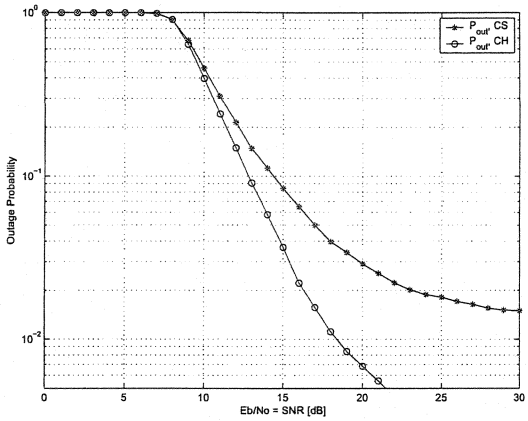

(b) GL(15) CH at 399.2 Mbps

Figure 4.26: Outage probability with 5 fingers over 7000 LOS1 channels, Th = 10^{-4}

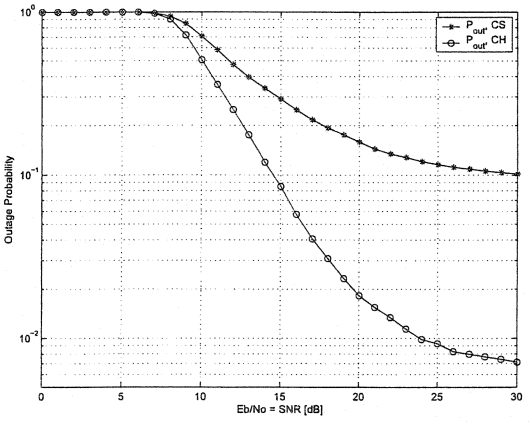

(a) WH(16) CH at 374.2 Mbps

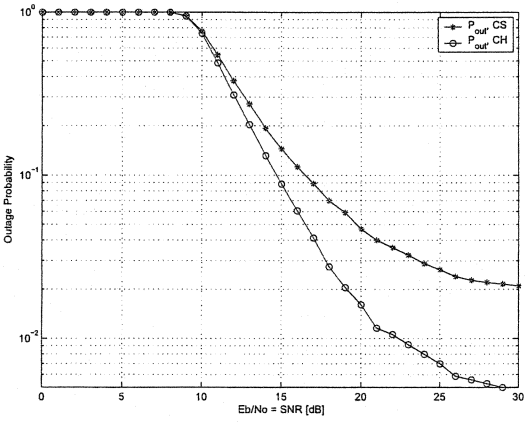

(b) GL(15) CH at 399.2 Mbps

Figure 4.27: Outage probability with 5 fingers over 7000 LOS1 channels, Th = 10^{-5}

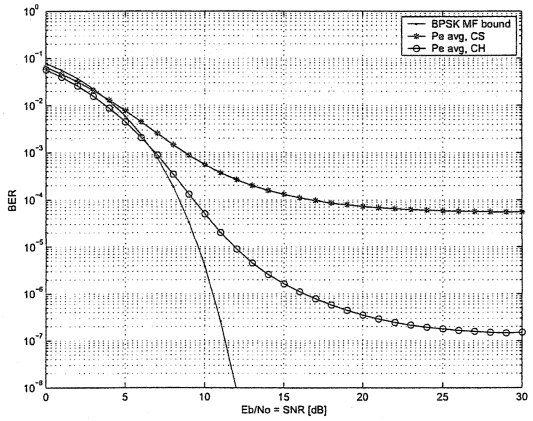

(a) WH(16) CH at 374.2 Mbps

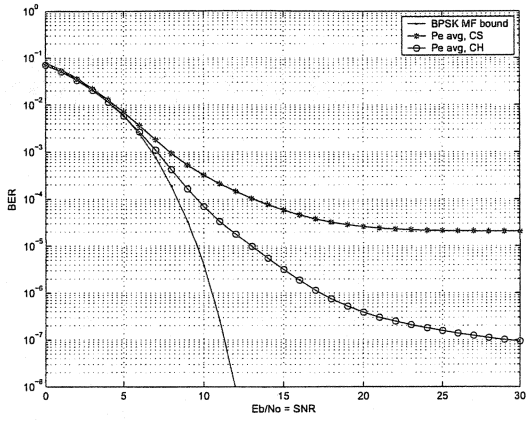

(b) GL(15) CH at 399.2 Mbps

Figure 4.28: Average BER with 10 fingers over 7000 LOS2 channels

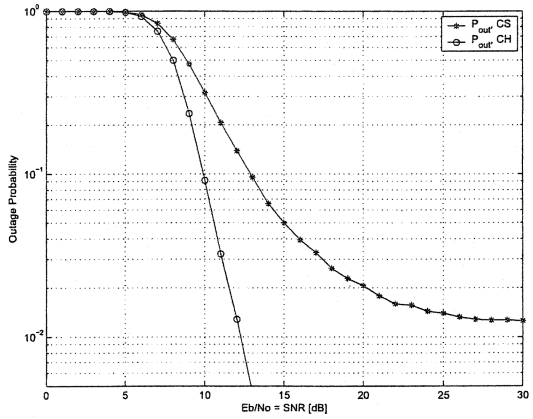

(a) WH(16) CH at 374.2 Mbps

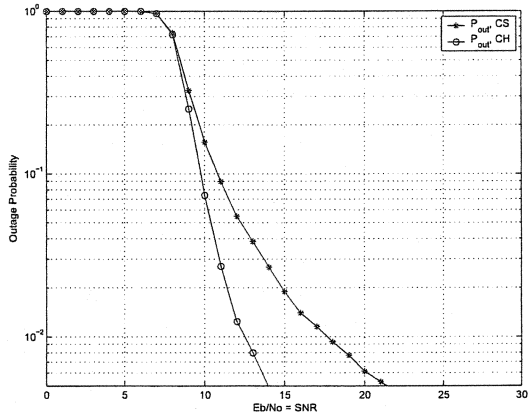

(b) GL(15) CH at 399.2 Mbps

Figure 4.29: Outage probability with 10 fingers over 7000 LOS2 channels, Th = 10^{-4}

channel has a lower number of multipath terms than those of the LOS1 channel, it requires less E_b/N_o to obtain the same BER. For CH with the WH(16) sequence, about a 6 dB gain is observed over CS at BER of 10^{-4}, while about a 3.5 dB gain is achieved with the GL(15) sequence at the same BER. The gain of CH over CS gets even bigger for lower target BER such as 10^{-5}.

Fig. 4.29 shows the outage probability for the LOS2 channel with the 10^{-4} threshold. If the target outage is 2%, then CH with the WH(16) sequence achieves a 8.5 dB gain over CS, and CH with the GL(15) sequence obtains a 3.5 dB gain over CS.

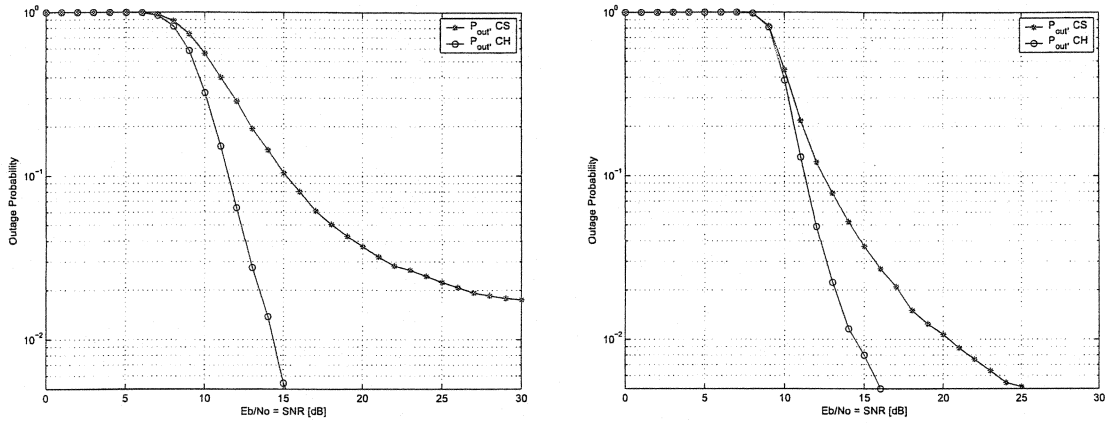

(a) WH(16) CH at 374.2 Mbps (b) GL(15) CH at 399.2 Mbps

Figure 4.30: Outage probability with 10 fingers over 7000 LOS2 channels, Th = 10^{-5}

The outage probability with the 10^{-5} threshold is shown in Fig. 4.30. CH with the WH(16) sequence shows around a 12 dB gain over CS for the 2% outage probability. CH with the GL(15) sequence shows around a 3.8 dB gain over CS.

If we assume that the LOS2 channel occurs at less than a 4 m separation of the transmitter and the receiver, not only the data rate over 200 Mbps should be supported, but also a even higher bit rate is preferred in a closer distance [37]. If CH is used for the LOS2 channel, it might not need the error-correction coding to achieve the target BER of 10^{-5} with given power constraint. Then it is possible for a CH system to achieve a bit rate higher than 200 Mbps. For example, CH needs around 13.5 dB to obtain 2% outage probability with the 10^{-5} threshold. Here the achievable bit rate is 374.2 Mbps with the WH(16) sequence and 399.2 Mbps with the GL(15) sequence.

Therefore, for the LOS2 channel, we have similar results to those for the LOS1 channel. Namely, CH is better than CS for all cases. It is noticeable that the performance of CH with both the WH(16) and the GL(15) sequences are very close to each other for the LOS1 and the LOS2 channel.

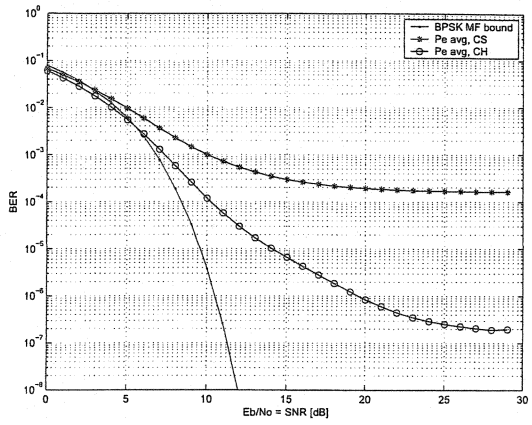

(a) WH(16) CH at 374.2 Mbps

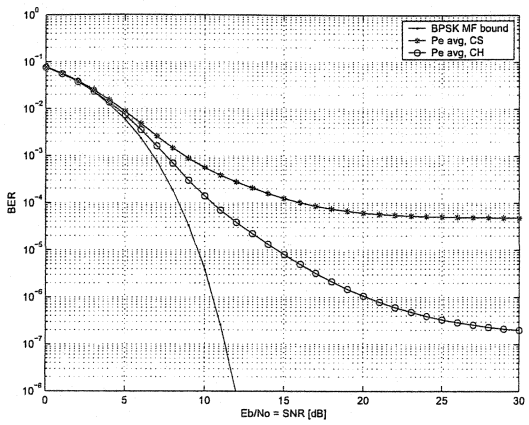

(b) GL(15) CH at 399.2 Mbps

Figure 4.31: Average BER with 5 fingers over 7000 LOS2 channels

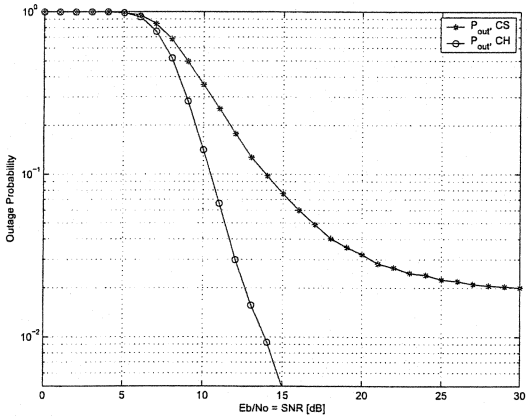

(a) WH(16) CH at 374.2 Mbps

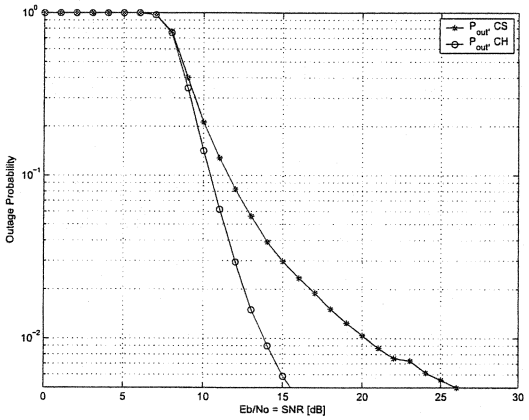

(b) GL(15) CH at 399.2 Mbps

Figure 4.32: Outage probability with 5 fingers over 7000 LOS2 channels, Th = 10^{-4}

Performance with 5 Rake fingers

We now decrease the number of fingers to 5 and evaluate the performance for the LOS2 channel. Fig. 4.31 shows the average BER with 5 fingers over 7000 LOS2 channels. Fig. 4.32 and Fig. 4.33 show the outage probability with 5 fingers over the 7000 LOS2 channels with the 10^{-4} and the 10^{-5} threshold, respectively.

As can be seen in the figures, if we use 5 fingers for the LOS2 channel, we need to increase approximately 1 dB more to achieve the same performance as with 10 fingers. Thus, there is not much loss observed by decreasing the number of fingers from 10 to

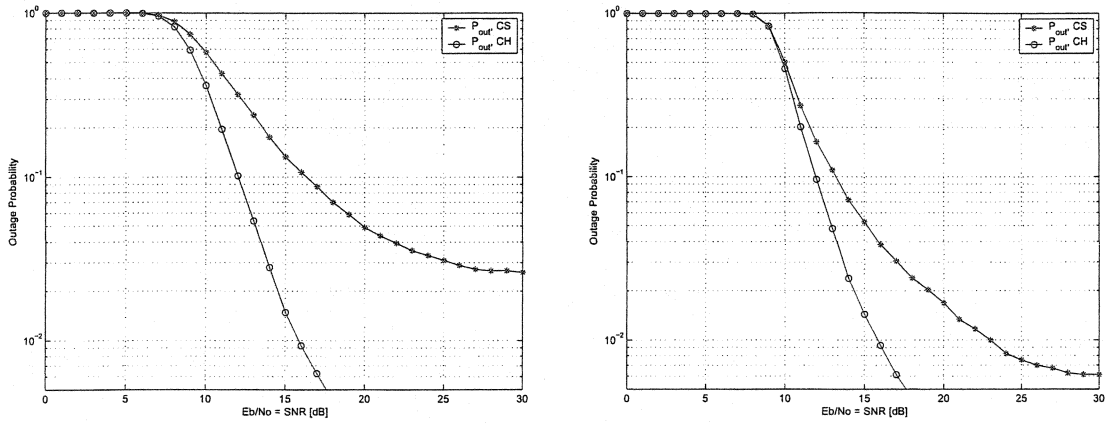

(a) WH(16) CH at 374.2 Mbps (b) GL(15) CH at 399.2 Mbps

Figure 4.33: Outage probability with 5 fingers over 7000 LOS2 channels, Th = 10^{-5}

5 for the LOS2 channel. This implies that the average number of significant arriving paths is not too large for the LOS2 channel. In fact, as is shown in Table 4.1, the average number of significant paths (NP_{10dB}) is 3.96 for the LOS2 channel.

4.3.3 The Average BER and the Outage Probability of the NLOS1 Channel

For the NLOS channel, our goal is to provide a possibility with CH to achieve at least a 110 Mbps data rate with the 2% total outage probability using the 10^{-5} threshold either with or without coding. First we evaluate the performance with length 15 or 16 sequences at a high rate (over 370 Mbps), and then we lower the bit rate.

A High Bit Rate with the WH(16) and the GL(15) sequences

Due to the large number of multipath terms in a NLOS1 channel ($NP_{10dB} = 35$), it is challenging to efficiently collect the received signal energy for a high rate system. Fig. 4.34 shows the average BER of CH with 40 fingers over 7000 NLOS1 channels. For the NLOS1 channel at a high rate, ISI seems to be the dominant factor of degradation. Although 40 Rake fingers were combined to collect received signal energy, the error floors are still high. For the NLOS1 channel, it seems that the GL(15) sequence shows slightly better performance than the WH(16) sequence.

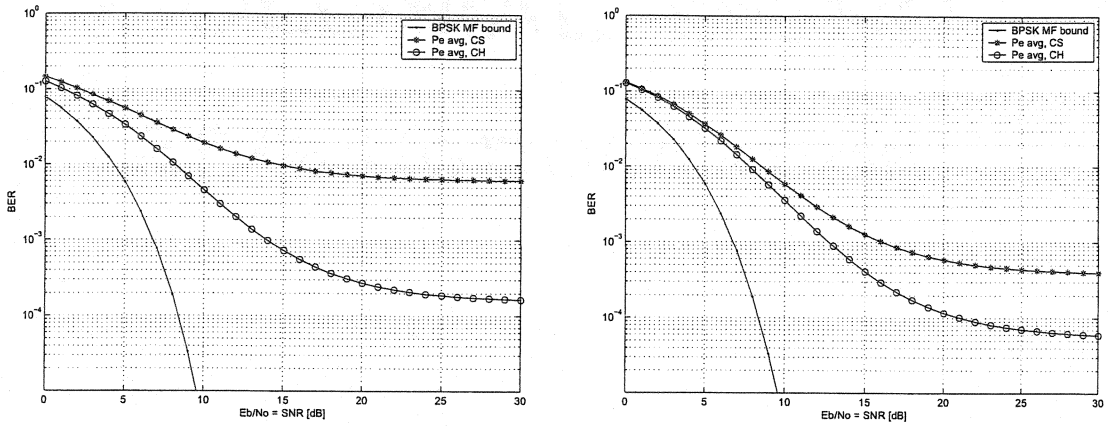

(a) WH(16) CH at 374.2 Mbps (b) GL(15) CH at 399.2 Mbps

Figure 4.34: Average BER with 40 fingers over 7000 NLOS1 channels

The outage probability with the 10^{-4} threshold is shown in Fig. 4.35. The target outage probability of 2% with the 10^{-4} threshold is not achieved even with 40 fingers. A possible solution is to loosen the threshold for the outage probability. One research group from Intel Corp.[41] suggested setting the uncoded BER to 10^{-3} and then lowering the total BER down to 10^{-5} by error-correction coding. Similar suggestion is also found in [36]. However, this requires further study in our case since we do not consider coding. In any case, assuming this error-correction coding can can be attained, we lower the threshold to 10^{-3} and compute the outage probability. Fig. 4.36 shows the outage probability with the 10^{-3} threshold. However, even with the 10^{-3} threshold, CH with the WH(16) sequence is unable to reach the 2% outage probability, while CH with the GL(15) sequence achieves the target. Thus, CH with the GL(15) sequence starts to perform better than CH with the WH(16) sequence for the NLOS1 channel, which was not observed in the LOS channel.

Lowering the threshold can be one solution with the GL(15) sequence but there is still a remaining concern that 40 Rake fingers are used to collect the signal energy. Although increasing the number of fingers generally improves BER and can provide a power efficient receiver, 40 is not the attractive number of Rake fingers from a practical point of view. Furthermore, CH with the WH(16) sequence needs even

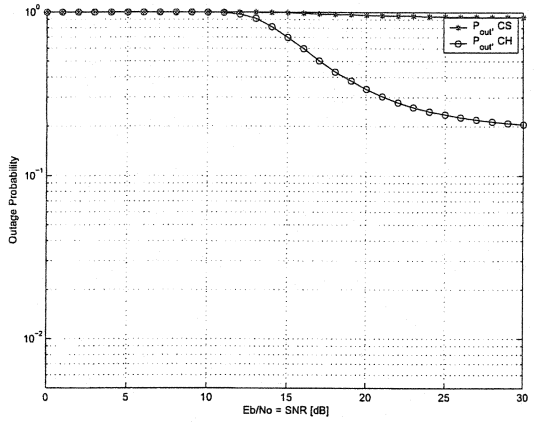

(a) WH(16) CH at 374.2 Mbps

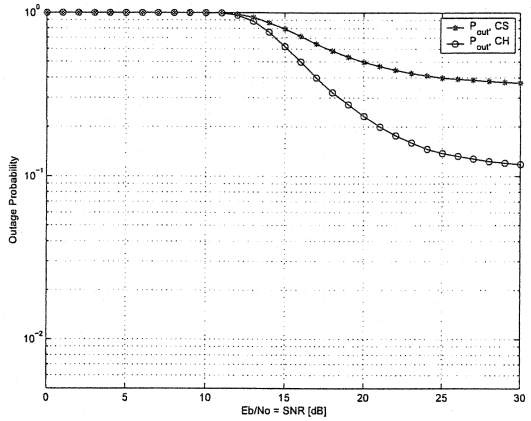

(b) GL(15) CH at 399.2 Mbps

Figure 4.35: Outage probability with 40 fingers over 7000 NLOS1 channels, Th = 10^{-4}

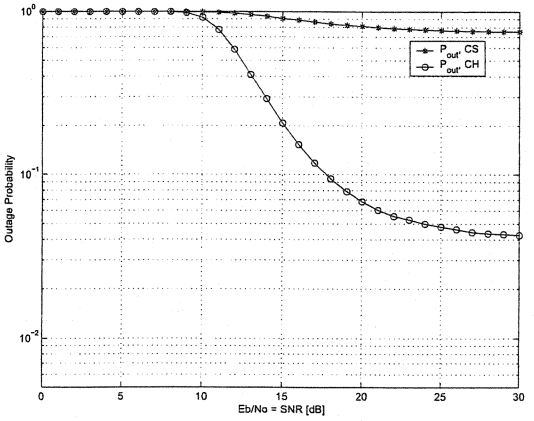

(a) WH(16) CH at 374.2 Mbps

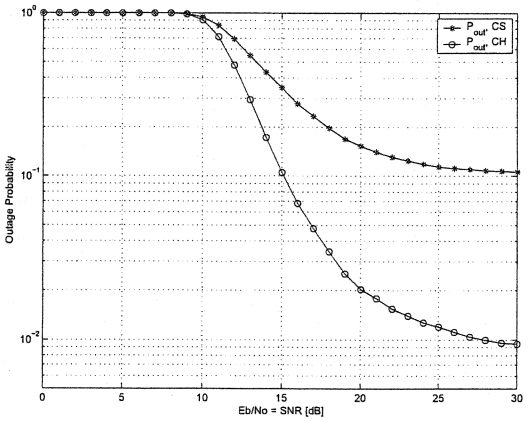

(b) GL(15) CH at 399.2 Mbps

Figure 4.36: Outage probability with 40 fingers over 7000 NLOS1 channels, Th = 10^{-3}

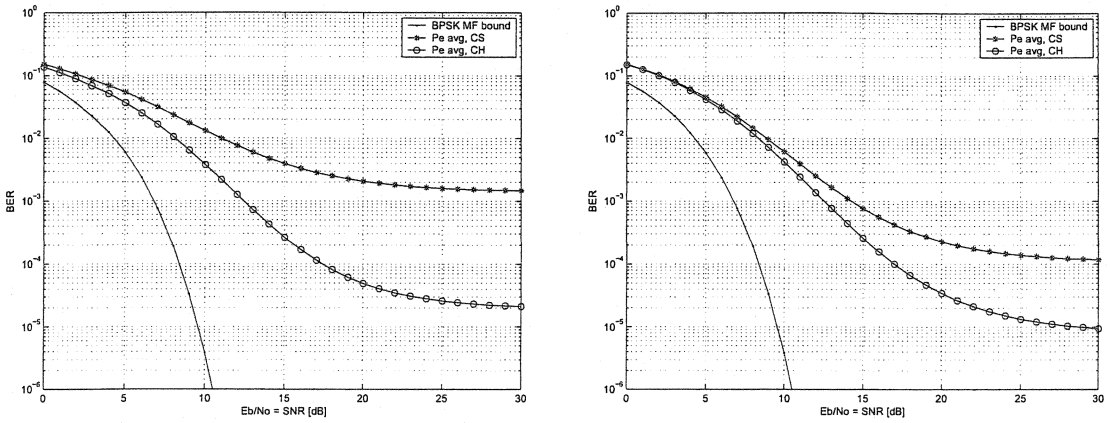

(a) Extended WH(32) sequence at 187.1 Mbps (b) Extended GL(30) sequence at 199.6 Mbps

Figure 4.37: Average BER of the extended WH(32) and the extended GL(30) sequences with 20 fingers over 7000 NLOS1 channels

more fingers to achieve the target outage. We empirically found that CH with the WH(16) sequence requires about 60 fingers to achieve the 2% outage probability with the 10^{-3} threshold.

A Lower Bit Rate with the extended WH(32) and the extended GL(30) sequences

First we use the extended WH(32) and the extended GL(30) sequences with length 32 and 30, respectively, for the lower rate system. Fig. 4.37 shows the average BER with 20 Rake fingers over 7000 NLOS1 channels. Both the extended WH(32) and the extended GL(30) sequences can reach 10^{-4} BER with 20 Rake fingers, and CH shows more than a 10 dB gain over CS. Hence it seems lowering the bit rate is more effective than increasing the number of Rake fingers if we compare the average BER of the original sequence with 40 fingers shown in Fig. 4.34.

The outage probability with the 10^{-4} threshold is shown in Fig. 4.38. Although CH enjoys a big gain over CS, the 2% target outage is only achieved at high E_b/N_o, even if the average BER of 10^{-4} has been reached at a reasonable E_b/N_o as shown in Fig. 4.37. As an alternative, if the 5% outage can be tolerated in the NLOS1 channel, CH can achieve the target outage with 10^{-4} threshold at around 21 dB for

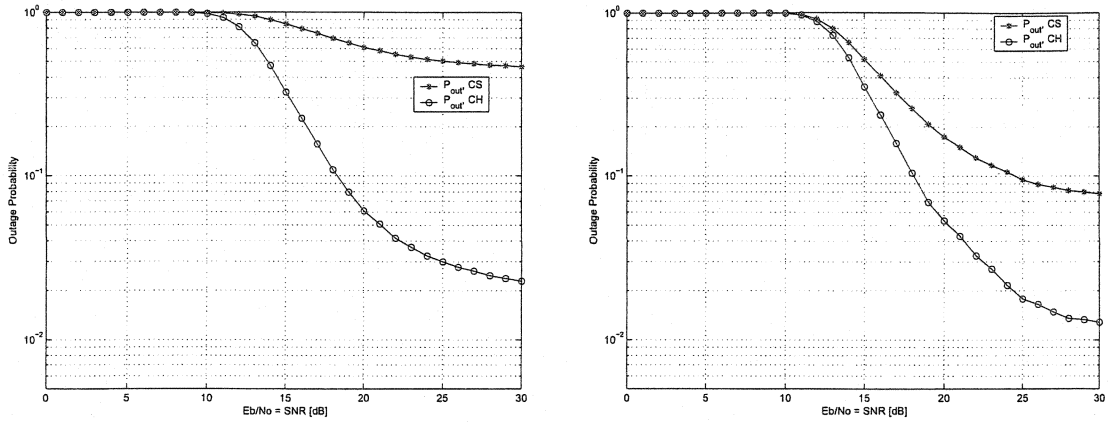

(a) Extended WH(16) sequence at 187.1 Mbps (b) Extended GL(15) sequence at 199.6 Mbps

Figure 4.38: Outage probability of the extended WH(32) and the extended GL(30) sequences with 20 fingers over 7000 NLOS1 channels, Th = 10^{-4}

both the extended WH(32) and the extended GL(30) sequences. Moreover the gain of CH over CS is well over 10 dB. Instead of increasing the target outage probability, if the threshold is set to 10^{-3}, shown in Fig. 4.39, the 2% outage probability can be achieved. The gain of CH over CS is well over 10 dB.

In summary, for the NLOS1 channel, the CH scheme with 20 Rake fingers can achieve the 5% outage probability with the 10^{-4} threshold and the 2% outage probability with the 10^{-3} threshold using the extended WH(32) and the extended GL(30) sequences. However the CS scheme fails to meet the target outage probability.

Next, we decrease the number of Rake fingers to 10 and examine the performance. Fig. 4.40 shows the average BER of the extended WH(32) and the extended GL(30) sequences. The average BER of both the sequences cannot reach 10^{-4} BER with 10 fingers. As can be expected, the outage probabilities with the 10^{-4} threshold, shown in Fig. 4.41, also fail to reach the target outage of 2% for CH. Fig. 4.42. shows the outage probability of 10 fingers with the 10^{-3} threshold. When CH is used, the outage probability of both sequences perform about the same. However only 5 % outage is achieved by CH with 10 Rake fingers in the high E_b/N_o region.

Therefore, 10 Rake fingers with the extended WH(32) and the extended GL(30)

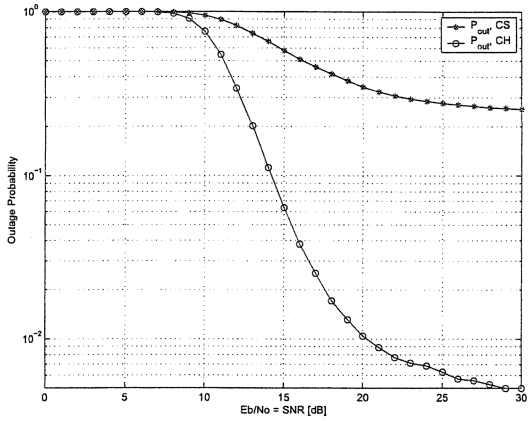

(a) Extended WH(16) sequence at 187.1 Mbps

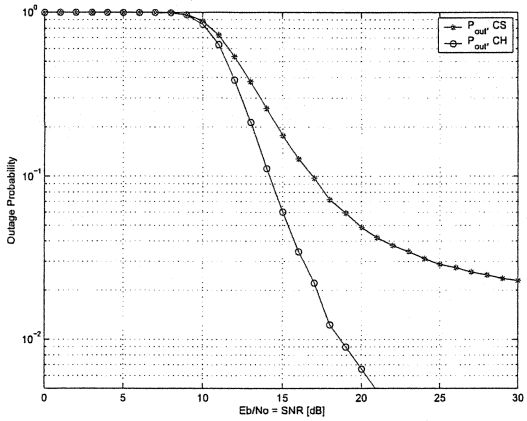

(b) Extended GL(15) sequence at 199.6 Mbps

Figure 4.39: Outage probability of the extended WH(32) and the extended GL(30) sequences with 20 fingers over 7000 NLOS1 channels, Th = 10^{-3}

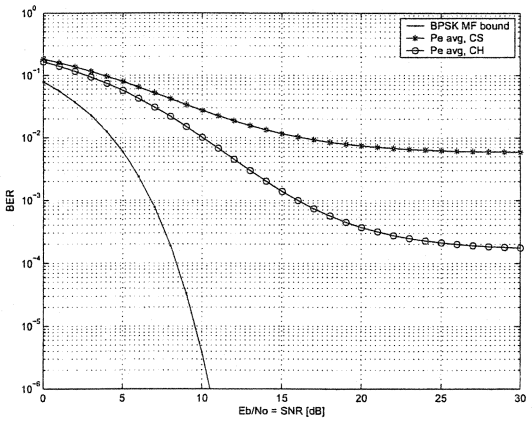

(a) Extended WH(16) sequence at 187.1 Mbps

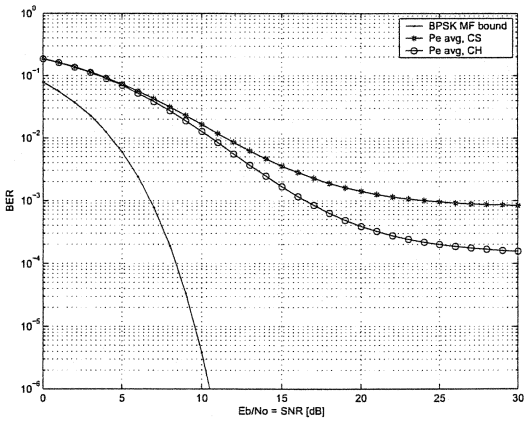

(b) Extended GL(15) sequence at 199.6 Mbps

Figure 4.40: Average BER of the extended WH(32) and the extended GL(30) sequences with 10 fingers over 7000 NLOS1 channels

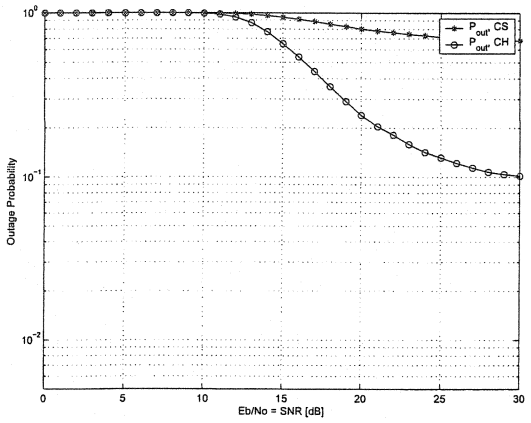

(a) Extended WH(16) sequence at 187.1 Mbps

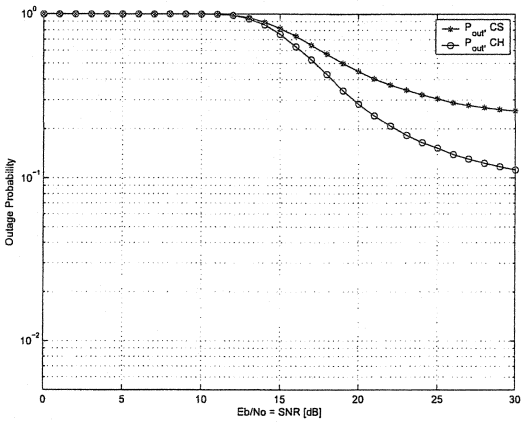

(b) Extended GL(15) sequence at 199.6 Mbps

Figure 4.41: Outage probability of the extended WH(32) and the extended GL(30) sequences with 10 fingers over 7000 NLOS1 channels, Th = 10^{-4}

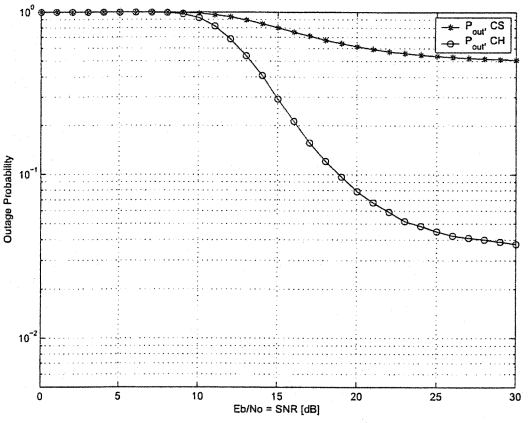

(a) Extended WH(16) sequence at 187.1 Mbps

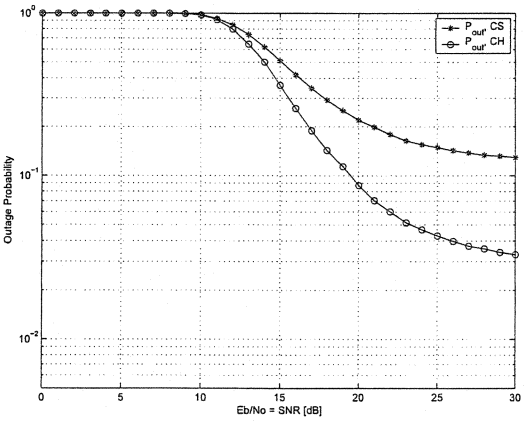

(b) Extended GL(15) sequence at 199.6 Mbps

Figure 4.42: Outage probability of the extended WH(32) and the extended GL(30) sequences with 10 fingers over 7000 NLOS1 channels, Th = 10^{-3}

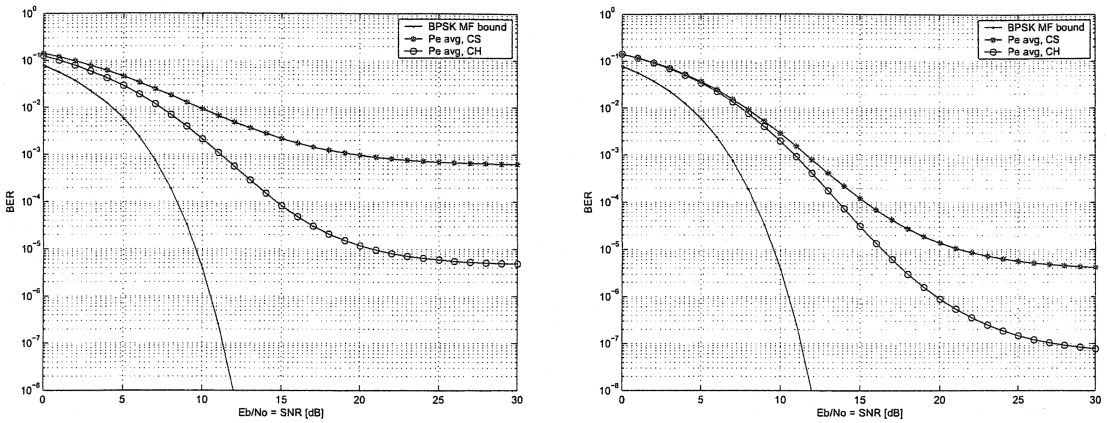

(a) WH(32) sequence at 187.1 Mbps

(b) Gold(31) sequence at 193.1 Mbps

Figure 4.43: Average BER of the WH(32) and the Gold(31) sequences with 20 fingers over 7000 NLOS1 channels

sequences are not sufficient to efficiently collect the received signal energy for the NLOS1 channel.

A Lower Bit Rate with the WH(32) and the Gold(31) sequences

We now examine the performance of the Gold(31) and the WH(32) sequences for the NLOS1 channel. Fig. 4.43 shows the average BER of the WH(32) and the Gold(31) sequences with 20 Rake fingers over the NLOS1 channel. If we compare with the results in Fig. 4.37, the WH(32) sequence shows better BER than the extended WH(32) sequence, and the Gold(31) sequence outperforms the extended GL(30) sequence. Note that the error floor of the Gold(31) sequence is much lower than that of the extended GL(30) sequence shown in Fig. 4.37(b).

The outage probability of the WH(32) and the Gold(31) sequences with 10^{-4} threshold is shown in Fig. 4.44. CH with both the WH(32) and the Gold(31) sequences reach the 2 % outage at 19 dB and 16.3 dB, respectively. Thus, the gain of CH over CS is well over 10 dB with the WH(32) sequence and 3.7 dB with the Gold(31) sequence. If we compare the outage probability of the WH(32) sequence with that of the Gold(31) sequence, the Gold(31) sequence is 2.7 dB better than the WH(32) sequence for the 2 % outage with the 10^{-4} threshold.

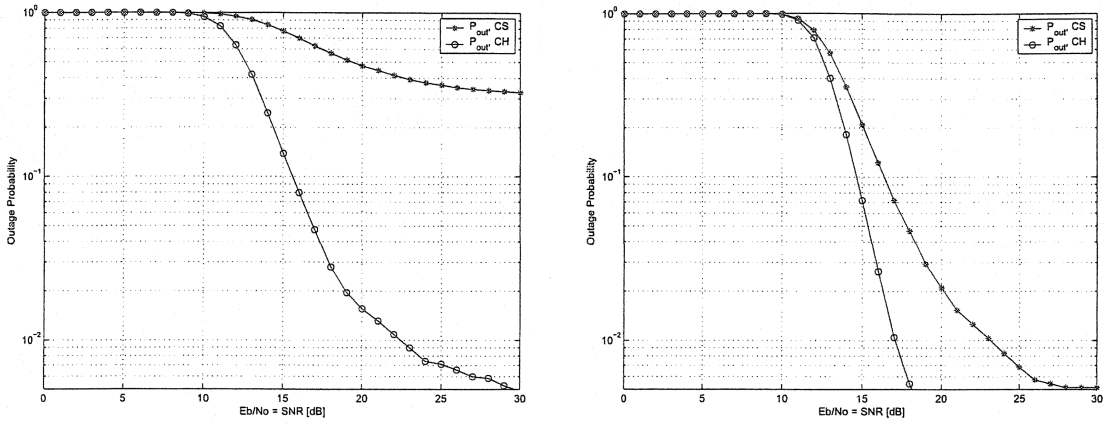

(a) WH(32) sequence at 187.1 Mbps (b) Gold(31) sequence at 193.1 Mbps

Figure 4.44: Outage probability of the WH(32) and the Gold(31) sequences with 20 fingers over 7000 NLOS1 channels, Th = 10^{-4}

The outage probability with the 10^{-5} threshold is illustrated in Fig. 4.45. Both sequences reach 2 % outage with 10^{-5} threshold, and the gain of CH over CS is well over 10 dB for the WH(32) sequence and 6.2 dB for the Gold(31) sequence. Note also that the gain of CH with the Gold(31) sequence over the WH(32) sequence is 5 dB. Therefore CH with the Gold(31) sequence has superior performance to CH with the WH(32) sequence for the NLOS1 channel, which was not observed in the LOS channel. It implies that the Gold sequence is more robust than the WH sequence in a dense multipath fading channel.

Next, we decrease the number of Rake fingers to 10 and evaluate the performance. Fig. 4.46 shows the average BER of the WH(32) and the Gold(31) sequences with 10 Rake fingers. By comparing this with Fig. 4.40, we can see the WH(32) and the Gold(31) sequences perform better than the extended WH(32) and the extended GL(30) sequences.

Fig. 4.47 shows the outage probability of the WH(32) and the Gold(31) sequences with 10 fingers with the 10^{-4} threshold. For the outage probability with 10 fingers, the WH(32) sequence fails to reach the 2% target outage, while the Gold(31) sequence can reached the target with 10^{-4} threshold. It is notable that, for the NLOS1 channel,

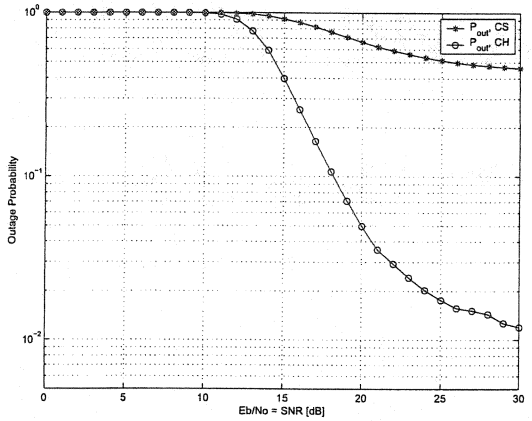

(a) WH(32) sequence at 187.1 Mbps

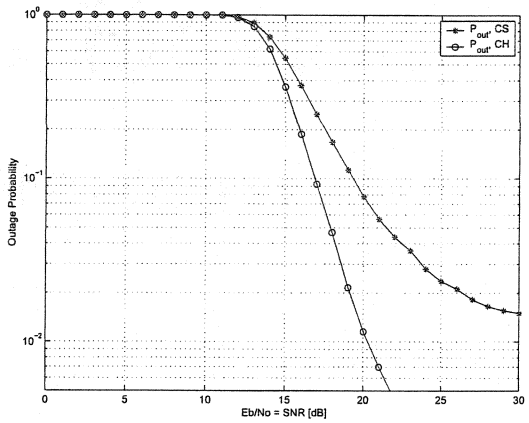

(b) Gold(31) sequence at 193.1 Mbps

Figure 4.45: Outage probability of the WH(32) and the Gold(31) sequences with 20 fingers over 7000 NLOS1 channels, Th = 10^{-5}

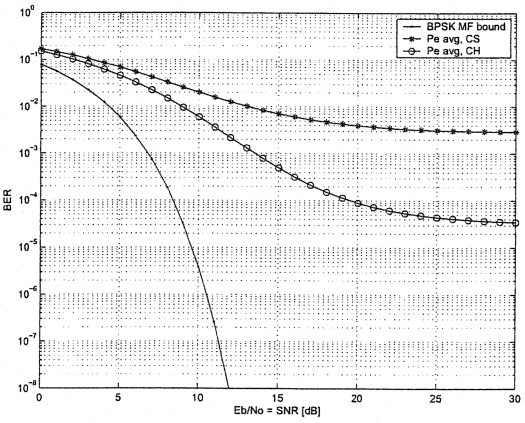

(a) WH(32) sequence at 187.1 Mbps

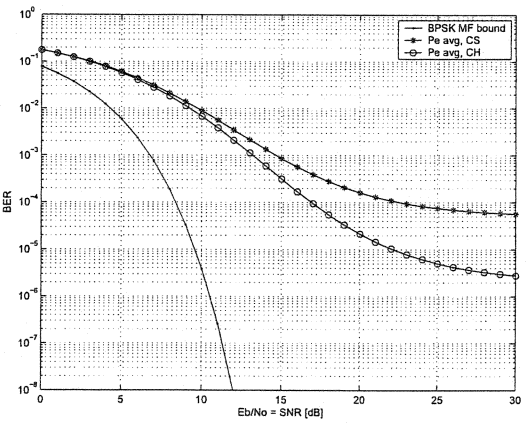

(b) Gold(31) sequence at 193.1 Mbps

Figure 4.46: Average BER of the WH(32) and the Gold(31) sequences with 10 fingers over 7000 NLOS1 channels

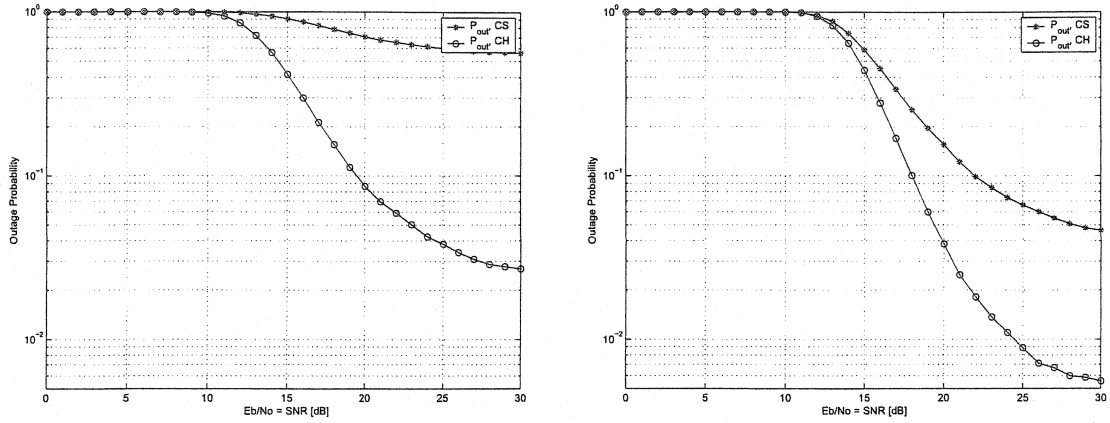

(a) WH(32) sequence at 187.1 Mbps (b) Gold(31) sequence at 193.1 Mbps

Figure 4.47: Outage probability of the WH(32) and the Gold(31) sequences with 10 fingers over 7000 NLOS1 channels, Th = 10^{-4}

using only 10 Rake fingers, CH with the Gold(31) sequence achieves the 2 % target outage at 22 dB. The gain of CH with the GL(31) sequence over CS is well over 10 dB.

The outage probability with the 10^{-3} threshold is shown in Fig. 4.48. It is seen that CH with both sequences has more than a 6 dB gain over CS for the 2 % outage with the 10^{-3} threshold. If we compare the WH(32) sequence with the Gold(31) sequence, CH with the Gold(31) sequence shows a 3 dB gain over CH with the WH(32) sequence for the 2 % outage probability.

In summary, CH with the WH(32) sequence and the Gold(31) sequence are better than CH with the extended WH(32) and the extended GL(30) sequences for the NLOS1 channel. Among all the sequences examined, CH with the Gold(31) sequence is shown to perform the best for the NLOS1 channel followed by CH with the WH(32) sequence. Moreover, the major result found in this work is that for the NLOS1 channel, CH with the Gold(31) sequence can provide the 2 % outage with the 10^{-3} threshold at $E_b/N_o = 17dB$ using 10 Rake fingers, as shown in Fig. 4.48(b). Also, CH with Gold(31) sequence showed a 6 dB gain over CS.

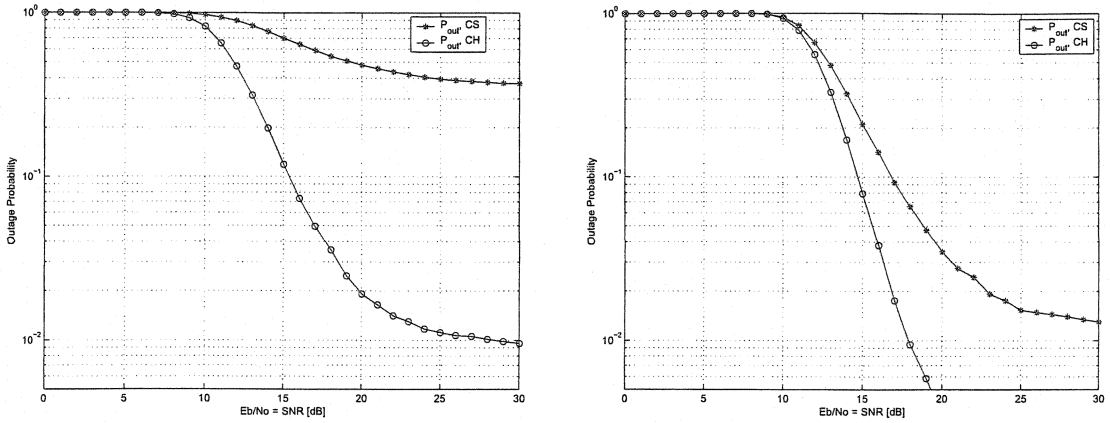

(a) WH(32) sequence at 187.1 Mbps

(b) Gold(31) sequence at 193.1 Mbps

Figure 4.48: Outage probability of the WH(32) and the Gold(31) sequences with 10 fingers over 7000 NLOS1 channels, Th = 10^{-3}

	CS	CH	avg. HP length
Gold(31)	48.01%	51.99%	1.69
WH(32)	6.50%	93.50%	2.84

Table 4.2: Usage of CS and CH with LOS1 channel

4.4 Characteristics of the Hopping Pattern Search Algorithm

In addition to the performance of CH shown in previous sections, there are also other things to be evaluated in order for CH to be applicable in practice. In this section, we examine some of the characteristics of the stage-wise CH pattern search algorithm described in Chapter 3.

4.4.1 Usage of Code Selection and Code Hopping

Since the stage-wise method chooses a CH pattern with the length from 1 to $N_{h,max}$, CS is also included. Table 4.2 shows the percentage of time the stage-wise method chose CS or CH for the Gold(31) sequence and the WH(32) sequence with 10 fingers simulated over 7000 NLOS1 channels. The stage-wise method chose CH 93.5% of the time for the WH(32) sequence for the statistically generated NLOS1 channels.

Code No.	1	2	3	4	5	6	7	8	9	10
%	4.94	4.90	3.19	3.47	3.39	3.14	2.07	2.37	3.55	3.57
Code No.	**11**	**12**	**13**	**14**	**15**	**16**	**17**	**18**	**19**	**20**
%	3.34	3.16	2.30	2.29	2.79	2.75	3.15	3.35	2.52	2.58
Code No.	**21**	**22**	**23**	**24**	**25**	**26**	**27**	**28**	**29**	**30**
%	3.26	2.94	3.09	3.01	2.45	2.73	3.00	2.93	2.78	2.85
Code No.	**31**	**32**								
%	4.16	3.99								

Table 4.3: The percentage of the WH(32) sequences chosen for the NLOS channels

Meanwhile, with the Gold(31) sequence, CH was chosen 51.99% of the time. This is due to the fact that the WH(32) sequence generally has lower cross-correlation values than auto-correlation values. Hence, the stage-wise method is able to find more CH patterns with the WH(32) sequence. However the Gold(31) sequence has generally well controlled both cross-correlation and auto-correlation functions, so the stage-wise method found less CH patterns that perform better than CS. Therefore this result implies that the WH sequences would give more performance gain by CH than that for the Gold sequences.

4.4.2 Usage of Spreading Sequences

It would also be ideal if the stage-wise CH pattern search algorithm choose all the spreading sequences with equal probability. Since the spreading sequence is also a precious resource, it is not desirable if the search method overwhelmingly chooses a specific code among the spreading sequences available. Table 4.3 and Table 4.4 show the percentage of spreading sequences chosen (including both CS and CH) from the WH(32) sequences and the Gold(31) sequences, respectively.

For both simulations, 7000 NLOS1 channels were used with 10 fingers. As we can see from both tables, the choice of spreading sequence is not exactly uniform but it seems most of them are evenly chosen to a certain degree.

Code No.	1	2	3	4	5	6	7	8	9	10
%	5.18	4.09	2.57	2.67	3.01	3.10	2.63	3.27	3.05	2.54
Code No.	**11**	**12**	**13**	**14**	**15**	**16**	**17**	**18**	**19**	**20**
%	4.20	2.95	3.33	3.55	3.16	2.97	2.26	3.27	2.97	3.71
Code No.	**21**	**22**	**23**	**24**	**25**	**26**	**27**	**28**	**29**	**30**
%	2.93	2.35	2.66	2.36	2.80	1.59	3.04	3.19	2.89	2.76
Code No.	**31**	**32**	**33**							
%	3.32	2.84	2.78							

Table 4.4: The percentage of the Gold(31) sequences chosen for the NLOS channels

4.4.3 Flexibility of the Hopping Pattern Search

If some receivers in a system have similar channel impulse responses, then it is possible that the CH pattern search algorithm finds the same CH pattern for more than two receivers. Then it may cause code collision between the receivers that use the same CH pattern. Therefore it would be desirable if the CH pattern search algorithm is able to find alternate CH patterns that also perform well for the same channel impulse response. This problem is directed as the flexibility of the CH pattern search. In this section we briefly investigate the possibility of the alternate CH pattern for a given channel.

To find the alternate CH pattern we slightly modify the CH pattern search algorithm. At the stage 1, in Chapter 3, we choose the second best code for CS. Then, at the stage 2, we also choose the second best CH pattern, and repeat the stage 2 until the search algorithm cannot find a better CH pattern. Fig. 4.49 compares the average BER of the suboptimal CH pattern with the alternate hoping pattern. The suboptimal CH pattern reaches 10^{-4} BER at 17 dB, while the alternate CH pattern reaches the same BER at 18 dB. We thus have a 1 dB loss for the alternative CH pattern.

Fig. 4.50 compares the outage probability of the suboptimal CH pattern with the alternate CH pattern. It is seen that the suboptimal CH pattern reaches 2 % outage at 16.8 dB, while the alternate CH pattern achieves the same outage at 18 dB. Thus

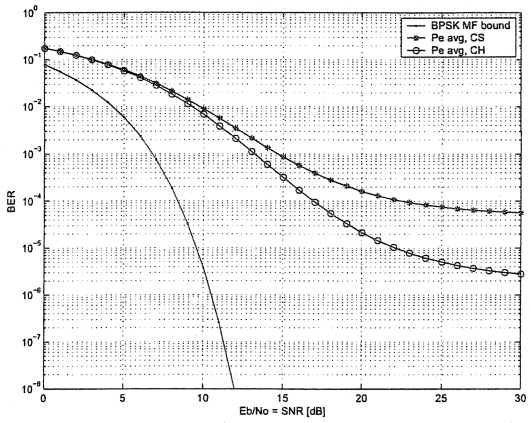

(a) Gold(31) suboptimal CH pattern

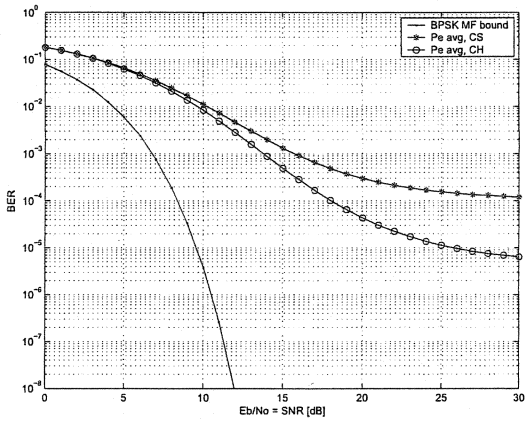

(b) Gold(31) alternate hoping pattern

Figure 4.49: Average BER comparison of the Gold(31) sequence with 10 fingers between the suboptimal and the alternate CH patterns (2nd CS and 2nd CH)

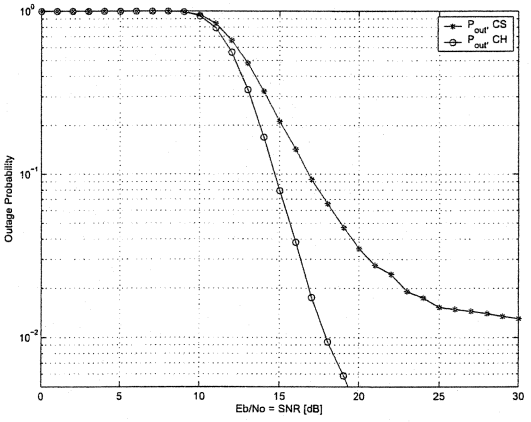

(a) Gold(31) suboptimal CH pattern

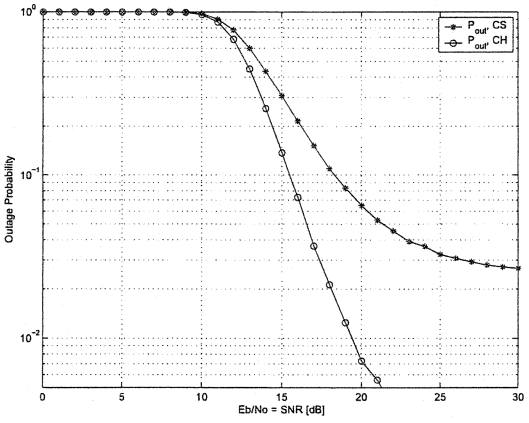

(b) Gold(31) alternate hoping pattern

Figure 4.50: Outage probability comparison of the Gold(31) sequence with 10 fingers between the suboptimal and the alternate CH patterns (2nd CS and 2nd CH), Th = 10^{-3}

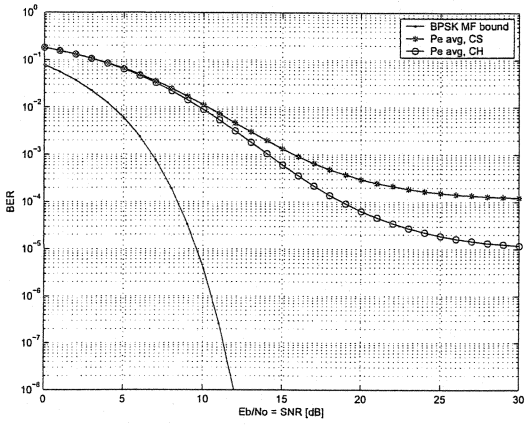

(a) Average BER, Gold(31)

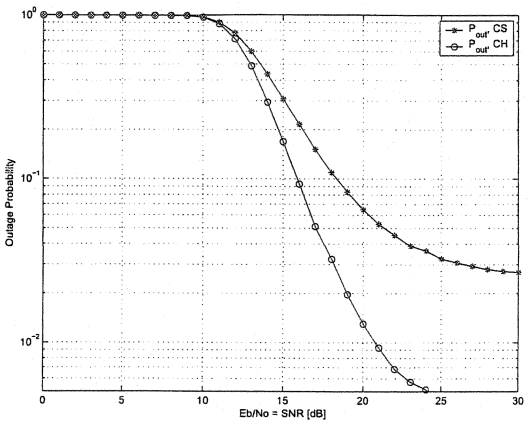

(b) Outage Probability, Gold(31)

Figure 4.51: The average BER and the outage probability of the Gold(31) sequence with 10 fingers and the alternate CH patterns (2nd CS and 3rd CH), Th = 10^{-3}

there is about a 1.2 dB loss in outage by using the alternate CH pattern.

Fig. 4.51 also shows the performance of another CH pattern chosen from the 2nd best CS and from the 3rd best CH. The CH pattern shown in the figure requires 19 dB both for the 10^{-4} BER and for the 2 % outage. Thus an extra 1 dB loss is caused by using yet another CH pattern from the CH pattern search algorithm.

Chapter 5

Conclusions

5.1 Conclusions

In a high rate indoor wireless UWB communication system, there is a large number of multipath terms in the channel impulse response. These cause intersymbol interference and make it hard to achieve good performance at a high rate. Although an equalizer is a strong scheme to suppress ISI, it increases complexity in the receiver. This thesis is concerned with providing an alternate method to compensate for ISI with simple receiver design, and proposes a CH-DSSS scheme. The following are the major conclusions drawn from this work.

1. The CH-DSSS scheme with the CH pattern search algorithm presented in this thesis is shown to suppress intersymbol interference and significantly improves the average BER and the outage probability for the wireless indoor UWB channel.

2. The analysis of the error probability can give the exact BER for the multipath fading channel. By using the Beaulieu series method, computational complexity is significantly reduced compared to the MC and the Q-MC method without compromising accuracy. It enabled the outage probability analysis to be possible. For example, for the simulation of a single NLOS1 channel with 10 fingers, the MC method took 9792 sec, and the Q-MC method took 77.4 sec to simulate

the BER. Meanwhile, the BSM took only 7.3 sec to compute the BER of the single NLOS1 channel.

3. The stage-wise CH pattern search algorithm does not search for the optimum CH pattern, but significantly reduces the computational complexity compared to the exhaustive search method. Furthermore CH with the stage-wise method is shown to always perform better than the CS method.

4. For the LOS channel, CS with the GL(15) sequence performs better than CS with the WH(16) sequence due to its good auto-correlation function. However, CH with the WH(16) sequence achieves significant improvement and performs about the same as CH with the GL(15) sequence.

5. For the NLOS1 channel, CH with the Gold(31) sequence performs the best among the sequences examined. Using 10 Rake fingers, CH with Gold(31) sequence achieved the 2 % outage probability with the 10^{-4} threshold at 22 dB, and the gain over CS is more than 10 dB. When the threshold is 10^{-3}, CH with both the WH(32) sequence and the Gold(31) sequence achieved the 2 % outage at 20 dB and 17 dB, respectively, and the gain of CH is more than 6 dB over CS. Therefore CH is recommended for the Gold(31) sequence with 10 fingers in the NLOS1 channel.

6. If the same number of fingers are used, CH can reduce the required E_b/N_o to get a target performance. On the other hand, if the same E_b/N_o is used, CH can reduce the number of Rake fingers required to get the target performance, inducing less complexity in the receiver.

5.2 Suggestions for Future Work

1. Although CH has shown significant improvement for a multipath fading channel with intersymbol interference, it is not verified in this thesis if CH with error-

correction coding meets the total BER requirement of 10^{-5} with the given power constraint by the FCC. Therefore, CH combined with coding should be further investigated.

2. The performance of CH is evaluated in a single user system. The performance of the CH scheme in a multiuser environment with an uncoordinated system is suggested for further study.

3. The pulse shaping and the spectral properties of a CH-DSSS system should also be studied.

4. Perfect knowledge of CSI is assumed throughout this thesis. One may wish to study CH and the CH pattern design with the imperfect knowledge of the channel state information.

5. As the number of multipath terms increase, the proposed CH pattern search takes a long time to find a CH pattern. One may wish to design more efficient CH pattern search algorithm.

6. The matched filter receiver with Rake combining may not be the best choice for a dense multipath fading UWB channel. One may wish to investigate CH with different types of receivers, such as a minimum mean-square-error (MMSE) receiver [64].

Bibliography

[1] A. M. Saleh and R. A. Valenzuela, "A Statistical Model for Indoor Multipath Propagation," *IEEE Journal on Selected Areas in Communications*, vol. 5, no. 2, pp. 128-137, Feb. 1987.

[2] J. G. Proakis, "Digital Communications, fourth edition," *McGraw Hill*, 2001.

[3] G. Ross, "A Time Domain Criterion for the Design of Wideband Radiation Elements," *IEEE Transactions on Antennas and Propagation*, vol. 16, no. 3, pp. 355-356, May 1968.

[4] C. L. Bennett and G. Ross, "Time-Domain Electromagnetics and its Applications," *IEEE Proceedings*, vol. 66, pp. 299-318, Mar. 1978.

[5] R. J. Fontana, "A Brief History of UWB Communications," *Multispectral Solutions Inc., [onlne]. Available: http://www.multispectral.com/history.html*, 2004.

[6] M. Z. Win and R. A. Scholtz, "Impulse radio: How It Works," *IEEE Communiactions Letters*, vol. 2, no. 2, pp. 36-38, Feb. 1998.

[7] M. Z. Win and R. A. Scholtz, "Ultra-wide Bandwidth Time-Hopping Spread-Spectrum Impulse Radio for Wireless Multiple-Access Communications," *IEEE Transactions on Communications*, vol. 48, no. 4, pp. 679-689, Apr. 2000.

[8] B. Hu and N. C. Beaulieu, "Exact Bit Error Rate Analysis of TH-PPM UWB Systems in the Presence of Multiple-Access Interference," *IEEE Communications Letters*, vol. 7, no. 12, pp. 572-574, Dec. 2003.

[9] F. R. Foerster, "The Performance of a Direct-Sequence Spread Ultrawideband System in the Presence of Multipath, Narrowband Interference, and Multiuser Interference," *IEEE Conference on Ultra Wideband Systems and Technologies*, Wyndham, Baltimore, pp. 87-91, May 2002.

[10] Q. Li and L. A. Rusch, "Multiuser Detection for DS-CDMA UWB in the Home Environment," *IEEE Journal on Selected Areas In Communications*, vol. 20, no. 9, pp. 1701-1711, Dec. 2002.

[11] T. Ogawa, A. Tomiki, and T. Kobayashi, "Development of Two Kinds of UWB Sources for Propagation, EMC and Other Experimental Studies: Impulse Radio and Direct-Sequence Spread Spectrum," *IEEE International Symposium on Antennas and Propagation Society*, Columbus, Ohio, vol. 4, pp. 273-276, Jun. 2003.

[12] K. Eshima, Y. Hase, and S. Oomori, "M-ary UWB System Using Walsh Codes," *IEEE Conference on Ultra Wideband Systems and Technologies, Digest of Papers*, Wyndham, Baltimore, pp. 37-40, May 2002.

[13] R. Gupta and A. H. Tewfik, "Capacity of Ultra-Wideband OFDM," *IEEE Semiannual Vehicular Technology Conference*, Jeju, Korea, vol. 2, pp. 1420-1424, Apr. 2003.

[14] D. Gerakoulis and P. Salmi, "An Interference Suppressing OFDM System for Ultra Wide Bandwidth Radio Channels," *IEEE Conference on Ultra Wideband Systems and Technologies, Digest of Papers*, Wyndham, Baltimore, pp. 259-264, May 2002.

[15] E. Saberinia and A. H. Tewfik, "Multi-User UWB-OFDM Communications," *IEEE Pacific Rim Conference on Communications, Computers and Signal Processing*, Victoria, BC, Cadana, vol. 1, pp. 127-130, Aug. 2003.

[16] A. H. Tewfik and E. Saberinia, "High Bit Rate Ultra-wideband OFDM," *IEEE Global Telecommunications Conference*, Taipei, Taiwan, vol. 3, pp. 260-2264, Nov. 2002.

[17] M. Weisenhorn and W. Hirt, "Performance of Binary Antipodal Signaling over the Indoor UWB MIMO Channel," *IEEE International Conference on Communications*, Anchorage, Alaska, vol. 4, pp. 2872-2878, May 2003.

[18] K. Tang, P. H. Siegel, and L. B. Milstein, "A Comparison of Long Versus Short Spreading Sequences in Coded Asynchronous DS-CDMA Systems," *IEEE Journal on Selected Areas in Communications*, vol. 19, no. 8, pp. 1614-1624, Aug. 2001.

[19] S. Parkvall, "Long vs Short Spreading Codes in Cellular DS-CDMA," *IEEE 5th International Symposium on Spread Spectrum Techniques and Applications*, Sun city, South Africa, vol. 3, pp. 681-685, Sep. 1998.

[20] S. Parkvall, "Variability of User Performance in Cellular DS-CDMA - Long versus Short Spreading Sequences," *IEEE Transactions on Communications*, vol. 48, no. 7, pp. 1178-1187, Jul. 2000.

[21] M. L. Honig and W. Veerakachen, "Performance Variability of Linear Multiuser Detection for DS-CDMA," *46th IEEE Vehicular Technology Conference*, Atlanta, Georgia, vol. 1, no. 28, pp. 372-376, May 1996.

[22] D. L. Noneaker and M. B. Pursley, "Selection of Spreading Sequences for Direct-Sequence Spread-Spectrum Communications over a Doubly Selective Fading Channel," *IEEE Transactions on Communications*, vol. 42, no. 12, pp. 3171-3177, Dec. 1994.

[23] B. Ünal and Y. Tanik, "Code-Hopping as a New Strategy to Improve Performance of S-CDMA Cellular Systems," *Global Telecommunications Conference*, London, England, vol. 2, pp. 1316-1319, Nov. 1996.

[24] B. Ünal and Y. Tanik, "Capacity Improvement by Code-Hopping in S-CDMA systems," *IEEE International Conference on Communications*, Atlanta, Georgia, vol. 2, pp. 989-993, Jun. 1998.

[25] S. Park and D. K. Sung, "Orthogonal Code Hopping Multiplexing," *IEEE Communications Letters*, vol. 6, no. 12, pp. 529-531, Dec. 2002.

[26] T. Onizawa and T. Hasegawa, "The Spread Spectrum Code Hopping System," *IEEE Third International Symposium on Spread Spectrum Techniques and Applications*, Oulu, Finland, vol. 1, pp. 287-291, Jul. 1994.

[27] T. Tsuzuki and R. Kohno, "Inter-Vehicle Communication Protocol Using Common Spreading Code," *Proceedings of the IEEE Intelligent Vehicles Symposium*, Parma, Italy, pp. 376-381, Oct. 2000.

[28] I. J. Kim, K. Kim, and B. Lim, "A Fast Cell Search Algorithm for Inter-Cell Asynchronous W-CDMA System using Code Hopping Method," *IEEE Global Telecommunications Conference*, Sydney, Australia, vol. 3, pp. 1373-1377, Nov. 1998.

[29] D. Noguet, J. R. Lequepeys, R. Lionti, and N. Daniele, "VICASSO: A New Flexible Base-band Transceiver ASIC for a Wide Range of DSSS Communication Applications," *IEEE Sixth International Symposium on Spread Spectrum Techniques and Applications*, Parsippany, New Jersey, vol. 2, pp. 506-509, Sep. 2000.

[30] J. K. Tugnait and J. Ma, "Blind Multiuser Detection for Code-Hopping DS-CDMA Signals in Asynchronous Multipath Channels," *IEEE Transactions on Wireless Communications*, vol. 3, no. 2, pp. 466-476, Mar. 2004.

[31] B. Parr, B. Cho, K. Wallace, and Z. Ding. "A Novel Ultra-Wideband Pulse Design Algorithm," *IEEE Communications Letters*, vol. 7, no. 5, pp. 219-221, May 2003.

[32] L. B. Michael, M. Ghavami, and R. Kohno. "Multiple Pulse Generator for Ultra-Wideband Communication using Hirmite Polynomial Based Orthogonal Pulses," *IEEE Conference on Ultra Wideband Systems and Technologies*, Wyndham, Baltimore, pp. 47-51, May 2002.

[33] E. Frazer, "UWB Applications and Interference," *UWB Colloquium [online]. Available: http://www.ofcom.org.uk/static/archive/ra/topics/uwb/uwb-applications-interference.pdf*, Jul. 2002.

[34] R. J. Fontana, "Experimental Results from an Ultra Wideband Precision Geolocation System," *[onlne]. Available: http://www.multispectral.com/pdf/GeoVGs.pdf*, 2000.

[35] "FCC notice of proposed rule making, revision of part 15 of the commission's rules regarding ultra-wideband transmission systems," *Federal Communications Commission*, Washington, DC, ET-Docket 98-153, 2002.

[36] S. Roy, J. R. Foerster, V. S. Somayazulu, and D. G. Leeper, "Ultrawideband Radio Design: The Promise of High-Speed, Short-Range Wireless Connectivity," *Proceedings of the IEEE*, vol. 95, no. 2, pp. 295-311, Feb. 2004.

[37] "SG3a Alternate PHY Selection Criteria," *IEEE P802.15-02/105r25 [online]. Available: http://grouper.ieee.org/groups/802/15/pub/2002/Sep02/*, 2002.

[38] "TG3a-Technical-Requirements," *IEEE P802.15-03/030r0 [onlne]. Available: http://www.ieee802.org/15/pub/TG3a.html*, Dec. 2002.

[39] G. R. Aiello and G. D. Rogerson, "Ultra-Wideband Wireless Systems," *IEEE microwave magazine*, vol. 4, no. 2, pp. 36-47, Jun. 2003.

[40] M. Hämäläinen, R. Tesi, J. Iinatti, and V. Hovinen, "On the Performance Comparison of Different UWB Data Modulation Schemes in AWGN Channel in the

Presence of Jamming," *IEEE Radio and Wireless Conference*, Boston, MA, pp. 83-86, Aug. 2002.

[41] J. Foerster, E. Green, S. Somayazulu, and D. Leeper, "Ultra-Wideband Technology for Short- or Medium- Range Wireless Communications," *Intel Technology Journal [online]. Available: www.intel.com/technology/itj/q22001/pdf/* Q2, 2001.

[42] "UWB Channel Modeling Contribution," Intel Corp., *IEEE P802.15-02/02 790r0-SG3a. [onlne]. Available: http://grouper.ieee.org/groups/802/15/pub/2002/Jul02/*, 2002.

[43] L. Rusch, C. Prettie, D. Cheung, Q. Li, and M. Ho, "Characterization of UWB Propagation from 2 to 8 GHz in a Residential Environment," *Intel Corporation, Intel Research Labs [online]. Available: www.intel.com/technology/ultrawideband/ downloads/*, 2001.

[44] H. Suzuki, "A Statistical Model for Urban Radio Propagation," *IEEE Transactions on Communications*, vol. 25, no. 7, pp. 673-680, Jul. 1977.

[45] H. Hashemi, "Impulse Response Modeling of Indoor Radio Propagation Channels," *IEEE Journal on Selected Areas in Communication*, vol. 11, no. 7, pp. 967-978, Sep. 1993.

[46] T. S. Rappaport, "Wireless Communications principles and practice 2nd. Ed," *Prentice Hall*, 2002.

[47] I. Vajda, "On Random Code-Hopping DS/SSMA System," *IEEE International Symposium on Spread Spectrum Techniques and applications*, London, England, pp. 47-52, Sep. 1990.

[48] R. E. Ziemer and R. L. Peterson, "Digital Communications and Spread Spectrum Systems," *Macmillan*, 1985.

[49] T. Hoholdt and J. Justesen, "Ternary sequences with Perfect Periodic Autocorrelation," *IEEE Transactions on Information Theory*, vol. 29, no. 4, pp. 597-600, Jul. 1983.

[50] S. R. Park, I. Song, and H. Kwon, "DS/CDMA Signature Sequences Based On PR-QMF Banks," *IEEE Transactions on Signal Processing*, vol. 50, no. 12, pp. 3043-3054, Dec. 2002.

[51] R. Gold, "Optimal Binary Sequences for Spread Spectrum Multiplexing," *IEEE Transactions on Information Theory*, vol. 13, no. 4, pp. 619-621, Oct. 1967.

[52] R. Gold, "Maximal Recursive Sequences with 3-value Recursive Cross-Correlation Function," *IEEE Transactions on Information Theory*, vol. 14, no. 1, pp. 154-156, Jan. 1968.

[53] D. V. Sarwate and M. B. Pursley, "Crosscorrelation Properties of Pseudorandom and Related Sequences," *IEEE Proceedings*, vol. 68, no. 5, pp. 593-619, May 1980.

[54] T. A. Dowing and R. J. McEliece, "Cross-correlation of Reverse Maximal-length Shift Register Sequences," *Technical Report, JPL Space Programs Summary*, vol. 3, pp. 192-193, 1968.

[55] P. Fan and M. Darnell, "Sequence Design for Communications Applications," *John Wiley and Sons*, New York, 1996.

[56] E. H. Dinan and B. Jabbari. "Spreading Codes for Direct Sequence CDMA and Wideband CDMA Cellular Networks," *IEEE Communications Magazine*, vol. 36, no. 9, pp. 48-54, Sep. 1998.

[57] B. J. Wysocki, "Signal Formats for Code Division Multiple Access Wireless Networks," *Ph.D. thesis, Curtin University of Technology*, Australia, Aug. 1999.

[58] N. C. Beaulieu, "A Simple Series for Personal Computer Computation of the Error Function Q(·)," *IEEE Transactions on Communications*, vol. 37, no. 9, pp. 989-991, Sep. 1989.

[59] N. C. Beaulieu, "The Evaluation of Error Probabilities for Intersymbol and Cochannel Interference," *IEEE Transactions on Communications*, vol. 39, no. 12, pp. 1740-1749, Dec. 1991.

[60] M. O. Sunay, "Performance Analysis of Direct Sequence Code Division Multiple Access Systems," *Ph.D. thesis, Queen's University*, Kingston, Ontario, Canada, 2000.

[61] J. M. Wozencraft and I. M. Jacobs, "Principles of Communication Engineering," *Waveland Press Inc.*, 1990.

[62] Y. K. J. Lau, "Arithmetic Errr Correcting Codes for Fault-Tolerant Digital Signal Processing in Satellite Applications," *Master's thesis, Queen's University*, Kingston, Ontario, Canada, 1992.

[63] R. W. Kerr, "Coherent Detection of Interleaved CPFSK on Various Shadowed Mobile Satellite Channels," *Master's thesis, Queen's University*, Kingston, Ontario, Canada, 1989.

[64] M. Thériault, L. A. Rusch, and P. Fortier, "Effect of RAKE Correlations on the Performance of Hybrid RAKE," *22nd Biennial Symposium on Communications, Queen's University*, Kingston, Ontario, Canada, pp. 322 - 324, Jun. 2004.

Appendix A

Confidence Intervals

For the BER simulation, the Monte Carlo(MC) method counted 200 errors for each E_b/N_0 until BER of 10^{-4} is reached. For the BER of 10^{-4}, at least $2 \cdot 10^6$ bits are used to simulate the BER. To get a guideline of the reliability of the simulation results, the statistical confidence intervals are derived from Chernoff bound [61], [63]. Table A.1 is excerpted from the results obtained in [62]. Similarly, Table A.2 shows how many channels are required to have a certain confidence interval for the outage probability.

BER	95% certain within 30%	95% certain within 20%
10^{-1}	8.00×10^2	1.755×10^3
10^{-2}	8.88×10^3	1.943×10^4
10^{-3}	8.97×10^4	1.962×10^5
10^{-4}	8.98×10^5	1.963×10^6
10^{-5}	8.98×10^6	1.964×10^7

Table A.1: Number of bits required to achieve a certain confidence interval

P_{outage}	95% certain within 30%	90% certain within 20%
0.05	1600	2900
0.04	2000	3600
0.03	2700	4900
0.02	4100	7400

Table A.2: Number of channels required to achieve a certain confidence interval